공학석사 학위논문

자가 조립 와이어프레임 DNA 구조체를 통한 설계 가능한 나노 수준 종이접기 기술 개발

Development of programmable nanoscale origami through self-assembled DNA wireframe structures

2022년 2월

서울대학교 대학원

기계공학부

김 명 석

자가 조립 와이어프레임 DNA 구조체를 통한 설계 가능한 나노 수준 종이접기 기술 개발

지도교수 김 도 년

이 논문을 공학석사 학위논문으로 제출함

2021년 10월

서울대학교 대학원

기계공학부

김 명 석

김명석의 공학석사 학위논문을 인준함

2021년 12월

위 원 장 이 호 원 (인)

부위원장 김 도 년 (인)

위 원 신 용 대 (인)

Abstract

The origami mechanism has provided effective solutions to many engineering problems related to structural reconfiguration through its transformable properties. However, the transfer of the origami-based reconfiguration mechanism from macroscale into nanoscale engineering remains a challenge due to the difficulties in effectively implementing high-precision structural design and programming various folding lines (crease patterns) of nanostructures. Here, we developed a nucleic-based crease patterning method on a planar sheet of DNA wireframe nanostructure (DNA wireframe paper) by harnessing the paper folding mechanism and implemented eight reconfigurable folding types of DNA wireframe papers using toehold-mediated strand displacement. The folding yield is optimized above 90% by increasing the binding probability and relieving the structural rigidity of the crease. Based on its high yield secured, folding properties such as orthogonal folding, repeatable folding and unfolding, and folding-based signal control were designed and demonstrated through atomic force microscopy and fluorescence measurements. Furthermore, environmental stimuli-responsive folding according to pH value and UV illumination time was designed and successfully controlled. Moreover, we adopt a hierarchical assembly strategy to program more complex crease patterns and finally achieved 10 types of the intended folding of larger-scale DNA papers polymerized in a quadruple area. With high yield, various programmability, and large scalability, we expect our origami-based structural reconfiguration methods for DNA assemblies to contribute to the advancement of folding-based engineering applications in nanoscale.

Keywords: DNA nanotechnology, DNA origami, Wireframe assemblies, Origami engineering, Structural reconfiguration, Finite element analysis

Student Number: 2020-28211

Table of contents

List of tables

List of notes

List of figures

Chapter 1. Introduction

Origami technology has been widely applied in various fields of macroscale engineering such as aerospace[1], robotics[2], architecture[3] with its advantages of effective shape change and corresponding functional implementation. In general, it has a polymorphic characteristic that a single planar structure of a flexible sheet could transform into numerous conformations by simply folding it along programmed crease patterns (folding lines), and moreover, structural abilities to reconfigure and deploy are naturally embodied through the fold and unfold sequences[4]. However, despite these advantages of simple mechanisms and desirable engineering properties, there have not been many studies that realize origami mechanisms at the nano-level engineering due to its general difficulties to implement the high-precision structural design and program various folds of the nanostructures.

Programmable self-assembly of DNA strands, DNA origami technology, could be one of the appropriate solutions to addressing that problem in that it enables the fabrication of nanometre-precise structures[5,6]. Through the development of prototyping software[7] and experimental methods to build DNA nanostructures with intended shapes[8, 9, 10, 11] and rigidities[12, 13], it has become more feasible to perform sophisticated structural designs of the desired form. Furthermore, the advances in quantitative computational analysis[14, 15] not only support the exquisite design of the DNA nanostructure through physical prediction of the equilibrium configuration, but recent studies on the hierarchical assembly[16, 17] have also enabled more complex structural design by polymerizing monomers with respective shapes patterns.

However, compared to the development of the precise structural design of DNA nanostructures, the reconfiguration system developed so far has limitations in implementing origami technology that enables numerous fold configurations at the nanoscale. First, a common way is to connect both sides of the DNA nanostructure with strands[18, 19, 20]. Since they usually had high internal rigidity to fold due to their densely designed sheet-type, they usually formed a tubular shape rather than completely folded. To avoid the curved form and obtain the entirely folded state,

various hinge systems have been introduced. In these systems, two tongs-like or planar DNA assemblies were connected to each other and pivoted at the joint consisting of single-stranded DNA (ssDNA), and their structural arms or leaves could be adjusted at an intended degree or state (between open and closed) by controlling mechanical properties[21, 22], binding interactions[23, 24], or stimulus-responsive actuation based on the cationic[25, 26] or acidic[27] concentrations. However, since the folding line was determined in advance by the hinge designs, various crease pattern designs were intrinsically limited in this system. Furthermore, while some studies on a Bennett linkage[28] or waterbomb-based[29] mechanism implemented its multifarious folded configurations of DNA assemblies through effective hinge designs and precise kinematic analysis, their transformations were still constricted by structurally engraved creases. Besides the hinge system, a reconfigurable shape transition for a wireframe DNA structure that was generally more bendable has also been studied[30]. However, it was rather close to forming a three-dimensional construction from the planar diagram, not a complete folding mechanism.

Here, we designed DNA wireframe assemblies (DNA wireframe paper) for the complete folding of nanostructures and demonstrated eight types of reconfigurable folding patterns using a modular crease patterning method based on single-stranded DNA (ssDNA) overhang and toehold-mediated strand displacement. The high folding success rate above 90% was obtained by increasing the binding probability between the overhangs and reducing the structural rigidity of the folding line. Orthogonal folding, repeatable folding and unfolding, and folding-based fluorescence signal control were successfully implemented as folding properties, and beyond the strand displacement, various environmental folding controls, such as pH-responsive structural reconfiguration and UV-based anti-folding system, were introduced and demonstrated. Finally, by polymerizing four original DNA papers, we synthesized a quadrupled DNA paper and realized 10 types of larger-scale and more complex folding patterns.

Chapter 2. Results

2.1. Design principle

In order to utilize a paper folding mechanism for reconfigurable DNA origami, we need to construct a reference, paper-like structure with crease patterns (or folding lines) about which it can be easily folded and unfolded. Toward this end, we designed a DNA origami wireframe whose edges were formed along the target crease patterns and the boundaries in paper folding (Figure 1a and Figures 2-3). Edges consisted of two-helix bundles as they were stiff enough to maintain overall structural integrity. Hereafter, we call this reference structure 'DNA wireframe paper'. To realize various folds in DNA wireframe papers (Figure 1b), we incorporated ssDNA overhangs denoted as crease handles into folding lines (Figure 1c) with two types: 3` (pink) and 5` (orange) crease handles. The overhang part of crease handles was composed of 8-nt-long ssDNA for bonding and 3-nt-long poly-T bases for spacer (black) where 'nt' denotes nucleotide. The folded state of DNA wireframe papers was activated by adding glue strands with complementary sequences to both crease handles. Each glue strand had a 5-nt-long toehold in its terminal, and hence, the folded structure could be unfolded via the toehold-mediated DNA displacement when releaser strands complementary to glue strands were added.

We first experimentally demonstrated the feasibility of the proposed folding mechanism by testing half-folding and unfolding of the square (SQ) DNA wireframe paper (Figure 1d). It was drafted using PERDIX[31] and only one pair of DNA edges placed on both sides of the target folding line was modified to have six 3` and 5` crease handles (Note 1 and Figure 4). The atomic force microscopy (AFM) images confirmed it could be successfully constructed into the unfolded, reference state. The heights of five peak points measured parallel to the folding line ranged from 0.6 to 0.8 nm. Randomly half-folded structures observed were 2% only. To fold the structure, we added glue strands ten times the concentration of crease handle pairs and incubated them at room temperature for an hour. Almost 60% of DNA wireframe papers were half-folded as intended. The measured heights

of five peak points were larger than 1.2 nm, suggesting the edges were laid over each other and hence the structure was well folded in half. Finally, releaser strands ten times more than glue strands were added and incubation at 37℃ was applied for an hour. They could successfully unfold the structure as the ratio of half-folded DNA wireframe papers was decreased to 2% again and the heights of five peak points were returned to their initial values. These results clearly show the possibility to build reconfigurable DNA origami with reversibility through programmable crease patterns in paper folding.

We further explored other types of folding of the SQ DNA wireframe paper (Figure 5a and Figure 6). Each crease was labeled with H (half) and Q (quarter) by the folding type. The AFM measurements confirmed that all eight types of folded configurations could be successfully realized as intended (Figure 5b, Figures 7-9, and Table 1). The equilibrium folded configurations in solution estimated using FE analysis, SNUPI[32], were similar to those observed on mica in AFM (Figure 5c, Figures 10-11, and Table 2). Agarose gel electrophoresis also showed higher mobility of a more folded structure (Figure 5d and Figure 12). These results suggested that the designed DNA wireframe papers were properly folded and maintained in solution rather than accidentally folded when deposited on mica and measured by AFM.

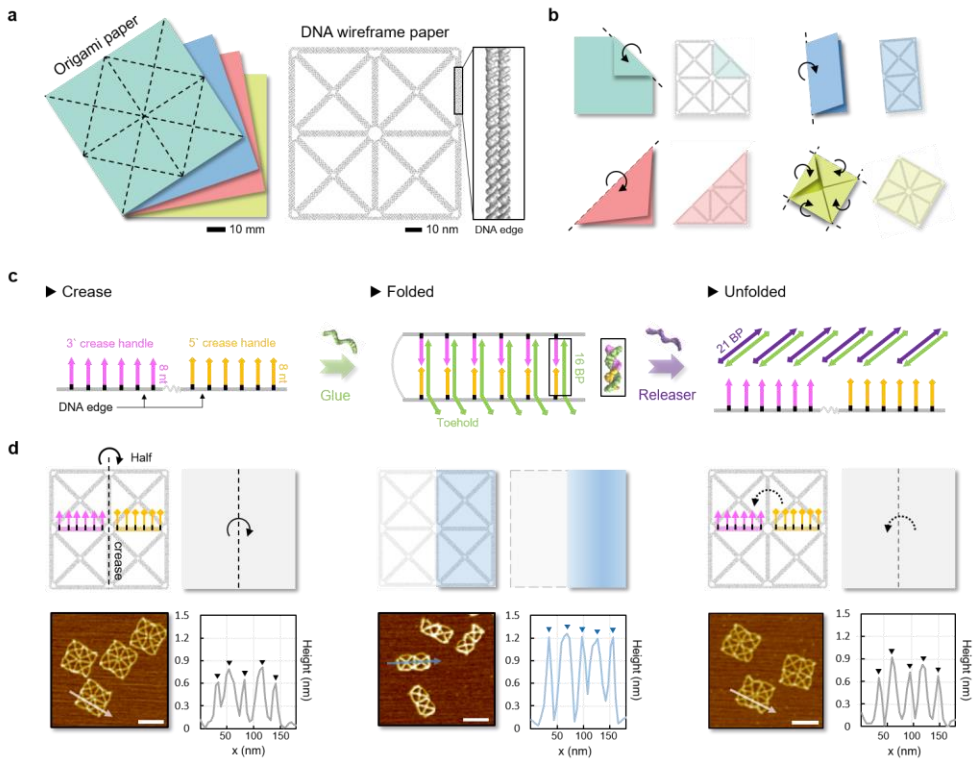

Figure 1. Scheme of nanoscale folding and unfolding of DNA wireframe paper. **(a)** Schematic representation of origami paper in macroscale (left) and DNA wireframe paper composed of DNA edges in nanoscale (right). **(b)** Conceptual illustration of transferring various folding lines from macroscale into nanoscale. **(c)** Basic principles of folding and unfolding of DNA wireframe paper. Crease: two types of crease handles, 3` and 5`, were designed to be overhung from the DNA edge and perpendicular to the plane of DNA paper. Folded: DNA wireframe paper was folded by adding glue strands (green) complementary to both crease handles. Unfolded: adding releaser strands (purple) fully complementary to the glue strand activates unfolding reaction through toehold-mediated strand displacement. **(d)** Experimental validation of folding mechanism with an example of half-folding of the DNA wireframe paper. The heights of five peak points of a DNA wireframe paper parallel to the folding line were measured by AFM and marked with reverse triangles in the height plot. Scale bars, 100 nm.

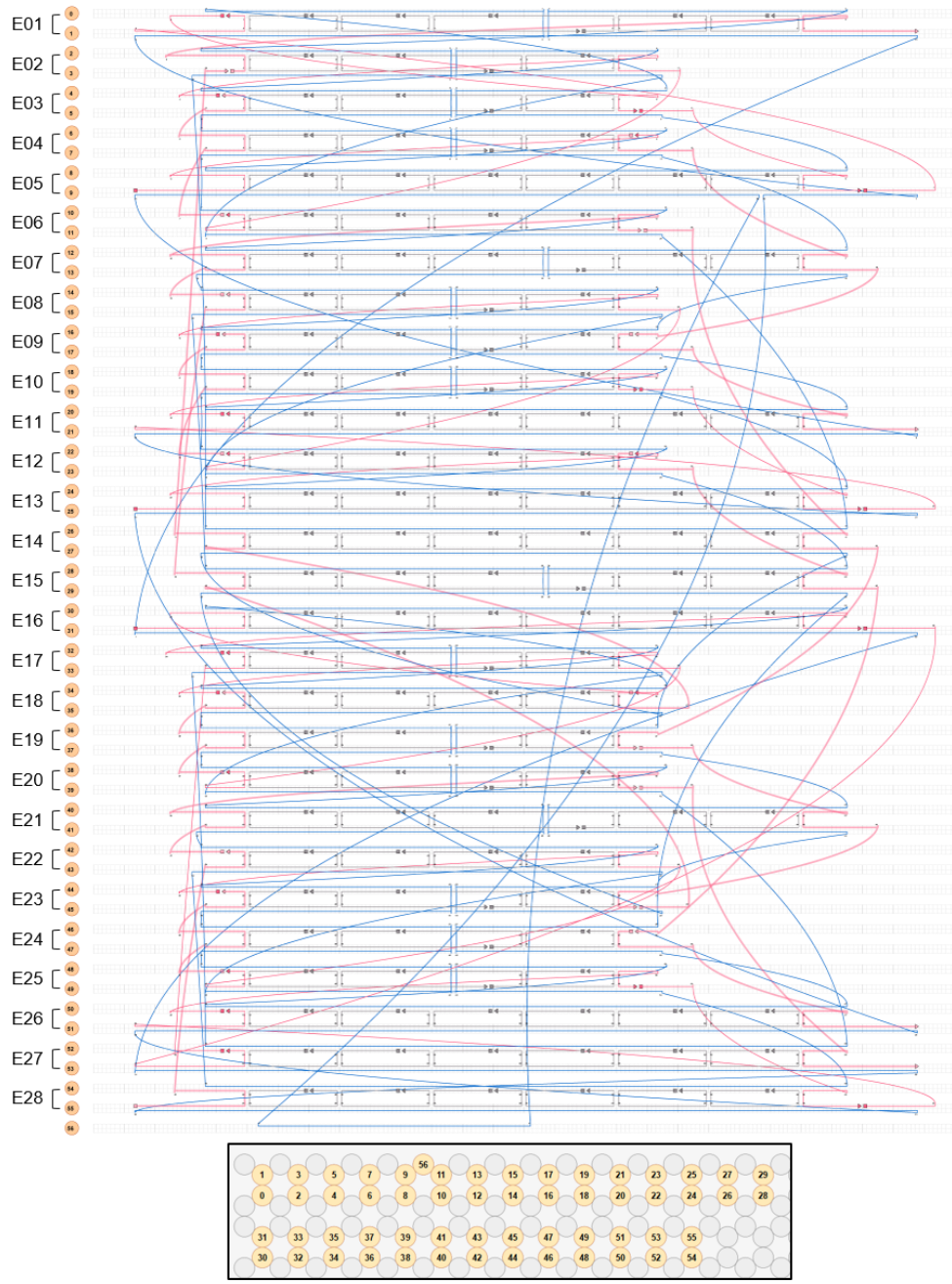

Figure 2. caDNAno blueprint of square DNA paper (SQ).

Gray and red-colored strands represent the edge and vertex staples, respectively. The DNA wireframe assemblies were designed based on the dual DNA duplex edge with a 7249-nt length of M13mp18 scaffold (blue) using PERDIX[31]. Sequences of the unpaired region of vertex staples are all designed with thymine (T). A scaffold loop was added in helix 56 to adjust the total length of the scaffold.

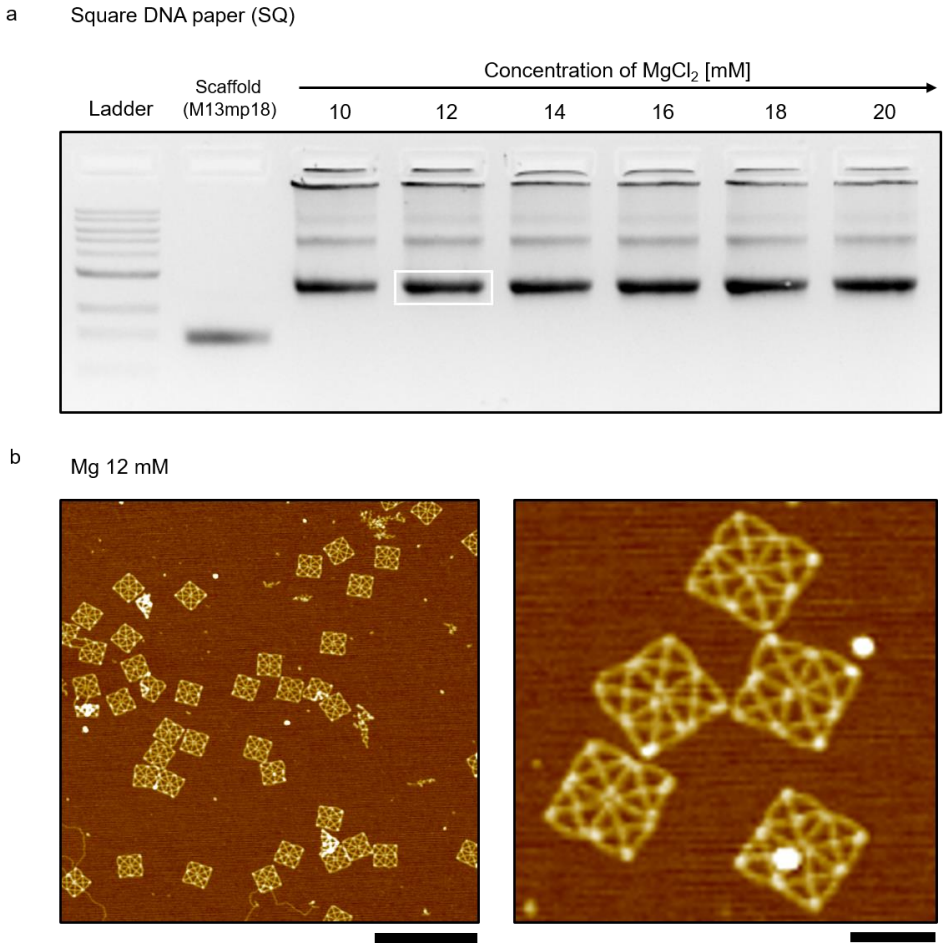

Figure 3. Synthesis of square DNA paper.

(a) Gel electrophoresis with Ethidium-Bromide stained 1.5wt% agarose gels for 90 min at 75 V by varying the cation concentration. Cation concentration of 12 mM $MgCl_2$ (white box) was used to synthesize square DNA papers (SQ). (b) Representative AFM images of SQ annealed with 12 mM $MgCl_2$. Scale bars, 500 nm and 100 nm.

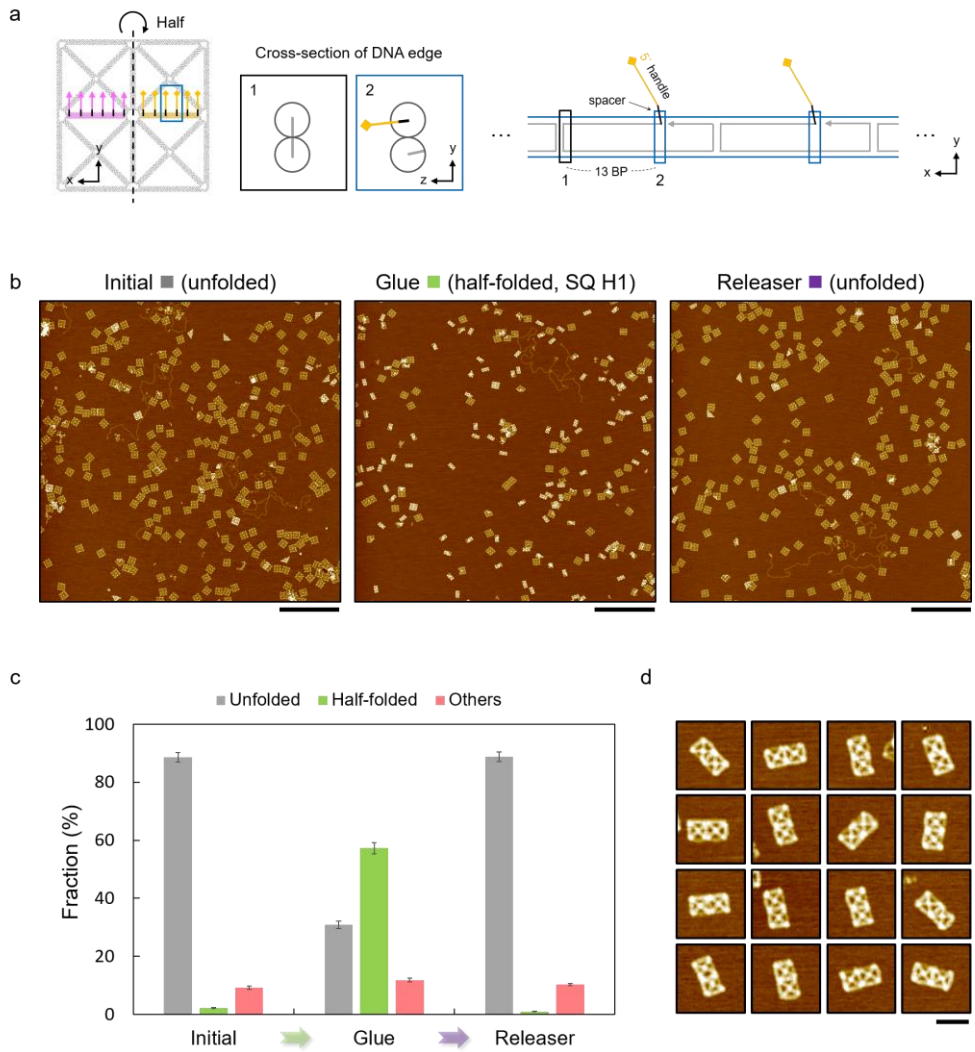

Figure 4. Crease handle design and experimental validation for half-folding and unfolding of SQ.

(a) Schematic illustration of crease handle designs for half-folding. The overhang direction of each crease handle was designed to be perpendicular to the crossover direction of DNA edge. (b) Representative AFM images of three states of the DNA wireframe papers. Scale bars, 1 μm. (c) The fraction of shapes at three states was described. (d) Exemplary AFM images of half-folding of SQ. Scale bar, 100 nm.

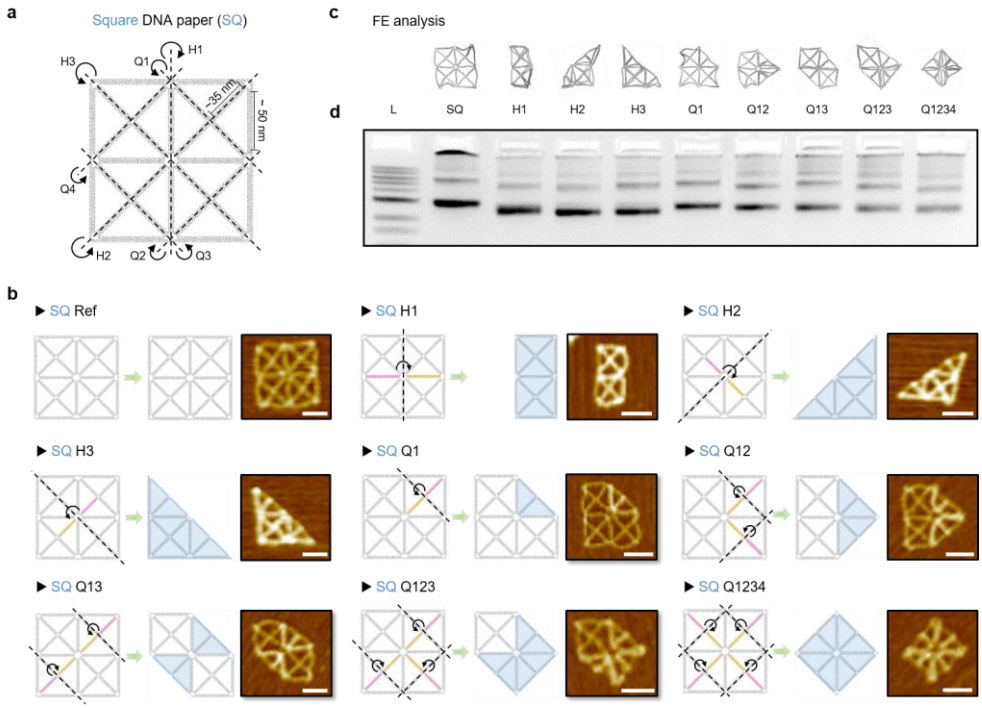

Figure 5. Implementation of various folding of DNA wireframe paper.

(a) Various folding patterns of square DNA wireframe papers (SQ). H: half-folding, Q: quarter-folding, and suffixal number: folding number. **(b)** Schematic illustration and representative AFM images of folded SQ after adding glue strands (green arrow). The pink and orange edges represented the DNA edges modified with 3` and 5` crease handles, respectively. Scale bars, 50 nm. **(c)** Equilibrated configurations of folded SQ estimated by finite element analysis in SNUPI[32]. **(d)** Gel electrophoresis with Ethidium-Bromide (EtBr) stained 1.5wt% agarose. Higher mobility of the band was observed for a more folded structure. L: ladder.

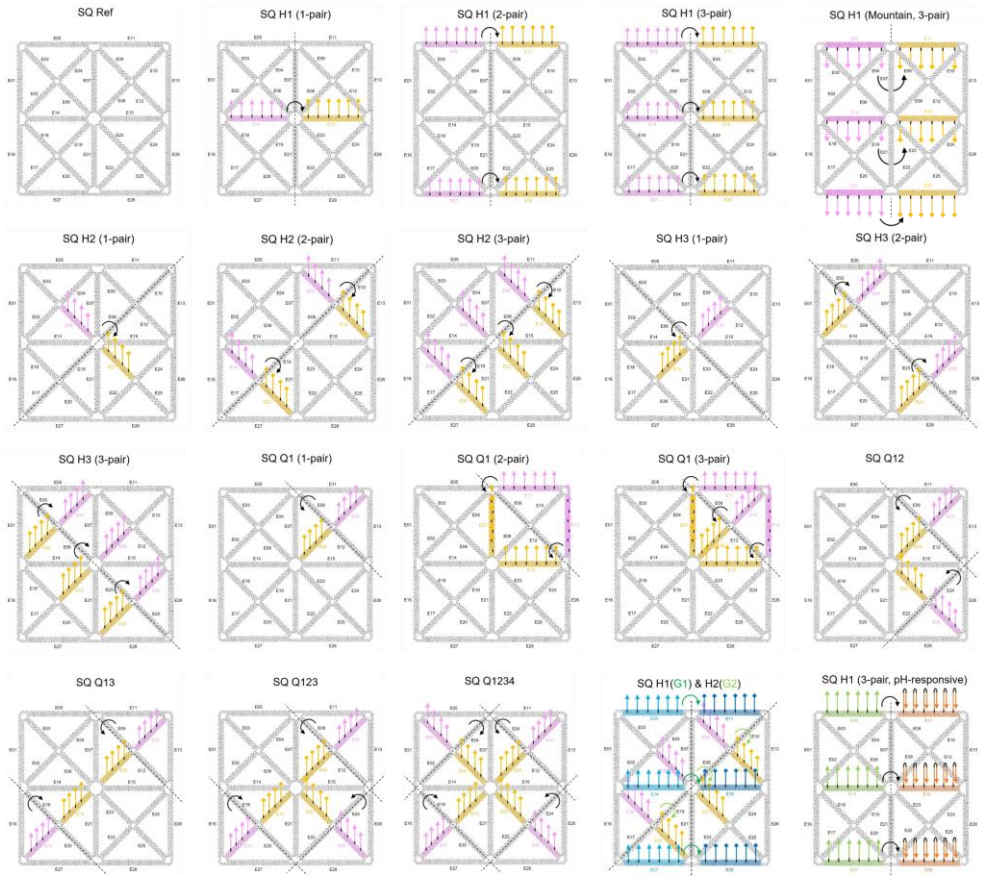

Figure 6. Detailed crease pattern of SQ folding.

Sky blue and blue edges indicate the modified DNA edges having 3` and 5` crease handles that bind with glue1 strands (G1), respectively. Pink and yellow edges indicate the modified DNA edges having 3` and 5` crease handles that bind with glue2 strands (G2), respectively. The downward direction of crease handles represents the crease handles for mountain fold (M) (see 5th crease pattern).

Figure 7. Exemplary AFM images of SQ folding (I).

Scale bars, 100 nm.

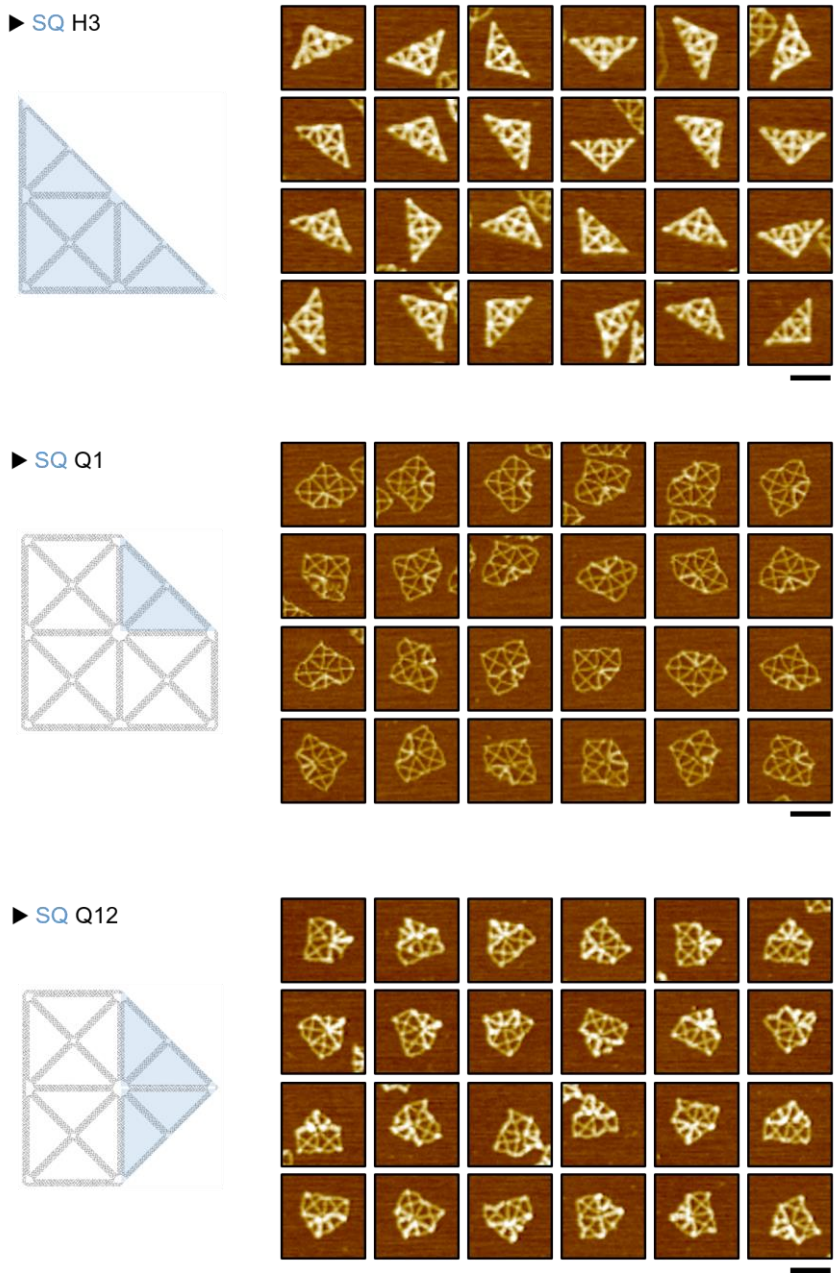

Figure 8. Exemplary AFM images of SQ folding (II).

Scale bars, 100 nm.

Figure 9. Exemplary AFM images of SQ folding (II).

Scale bars, 100 nm.

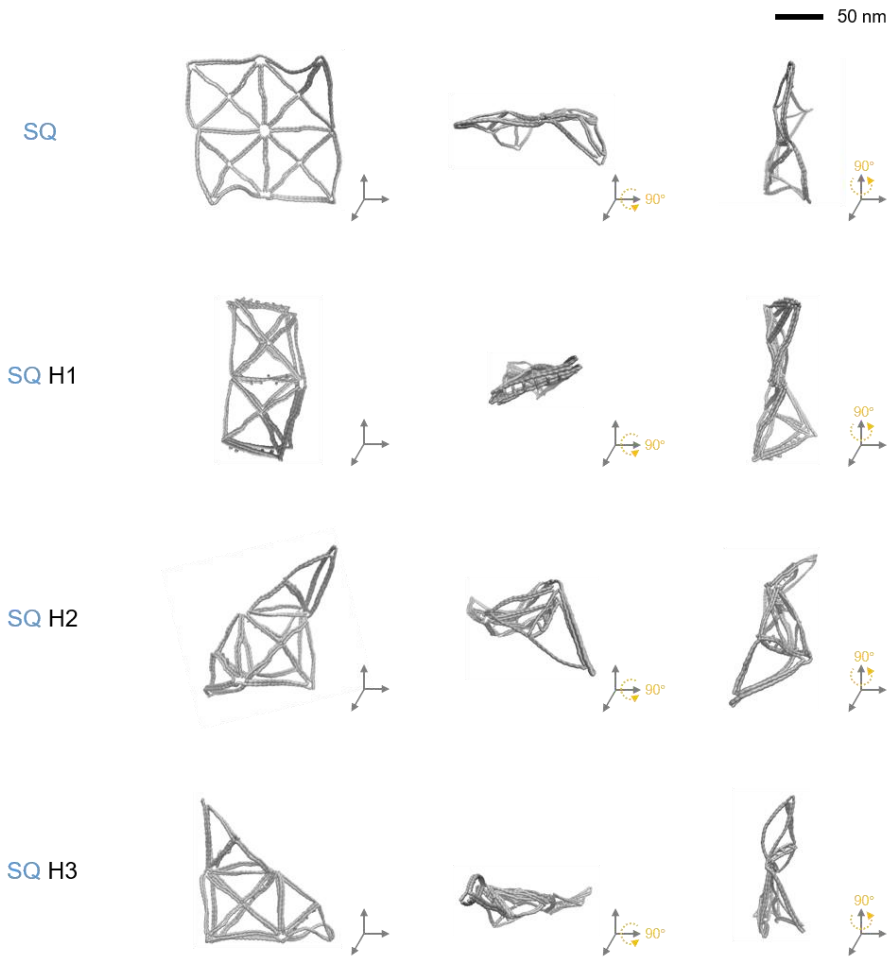

Figure 10. FE analysis results of equilibrated configurations of SQ folding (I).

Complete binding between glue strands and designed crease handles was assumed.

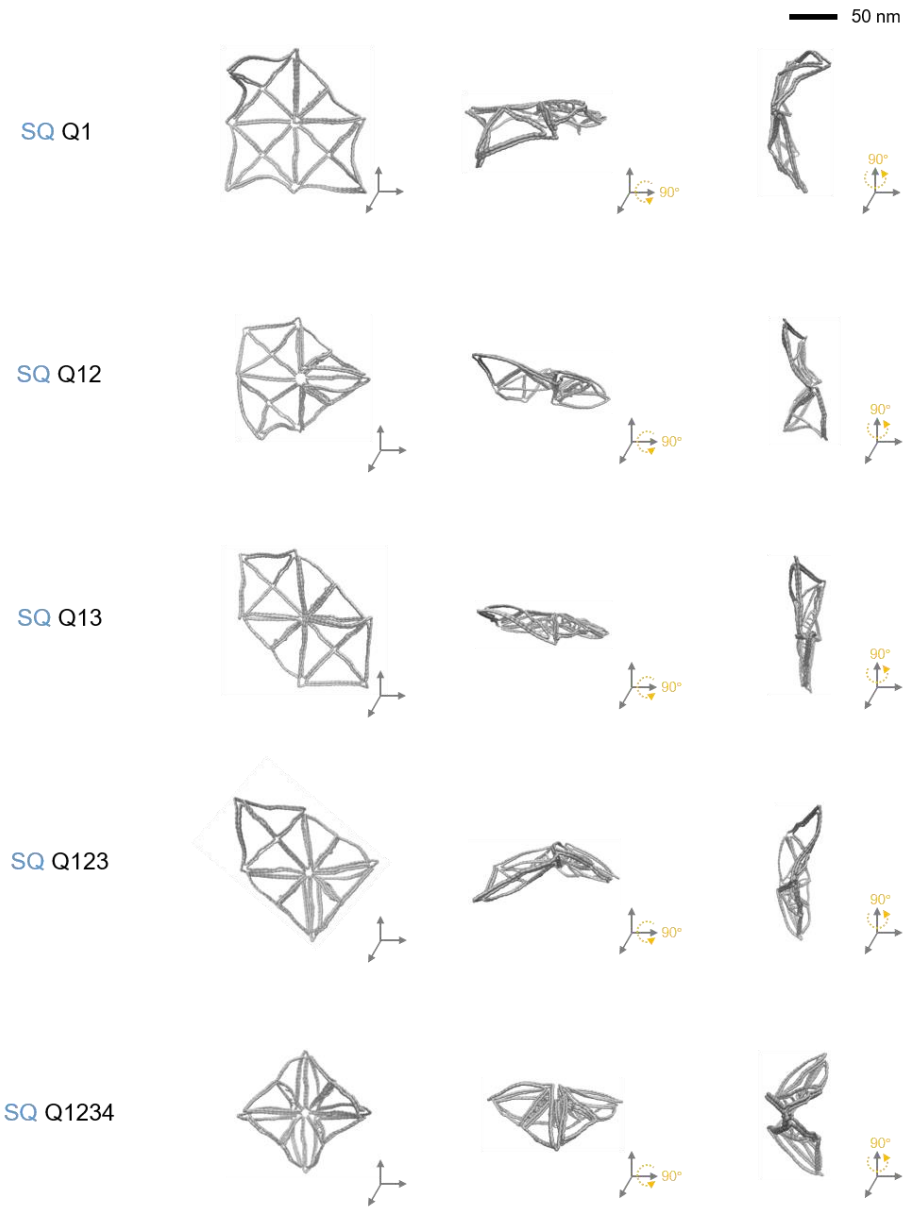

Figure 11. FE analysis results of equilibrated configurations of SQ folding (II).

Complete binding between glue strands and designed crease handles was assumed.

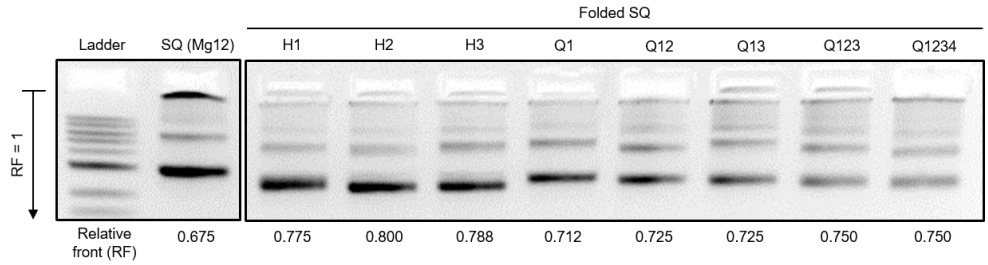

Figure 12. Gel electrophoresis of folded SQ.

Gel electrophoresis with Ethidium-Bromide stained 1.5wt% agarose gels for 90 min at 75 V to compare the migration of folded square DNA wireframe papers (SQ). Each value of relative front (RF) was measured from the relative distance between the entrance and the band position of the gel using Image Lab v5.1 program (Bio-Rad). Agarose gel electrophoresis showed higher mobility of a more folded structure.

Table 1. Folding yield of DNA wireframe paper.

• Single folding

Name	Number of pair	Number of gap (state)	Number of DNA structures			Yield (%)	Standard error (%)
			Folded	Others	Total		
SQ ref	0	nick	256	24	280	91.4	1.60
SQ H1	1	nick	343	165	508	67.5	1.71
		1-gap	404	120	524	77.1	1.61
		3-gap	457	137	594	76.9	1.52
		5-gap	485	112	597	81.2	1.44
	2	nick	227	35	262	86.6	1.96
		1-gap	337	47	384	87.8	1.57
		3-gap	378	58	436	86.7	1.51
		5-gap	417	51	468	89.1	1.36
	3	nick	91	14	105	86.7	3.09
		1-gap	140	19	159	88.1	2.41
		3-gap	267	34	301	88.7	1.72
		5-gap	176	13	189	93.1	1.78
SQ H2	1	-	119	192	311	38.3	1.70
	2	-	393	75	468	84.0	1.55
	3	-	445	29	474	93.9	1.07
SQ H3	1	-	69	190	259	26.6	1.42
	2	-	272	87	359	75.8	1.97
	3	-	407	88	495	82.2	1.56
SQ Q1	1	nick	126	47	173	72.8	2.89
	2	nick	270	71	341	79.2	1.96
	3	nick	291	40	331	87.9	1.68
		1-gap	512	67	579	88.4	1.25
		5-gap	468	97	565	82.8	1.44

Table 1 (continued).

• Multiple quarter-folding (1-pair and nick)

Name	Number of DNA structures								Yield (%)	Standard error (%)
	SQ	Q1	Q12	Q13	Q123	Q1234	Others	Total		
SQ Q1	30	**126**	4	4	0	0	9	173	72.8	2.89
SQ Q12	32	122	**150**	4	1	0	42	351	42.7	1.73
SQ Q13	24	115	3	**102**	6	0	36	286	35.7	1.69
SQ Q123	9	38	57	27	**74**	0	16	221	33.5	1.84
SQ Q1234	5	15	21	22	59	**25**	33	180	13.9	0.96

• Orthogonal folding (H1: 3-pair and nick, H2: 3-pair)

Name	State	Number of DNA structures						Yield (%)	Standard error (%)
		SQ	H1	H2	Q1	Others	Total		
Orthogonal SQ (H1, H2)	no Glue	**242**	7	7	28	9	293	82.6	2.01
	Glue1	1	**453**	4	2	11	471	96.2	0.87
	Glue2	5	1	**369**	3	17	395	93.4	1.21

• Repeatable folding (H1: 3-pair and nick & Gel extraction)

Name	State	Number of DNA structures				Yield (%)	Standard error (%)
		SQ	H1	Others	Total		
SQ H1	Unfolded	**128**	7	23	158	81.0	2.81
	Folded	0	**761**	19	780	97.6	0.55

Table 1 (continued).

• Folding-dependent signal control (H1: 3-pair and nick, H2: 3-pair)

Name	State	Number of DNA structures				Yield (%)	Standard error (%)
		Folded	Unfolded	Others	Total		
SQ H1	Initial	17 (H1)	**265**	60	342	77.5	1.99
	Glue	**276 (H1)**	0	5	281	98.2	0.78
	Releaser	11 (H1)	**178**	23	212	84.0	2.31
SQ H2	Initial	23 (H2)	**397**	75	495	80.2	1.60
	Glue	**549 (H2)**	4	31	584	94.0	0.95
	Releaser	36 (H2)	**349**	70	455	76.7	1.74

* 2-pair of reporters and quenchers was used.

• Mountain and valley fold (H1: 3-pair and nick)

Name	State	Number of DNA structures				Yield (%)	Standard error (%)
		H1	Unfolded	Others	Total		
SQ H1	Mountain	213	3	1	217	98.2	0.80
	Valley	276	0	5	281	98.2	0.78

* 2-pair of reporters and quenchers was used.

• pH-responsive folding and unfolding (3-pair)

Name	State	Number of DNA structures				Yield (%)	Standard error (%)
		Folded	Unfolded	Others	Total		
SQ H1	pH 5.95	398	7	37	440	90.1	1.35
	pH 6.67	318	24	37	379	83.9	1.73
	pH 7.29	208	74	37	319	65.2	2.15
	pH 7.68	79	194	29	302	26.2	1.29
	pH 8.11	6	200	24	230	2.61	0.17
	pH 8.41	6	238	46	290	2.07	0.00

* 2-pair of reporters and quenchers was used.

Table 1 (continued).

• UV-responsive unfolding (3-pair & PC-glue)

Name	UV illumination	Number of DNA structures				Yield (%)	Standard error (%)
		Folded	Unfolded	Others	Total		
SQ H1	0 min	165	18	11	194	85.1	2.36
	1 min	169	20	6	195	86.7	2.27
	5 min	87	62	21	170	51.2	2.74
	10 min	18	101	32	151	11.9	0.91
	15 min	6	115	18	139	4.32	0.36
	30 min	9	258	18	285	3.16	0.18
SQ H2	0 min	109	26	14	149	73.2	3.11
	15 min	16	146	10	172	9.30	0.68
SQ Q1	0 min	180	14	12	206	87.4	2.16
	15 min	9	144	3	156	5.77	0.45

Table 2. Main parameter of finite element analysis.

Option	Abbreviation	Value	Unit
1. Base-pair (BP) and crossover (CO) steps			
- Coefficient function	BP_CF_IND	Order 1	-
2. Single-stranded DNA (ssDNA)			
- Contour length per nucleotide	SS_LC1	0.67	[nm/nt]
- Persistence length	SS_LB	0.74	[nm]
- Stretching rigidity when stretched	SS_EA_H	710	[pN]
- Stretching rigidity when relaxed	SS_EA_L	5	[pN]
- Coefficient function	SS_CF_IND	Order 1	-
3. Electrostatic interaction (ES)			
- Temperature	ES_TEMP	300	[K]
- Mg concentration	ES_MG	20	[mM]
- Cutoff distance	ES_R_CUT	20	[nm]
- Coefficient function	ES_CF_IND	Quadratic	-

Prior to the FE analysis, the partition and relocation methods for DNA wireframe assemblies were applied. For other parameters, in general, the default value described in SNUPI[32] was used.

Table 3. Staple sequence for constructing DNA wireframe paper.

• Square DNA paper (scaffold = M13mp18, edge ■, vertex ■)(H: helix)

Name	Sequence (5`→3`)
E01-1_H00 ■	ACTATGGTTGCTTTCGTGGCGAGAAAGGAAGGGAAGGCGCGT
E01-2_H00 ■	ATGCGCCGCTACAGGAAAGCGAAAGGAGCGGGCGCGCGCTTA
E01-3_H00 ■	CCACCACACCCGCCTAGGGCGCTGGCAAGTGTAGCGGTCAGGGTGAGA
E01-4_H01 ■	AAGGCCGGAGGTAAAGATTCAAAACGCTGCGCGTAA
E01-5_H00 ■	CCTGAGTAATGTGTAGACAGTCAAATCACCATCAATGCAATG
E01-6_H00 ■	TCATATATTTTAAATATGATATTCAACCGTTCTAGAGAACCC
E02-1_H02 ■	AGAAGCCTTTATTTAAATTAAGCAATAAAGCCTCATTGCGGG
E02-2_H02 ■	ACCCTGTAATACTTGAGCATAAAGCTAAATCGGTTGTACCTTGCTCCT
E02-3_H03 ■	TTTGATAATAGAGAGTACCTTTAAAAAAACATTATG
E02-4_H02 ■	CAACAGGTCAGGATGAGGTCATTTTTGCGGATGGCCAAACTC
E03-1_H04 ■	TTTAATTCGAGCTTCCCTGACTATTATAGTCAGAAATCGCGT
E03-2_H04 ■	GAAAGACTTCAAATGCAAAGCGGATTGCATCAAAAAGATTCGATTAAA
E03-3_H05 ■	GGGATTTTGAGCTAAACAGGAGGCAAGAGGAAGCCC
E03-4_H04 ■	TAGAATCAGAGCGGAGACAGGAACGGTACGCCAGATCCTCGT
E04-1_H06 ■	AACGAGAATGACCATAGACTGGATAGCGTCCAATATTCAGAA
E04-2_H06 ■	AATGCTTTAAACAGCTGCGGAATCGTCATAAATATTCATTTACATTTT
E04-3_H07 ■	GACGCTCACGCTCATGGAAATACCGAATCCCCCTCA
E04-4_H06 ■	TGCAACAGGAAAAAATCGTCTGAAATGGATTATTTCAGCCAT
E05-1_H08 ■	CGGCCTTGCTGGTACCTTATAAATCAAAAGAATAGAAACTAT
E05-2_H08 ■	GAGTAGAAGAACTCCCCGAGATAGGGTTGAGTGTTCTTGCCT
E05-3_H08 ■	TAGTAATAACATCAGTTCCAGTTTGGAACAAGAGTCTTTGAT
E05-4_H08 ■	TTGTAGCAATACTTCCACTATTAAAGAACGTGGACTTAACCG
E05-5_H08 ■	GTCCATCACGCAAATCCAACGTCAAAGGGCGAAAAAGAGTCT
E05-6_H08 ■	GGCCACCGAGTAAAACCGTCTATCAAGCACTAAATTCAGTGA
E06-1_H10 ■	AAGAAGTTTTGCCATAATGCTGTAGCTCAACATGTTTTGCAA
E06-2_H10 ■	AATAGCGAGAGGCTTTTAAATATGCAACTAAAGTAAAACCAA
E06-3_H10 ■	CCAGACGACGATAACGGTGTCTGGAAGTTTCATTCTCGTTTA
E06-4_H10 ■	CACTATCATAACCCCATATAACAGTTGATTCCCAAAGAGCAA
E07-1_H12 ■	GATACATAACGCCATATACCAGTCAGGACGTTGGGTAATGCA
E07-2_H12 ■	ATACCACATTCAACAAGAAAAATCTACGTTAATAATTTAGGA
E07-3_H12 ■	TTCATCAGTTGAGAAACGAACTAACGGAACAACATTATTAAAGCGTAA
E07-4_H13 ■	GAATACGTAACCCTTCTGACCTGACAGGTAGAAAGA

E07-5_H12 ■	GCCAACAGAGATAGGGCACAGACAATATTTTTGAACATTCTG
E07-6_H12 ■	AGTAATAAAAGGGATGGCTATTAGTCTTTAATGCGCACGACC
E08-1_H14 ■	TGTGAATTACCTTAGAATAAGGCTTGCCCTGACGATAATCAT
E08-2_H14 ■	TTTAATTTCAACTTGAAACACCAGAACGAGTAGTAAATTGAAAACATA
E08-3_H15 ■	GCGATAGCTCCCTTAGAATCCTTGGGCTTGAGATGG
E08-4_H14 ■	CTATTAATTAATTTTTAGATTAAGACGCTGAGAAGATCGTCG
E09-1_H16 ■	TCAATATATGTGAGAACAAACATCAAGAAAACAAAACATAAA
E09-2_H16 ■	TTAATGGAAACAGTATTAATTACATTTAACAATTTCATTTATAAAACA
E09-3_H17 ■	GAGGTGAGGAACCACCAGCAGAAGGAATTACCTTTT
E09-4_H16 ■	TAAAAATACCGAACGCGGTCAGTATTAACACCGCCTCGCCAT
E10-1_H18 ■	ATTCATTTCAATTACCTTTTACATCGGGAGAAACAGCGAATT
E10-2_H18 ■	AAAATCGCGCAGAGATAACGGATTCGCCTGATTGCTTTGAAGAAGTAT
E10-3_H19 ■	TAGACTTTATACATTTGAGGATTTATACCAAGTTAC
E10-4_H18 ■	GCCGTCAATAGATAACAAACAATTCGACAACTCGTGATTAGA
E11-1_H20 ■	TATCTAAAATATCTCGGGGAGAGGCGGTTTGCGTAGGAAGGT
E11-2_H20 ■	TTGAAAGGAATTGATTGGGCGCCAGGGTGGTTTTTTCAACAG
E11-3_H20 ■	GGTCAGTTGGCAAACTTTTCACCAGTGAGACGGGCAATATCT
E11-4_H20 ■	TCAAACCCTCAATCAACAGCTGATTGCCCTTCACCTCAAATA
E11-5_H20 ■	CACCTTGCTGAACCGCCTGGCCCTGAGAGAGTTGCAAAGCAT
E11-6_H20 ■	CAAATGAAAAATCTAGCAAGCGGTCCACGCTGGTTCCAGCAG
E12-1_H22 ■	TCAGGTTTAACGTCAATCATAGGTCTGAGAGACTATAGATTT
E12-2_H22 ■	ATAAAGAAATTGCGCCTTTTTAACCTCCGGCTTAGAACAGAA
E12-3_H22 ■	TTATTTGCACGTAAGTTGGGTTATATAACTATATGATCAAAA
E12-4_H22 ■	TTAGAACCTACCATTAAATGCTGATGCAAATCCAAGGAAGGG
E13-1_H24 ■	ATAATCCTGATTGTTCCTGTGTGAAATTGTTATCCCATCAAT
E13-2_H24 ■	AGATGATGGCAATTGCTCACAATTCCACACAACATGATTATC
E13-3_H24 ■	ATCATCATATTCCTACGAGCCGGAAGCATAAAGTGCGGAATT
E13-4_H24 ■	ACCACCAGAAGGAGTAAAGCCTGGGGTGCCTAATGCAAAGAA
E13-5_H24 ■	ATCATTTTGCGGAAAGTGAGCTAACTCACATTAATTAACATT
E13-6_H24 ■	TTTAAAAGTTTGAGTGCGTTGCGCTCACTGCCCGCTATTAAT
E14-1_H26 ■	ATCCAATAAATCATAGGCTCCAAAAGGAGCCTTTACATTAAC
E14-2_H26 ■	ACTAATAGTAGTAGATTGTATCGGTTTATCAGCTTCAATTCT
E14-3_H26 ■	TGAAAAGGTGGCATGCTTTCGAGGTGAATTTCTTACGCGAGC
E14-4_H26 ■	ATTTTCATTTGGGGAACAGCTTGATACCGATAGTTTAGCTAT
E14-5_H26 ■	GTCAATAACCTGTTGCGCCGACAATGACAACAACCGCAAATG
E14-6_H26 ■	ATTAGATACATTTCATCGCCCACGCATAACCGATATTTGACC

E15-1_H28 ■	ATTACCCAAATCAACGGTCAATCATAAGGGAACCGGATATTC
E15-2_H28 ■	CTTGACAAGAACCGAACTGACCAACTTTGAAAGAGGAGTAAT
E15-3_H28 ■	CTGACCTTCATCAAGACAGATGAACGGTGTACAGACCAGGAAATACCG
E15-4_H29 ■	ACCGTGTGTAAATTTAATGGTTTGCGCATAGGCTGG
E15-5_H28 ■	TTCATCTTCTGACCATAAATAAGGCGTTAAATAAGAGTTAAT
E15-6_H28 ■	TTCAAATATATTTTAATAAACACCGGAATCATAATAAACTTT
E16-1_H30 ■	TGGTAATAAGTTTTATCAGGTCATTGCCTGAGAGTAGTGTAC
E16-2_H30 ■	TTTGATGATACAGGCTGGAGCAAACAAGAGAATCGCATGGCT
E16-3_H30 ■	CAGTAAGCGTCATAATGAACGGTAATCGTAAAACTACCGTTC
E16-4_H30 ■	CAGTCTCTGAATTTAGCATGTCAATCATATGTACCGAAAGCG
E16-5_H30 ■	TTAAAGCCAGAATGCCGGTTGATAATCAGAAAAGCATCCTCA
E16-6_H30 ■	TCACAAACAAATAACCCAAAAACAGGAAGATTGTATTGATAT
E17-1_H32 ■	ATTGACAGGAGGTTCCGCCACCCTCAGAACCGCCACGCCAGC
E17-2_H32 ■	ACCACCAGAGCCGCCCCTCAGAGCCACCACCCTCAGAGCCCGTCGAGA
E17-3_H33 ■	GGGTTGATCCAGGCGGATAAGTGCGCCACCAGAACC
E17-4_H32 ■	GGTTTTGCTCAGTAATAAGTATAGCCCGGAATAGGTTAGCGG
E18-1_H34 ■	TAAGAGGCTGAGACGATTTTGCTAAACAACTTTCAAAAGTAT
E18-2_H34 ■	TATTCTGAAACATGACAGTTTCAGCGGAGTGAGAAAACCTAT
E18-3_H34 ■	CCTGCCTATTTCGGTAGAAAGGAACAACTAAAGGAAATGCCC
E18-4_H34 ■	CCGTATAAACAGTTATTGCGAATAATAATTTTTTCACAGTGC
E19-1_H36 ■	TCTTTCCAGACGTTCGTCACCAGTACAAACTACAATTTGTCG
E19-2_H36 ■	TAACGATCTAAAGTCGCCTGTAGCATTCCACAGACAGCCCCAGCAGCG
E19-3_H37 ■	AAAGACAGGCGGGATCGTCACCCTTCATAGTTAGCG
E19-4_H36 ■	TAAAGGCCGCTTTTCATCGGAACGAGGGTAGCAACAGGGAGT
E20-1_H38 ■	GCCCAATAGGAACCTTTAGTACCGCCACCCTCAGAATAGCAA
E20-2_H38 ■	CCTCATTTTCAGGGACCGCCACCCTCAGAACCGCCACCCTACCATTAG
E20-3_H39 ■	CAAGGCCGCACCAGTAGCACCATTCAGAGCCACCAC
E20-4_H38 ■	AGAGCCAGCAAAATGAAACGTCACCAATGAAACCAGGGAATT
E21-1_H40 ■	AAGGTGAATTATCAGAATAAGTTTATTTTGTCACATTCATTA
E21-2_H40 ■	ATTGACGGAAATTAATCAATAGAAAATTCATATGGGGTAAAT
E21-3_H40 ■	ATTGAGGGAGGGAATTTACCAGCGCCAAAGACAAAAGGGCAAGGCACC
E21-4_H41 ■	AACCTAAAACGTAATGCCACTACGGACATTCAACCG
E21-5_H40 ■	TAAACGGGTAAAATACGAAAGAGGCAAAAGAATACTTTCCAT
E21-6_H40 ■	TTTTCATGAGGAAGACTAAAACACTCATCTTTGACAAAGACT
E22-1_H42 ■	AGGTGGCAACATATGGTTTTGAAGCCTTAAATCAATACATAA
E22-2_H42 ■	ACGTAGAAAATACAGATTAGTTGCTATTTTGCACCTTAGCAA

E22-3_H42 ■	TATTACGCAGTATGCAGCTACAATTTTATCCTGAAGACTCCT
E22-4_H42 ■	ACTGGCATGATTAATCTTACCAACGCTAACGAGCGCAAAAGA
E23-1_H44 ■	AGGAAACCGAGGAAGAAACAATGAAATAGCAATAGTACCAGA
E23-2_H44 ■	TAGCCGAACAAAGTCTATCTTACCGAAGCCCTTTTTAAGAATAAATTG
E23-3_H45 ■	TGTCGAAATTTGTATCATCGCCTGAAAGTAAGCAGA
E23-4_H44 ■	AAGTACAACGGAGATCCGCGACCTGCTCCATGTTACGAAACA
E24-1_H46 ■	CCACAAGAATTGAGAAGCGCATTAGACGGGAGAATAGATAAC
E24-2_H46 ■	CGCTAATATCAGAGTAACTGAACACCCTGAACAAAGTCAGCCAACGCT
E24-3_H47 ■	CAACAGTATCTTACCAGTATAAAGAGGGTAATTGAG
E24-4_H46 ■	TGCGTTATACAAATGGGCTTAATTGAGAATCGCCATATCATA
E25-1_H48 ■	AGCAGCCTTTACAGCAGTTACAAAATAAACAGCCATGAAAAT
E25-2_H48 ■	TTTAACGTCAAAAATATTATTTATCCCAATCCAAATAAGAAGAAACCA
E25-3_H49 ■	ATCAATAATAATTTACGAGCATGTAACGATTTTTTG
E25-4_H48 ■	ATAATATCCCATCCTCGGCTGTCTTTCCTTATCATAAGAAAA
E26-1_H50 ■	ACGCGCCTGTTTATTATTACGCCAGCTGGCGAAAGATGCAGA
E26-2_H50 ■	AACATGTTCAGCTAGGGGATGTGCTGCAAGGCGATAATAAAC
E26-3_H50 ■	GTCCAGACGACGACTAAGTTGGGTAACGCCAGGGTTAATTCT
E26-4_H50 ■	GACAAAAGGTAAAGTTTCCCAGTCACGACGTTGTAAAGTACC
E26-5_H50 ■	AATAAGAGAATATAAAACGACGGCCAGTGCCAAGCAGCCAGT
E26-6_H50 ■	CAGAGGCATTTTCGTTGCATGCCTGCAGGTCGACTATTTAGG
E27-1_H52 ■	GGAACCAGAGCCACTTTTTGTTAAATCAGCTCATTAATCACC
E27-2_H52 ■	CTTTTCATAATCAATTTTAACCAATAGGAACGCCATTGCCAT
E27-3_H52 ■	CCCCTTATTAGCGTTCAAAAATAATTCGCGTCTGGTCATAGC
E27-4_H52 ■	ATCGGCATTTTCGGCCTTCCTGTAGCCAGCTTTCACGTTTTC
E27-5_H52 ■	GTCAGACTGTAGCGTCAACATTAAATGTGAGCGAGCTTTAGC
E27-6_H52 ■	AGAATCAAGTTTGCTAACAACCCGTCGGATTCTCCTAGCGAC
E28-1_H54 ■	ACGCGAGGCGTTTTGGGCGCATCGTAACCGTGCATTCTAAGA
E28-2_H54 ■	GGCTTATCCGGTATCTGCCAGTTTGAGGGGACGACTATAGAA
E28-3_H54 ■	GCAAGCAAATCAGAGACAGTATCGGCCTCAGGAAGCCCAATA
E28-4_H54 ■	GAATCATTACCGCGATCGCACTCCAGCCAGCTTTCATCGTAG
E28-5_H54 ■	CCGTTTTTATTTTCCGGCACCGCTTCTGGTGCCGGAAGCAAG
E28-6_H54 ■	CACTCATCGAGAACAAACCAGGCAAAGCGCCATTCAGTACCG
V01-1_H00 ■	GCACGTTTTTTTTTAACGTGCTTATCCT
V01-2_H05 ■	GAGAAGTTTTTTTTGTTTTTATAACGGAACCCTAAAGG
V01-3_H09 ■	GAGCCCCCGATTTTTTTAGAGCTTGACGGGGAAAGCCGGCGAAGACGA
V02-1_H09 ■	ATGGTGGTTCCGAAATCGGCAAAATCATATCCAGAATTTTTTTTATATTA

V02-2_H06 ■	CCGCACATTGGCAGATTTTTTTTTCACCAGTCACGAACTGATAGTTTTTTTCCCTAA
V02-3_H16 ■	AACATGCAACAGTGCTTTTTTTCACGCTGAGAGTGCCCCAGCAGGCGAAAATCCTGTTTG
V03-1_H20 ■	AGCACTTTTTTTTACAACTAATAATTAA
V03-2_H19 ■	ATCCTTTTTTTTTTGCCCGAACGTTTTCCAGTCGGGAA
V03-3_H25 ■	ACCTGTCGTGCCATTTTGCTGCATTAATGAATCGGCCAACGCGTTAGG
V04-1_H31 ■	CTATTTTTGAGAGATCTACAAAGGCTAACGGGGTCATTTTTTTTGCCTTG
V04-2_H03 ■	AGCACAACGCAAGGATTTTTTTTTAAAAATTTTTCTGATAAATTAATGCCGGAGAGGGTAG
V04-3_H34 ■	AGTAACGTTGAAAATTTTTTTTCCAAAAAAAACAGGCAAGGTTTTTTTAGAATT
V05-1_H14 ■	TTTTAATTTTTTTACTGGCTCATAAAGGAATTATTTTTTTTAGGCATAGTATTCTGC
V05-2_H37 ■	CAGAGGTTTTTTTCTTTGAGGACTCCCCAGCGATTTTTTTTTATACCAAGCGCTTAG
V05-3_H45 ■	CCGGAATTTTTTGAGGCGCAGACGTAACAAAGTTTTTTTCTCATTCAGTTGCGA
V05-4_H11 ■	GAACGTTTTTTTAGTAGATTTAGTATTCGGTCGCTTTTTTTTGAGGCTTGCGGCTA
V06-1_H25 ■	AATTCGTAATCATGGTCATAGCTGTTTTGGATTATATTTTTTTTTCTGAA
V06-2_H22 ■	TAATTCGCAAGACAATTTTTTTAGAACGCGAGATACTAGAAAAATTTTTTTGCCTGT
V06-3_H46 ■	TTAGTATTTAACAACTTTTTTTTGCCAACATGTACTAGAGGATCCCCGGGTACCGAGCTCG
V07-1_H32 ■	AGGTCATTTTTTTTGACGATTGGCCTAAGCAAATATTTA
V07-2_H52 ■	GAACCTTTTTTTTCCCTCAGAGGAGGC
V07-3_H31 ■	AATTGTAAACGTTTTTTAATATTTTGTTAAAATTCGCATTAAACACCG
V08-1_H55 ■	ATGGGATAGGTCACGTTGGTGTAGATAGCGAACCTCTTTTTTTACTTGCGGGAAAAAG
V08-2_H42 ■	AAACGCTTTTTTTAGACACCACGCCGTCACCGATTTTTTTTTGAGCCATTTTCGAT
V08-3_H39 ■	AGCAGCTTTTTTTACCGTAATCAGGTGGGAACAAACGGCGGATTGACCGTA
V09-1_H50 ■	ATAGATTTTTTTTAGTCCTGAACTCCAA
V09-2_H49 ■	GAACGGTTTTTTTGTATTAAACCAGCCATTCAGGCTGC
V09-3_H55 ■	GCAACTGTTGGGATTTTAGGGCGATCGGTGCGGGCCTCTTCGCCAACA
V10-1_H04 ■	GAACCTTTTTAGACCGGAAGTTAGAGCTTAATTTTTTGCTGAATAGAGGG
V10-2_H10 ■	GGTAATTTTTTGTAAAATGTTTAAATCAAAAATTTTTCAGGTCTTTACAAAGC
V11-1_H16 ■	ACCTTTTTTTGCTTCTGTAAAGTCAATAGTGTTTTAATTTATCAAAGATG
V11-2_H22 ■	AATATATTTTTAGTAACAGTACCTGAGCAAAATTTTTAAGATGATGATGAATA
V12-1_H34 ■	AGAGATTTTTAGGATTAGGATGTATCACCGTTTTTACTCAGGAGGCATGT
V12-2_H38 ■	ACCGTATTTTTCACTGAGTTTAGTAAATGAATTTTTTTTCTGTATGGTCCTCA
V13-1_H44 ■	TAATATTTTTACGGAATACCTCTTTCCAGAGTTTTCCTAATTTGCAGAGA
V13-2_H48 ■	ATAACATTTTTAAAAACAGGGTTAAGCCCAATTTTTTATAAGAGCAAACGCAA

Note 1. Design of DNA wireframe nanostructure.

Draft for the square DNA wireframe paper (SQ) was designed using PERDIX[31]. The SQ was composed of 9 vertices, 16 edges with 104 BP and 12 edges with 146 BP, and 16 faces. Edges were designed based on a dual DNA duplex with antiparallel double crossover. The name of edges (E) and vertices (V) were labeled as shown in the figure below. A scaffold loop was added to adjust the total length of the scaffold, and edge staples were modified to have the direction of nicks perpendicular to the plane. Detailed caDNAno design and sequences were described in Figure 2 and Table 3.

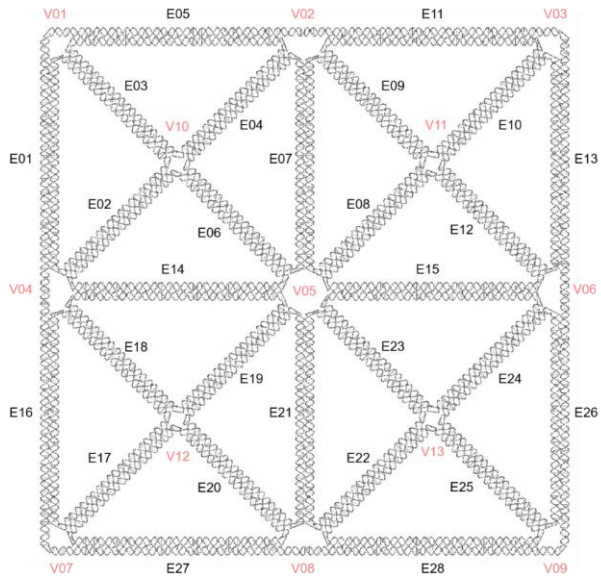

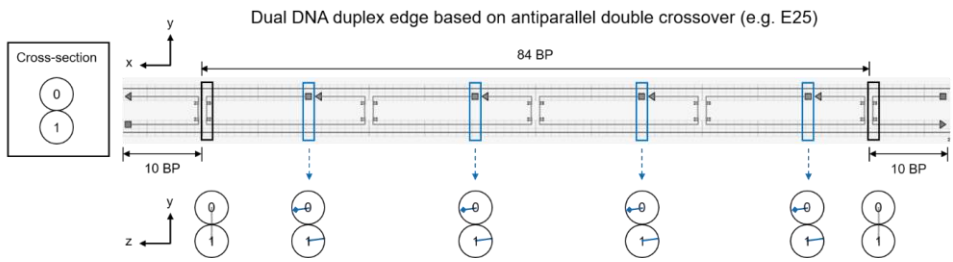

2.2. Yield optimization

The estimated yield based on AFM images (Figure 13) was below 70% for the folding patterns in the previous section (Table 1). This relatively low yield was because the number of crease handle pairs was insufficient and the edges were too stiff. To enhance the yield of folded structures, we explored the effect of the number of crease handle pairs and the stiffness of edges on the structural yield.

First, we varied the number of crease handle pairs controlling the binding probability between glue strands and crease handles (Figure 14a). In the case of H2 folding which showed the lowest yield with a single pair of crease handles, the yield increased drastically from 38.3% to 84.0% and eventually 93.9% when the number of crease handle pairs increased from one to two and three, respectively (Figure 14c, Figure 15, and Table 1). The yields of Q1 and H1 foldings were improved from 72.8% to 87.9% and from 67.5% to 86.7%, respectively, when three pairs were used (Figure 14c and Figures 15-20). Hence, the use of a sufficient number of crease handle pairs would be important to implement a paper folding mechanism with a high yield.

For further enhancement, we investigated the influence of the edge stiffness as well. In the SQ DNA wireframe paper designed by PERDIX, most vertices where wireframe edges meet have unpaired single-stranded parts. However, the vertices at the middle of outer boundaries have a nicked double helix making them stiffer than other vertices (Figure 14d, black box), which may deteriorate the success rate of folding about them. Hence, we systematically reduced their bending stiffness by replacing a nick with a gap of different lengths through the modular change of staple strands around the nick position[33]. First, its effect was examined with H1 folding where two stiff vertices were involved. In total, 9 structures were additionally constructed by considering four gap lengths (1-, 3-, and 5-nt-long gaps) for three cases in the number of crease handle pairs (Figure 14e and Figure 21). 5-gap designs showed the highest yield for all cases in the number of crease handle pairs as it was improved from 67.5%, 86.6%, and 86.7% to 81.2%, 89.6%, and 93.1% for one, two, and three pairs, respectively (Figures 16-18 and Table 1). Note that the softening of these vertices using gaps did not affect overall structural integrity as the unfolded portion of 5-gap designs without glue strands was

maintained near 80%, similar to original, non-gap designs (Figure 22). Hence, the modulation of the vertex stiffness locally using gaps would be an effective way of enhancing the folding yield without hurting the overall structural integrity of DNA wireframe papers.

To quantitatively compare the effect of the edge stiffness, we estimated the strain energy of folded structures using SNUPI[32] (Figure 14f and Note 2). As expected, the normalized flexural rigidity globally decreased as the length of the gap increased, and eventually, the value of 5-gap was measured to be about 30% of those of nick. Furthermore, we simply designed a cost model for the elastic energy required for folding using the polymer theory, and the results supported our prediction of yield improvement by the gap (Note 3).

Finally, based on these findings, we then investigated the optimal yield for other cases of single folding (Figure 14g and Table 1). It was measured for SQ with 93.1% of H1 (3-pair and 5-gap), 93.9% of H2 (3-pair), and 88.4% of Q1 (3-pair and 1-gap). Through the observation for the increased yield of randomly more quarter folded SQ, the slightly lower yield of SQ Q1 with 5-gap than 1-gap could be explained (Figure 23).

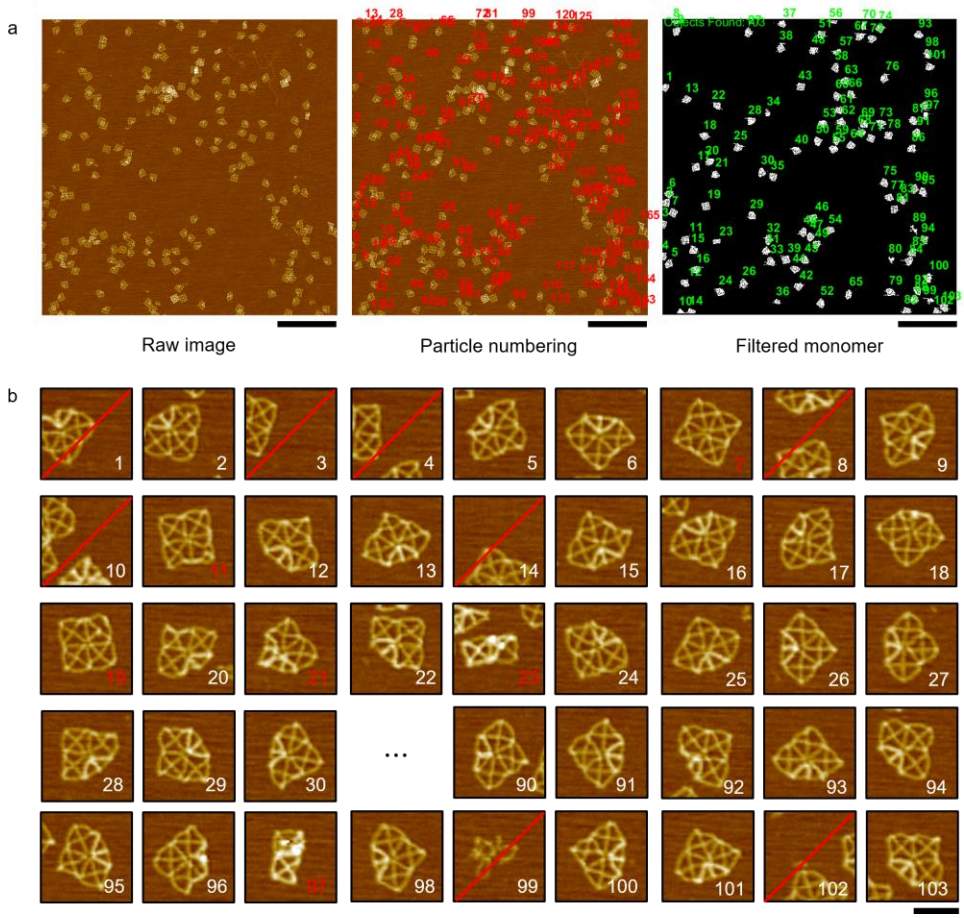

Figure 13. The procedure of estimating folding yield based on AFM image.

(a) Image process for estimating the folding yield with an example of SQ Q1. All particles in the raw AFM image (left) were systematically numbered (middle), filtered depending on their size to remove aggregated particles, and renumbered using customized MATLAB codes (right). Scale bars, 1 μm. (b) Partially displayed or irregularly shaped particles were excluded from the yield estimation (red diagonal cancel lines). Individual images with white and red numbers indicate the monomers with intended and unintended shapes, respectively. Scale bar, 100 nm.

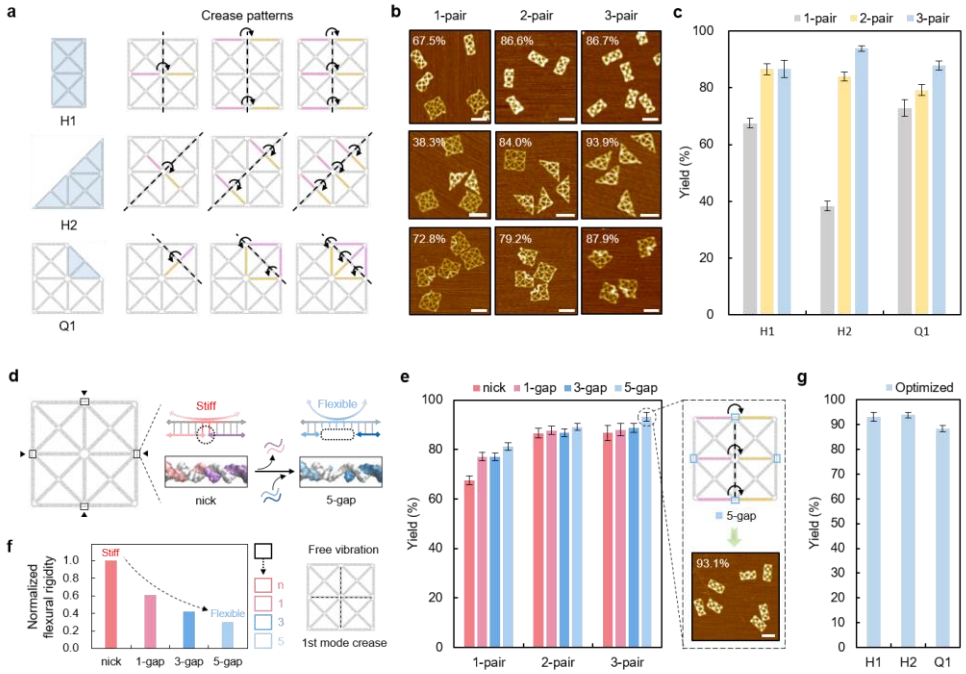

Figure 14. Optimization of folding yield.

(a) Crease patterns of H1, H2, and Q1 fold with the increasing number of crease handle pairs. **(b)** Representative AFM images of H1, H2, and Q1 with the different number of pairs after adding glue strands. Scale bars, 100 nm. **(c)** Folding yield of H1, H2, and Q1 according to the number of pairs. **(d)** Modular gap design on four nick vertices of SQ (black box). **(e)** Folding yield of H1 according to the number of pairs and gaps. (Inset) SQ H1 with 3-pair and 5-gap represented the best yields of 93.1% in AFM images. Scale bar, 100 nm. **(f)** The normalized flexural rigidity of a DNA paper with gaps from nick (0-gap) to 5-gap. The flexural rigidity of plate theory was derived from the free vibration analysis using SNUPI[32] and normalized based on the value of nick (Note 2). **(g)** The optimal yield results of SQ H1, H2, and Q1 folding by varying the number of pairs and gaps. (c, e, g) At least three AFM measurements were conducted to estimate the yield and standard error.

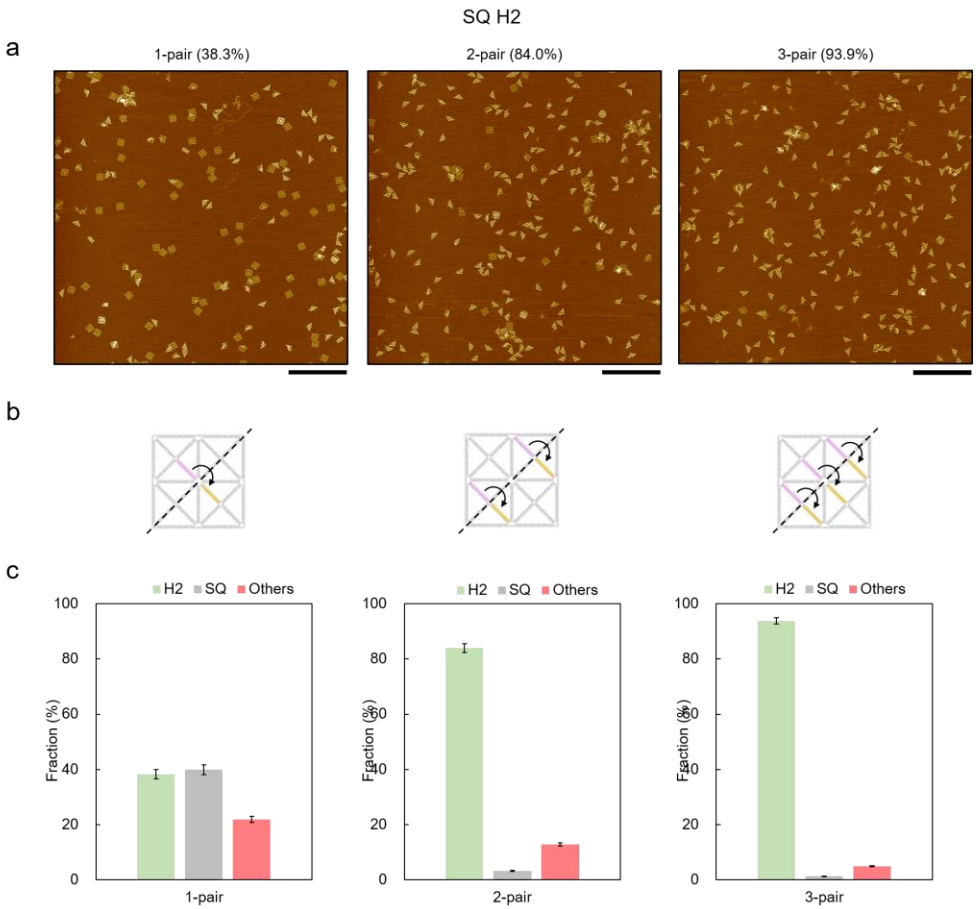

Figure 15. Representative AFM images of SQ H2 (pair).

(a) Representative AFM images of SQ H2 with three different numbers of crease handle pairs from one to three. Scale bars, 1 μm. (b) Crease patterns of corresponding SQ H2. Pink and orange edges represent DNA edges modified with 3` and 5` crease handles, respectively. (c) The fraction of H2, SQ (unfolded), and Others estimated by AFM measurements. At least three AFM measurements were conducted to estimate the folding yield and standard error. Detailed data were described in Table 1.

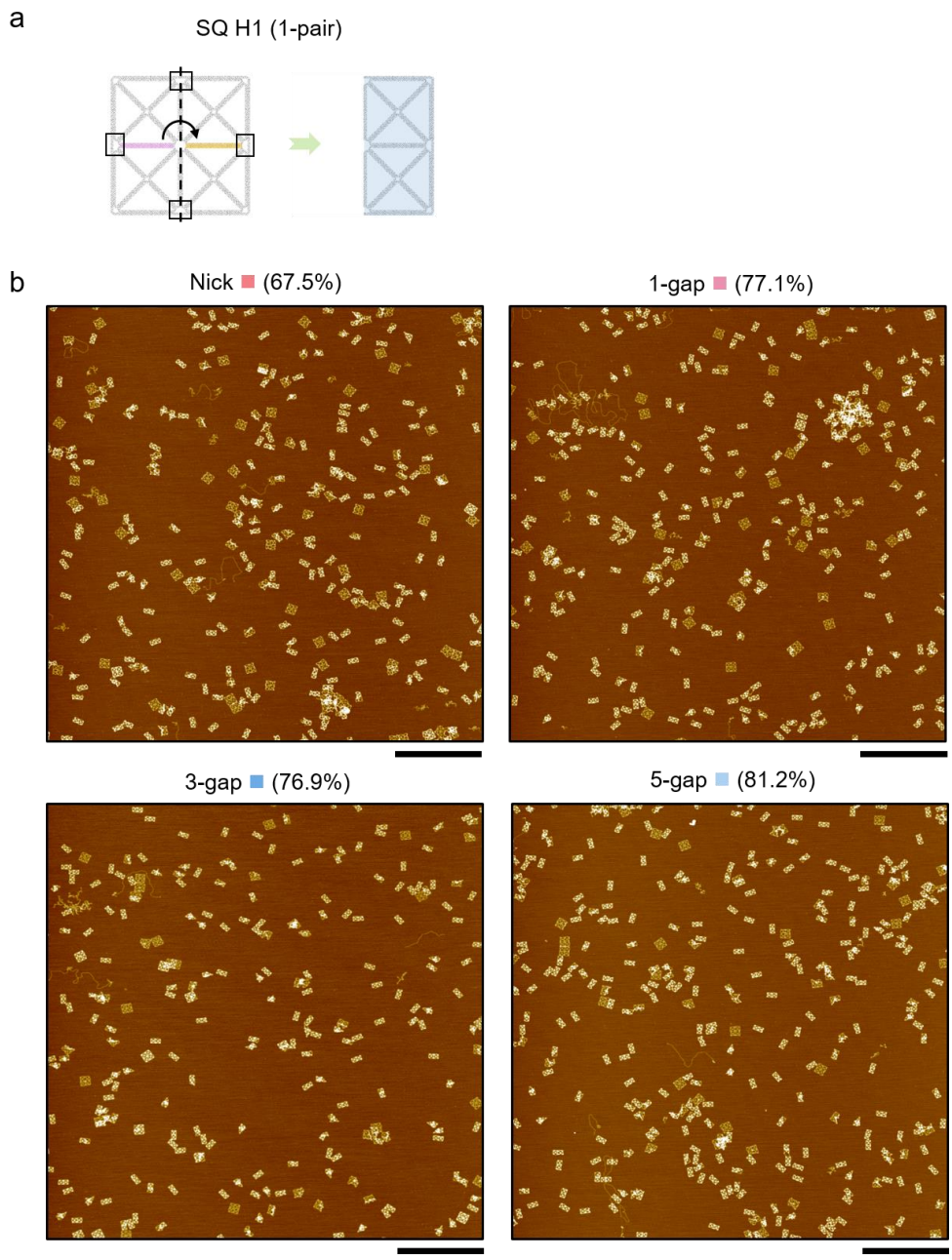

Figure 16. Representative AFM images of SQ H1 (1-pair, gap).

(a) Crease pattern of SQ H1 with single pair of crease handles and different lengths of gaps on the four vertices (black box). (b) Representative AFM images of SQ H1 1-pair with nick, 1-, 3-, and 5-nt long gaps. At least three AFM measurements were conducted to estimate the folding yield and standard error. Scale bars, 1 μm.

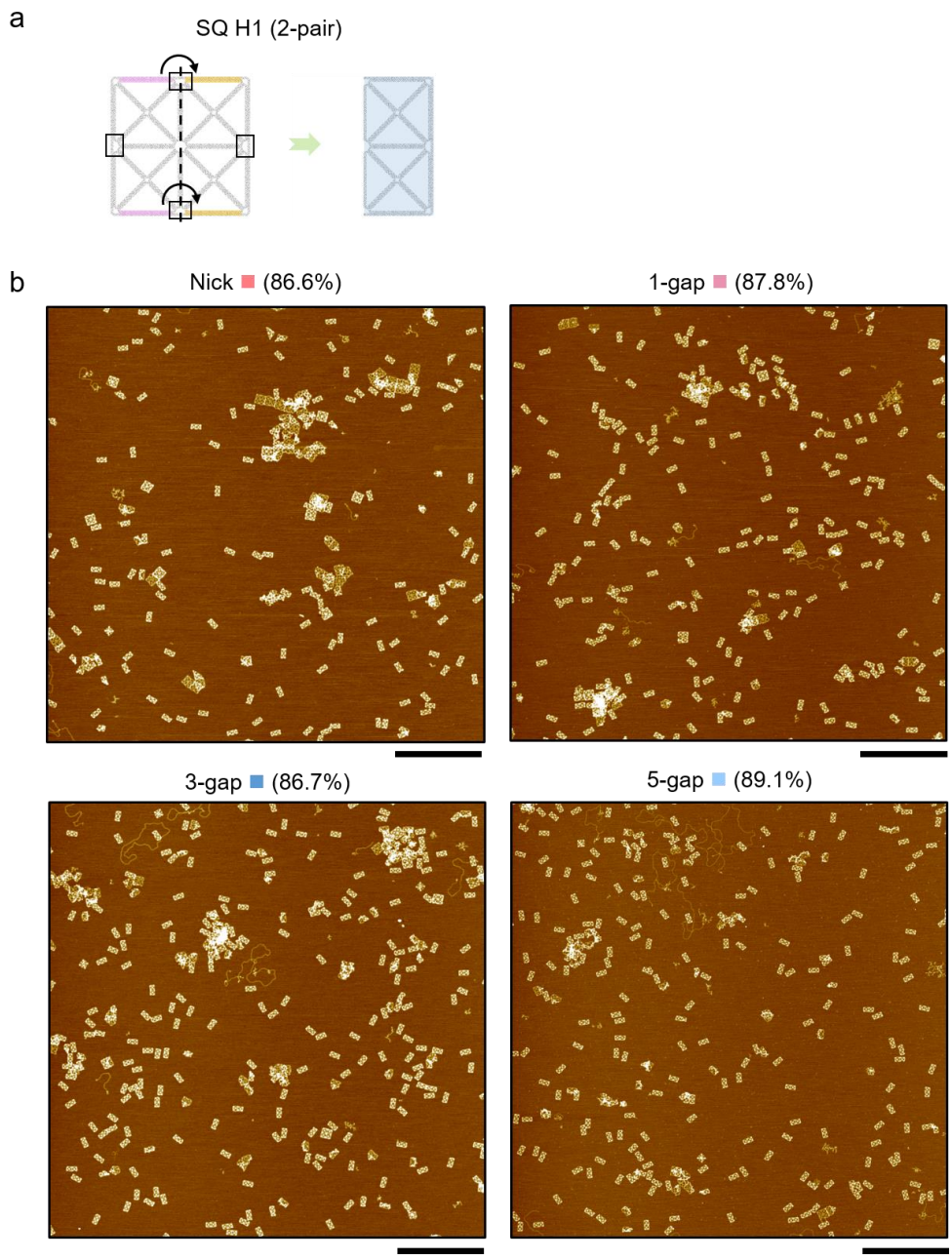

Figure 17. Representative AFM images of SQ H1 (2-pair, gap).

(a) Crease pattern of SQ H1 with two pairs of crease handles and different lengths of gaps on the four vertices (black box). (b) Representative AFM images of SQ H1 2-pair with nick, 1-, 3-, and 5-nt long gaps. At least three AFM measurements were conducted to estimate the folding yield and standard error. Scale bars, 1 μm.

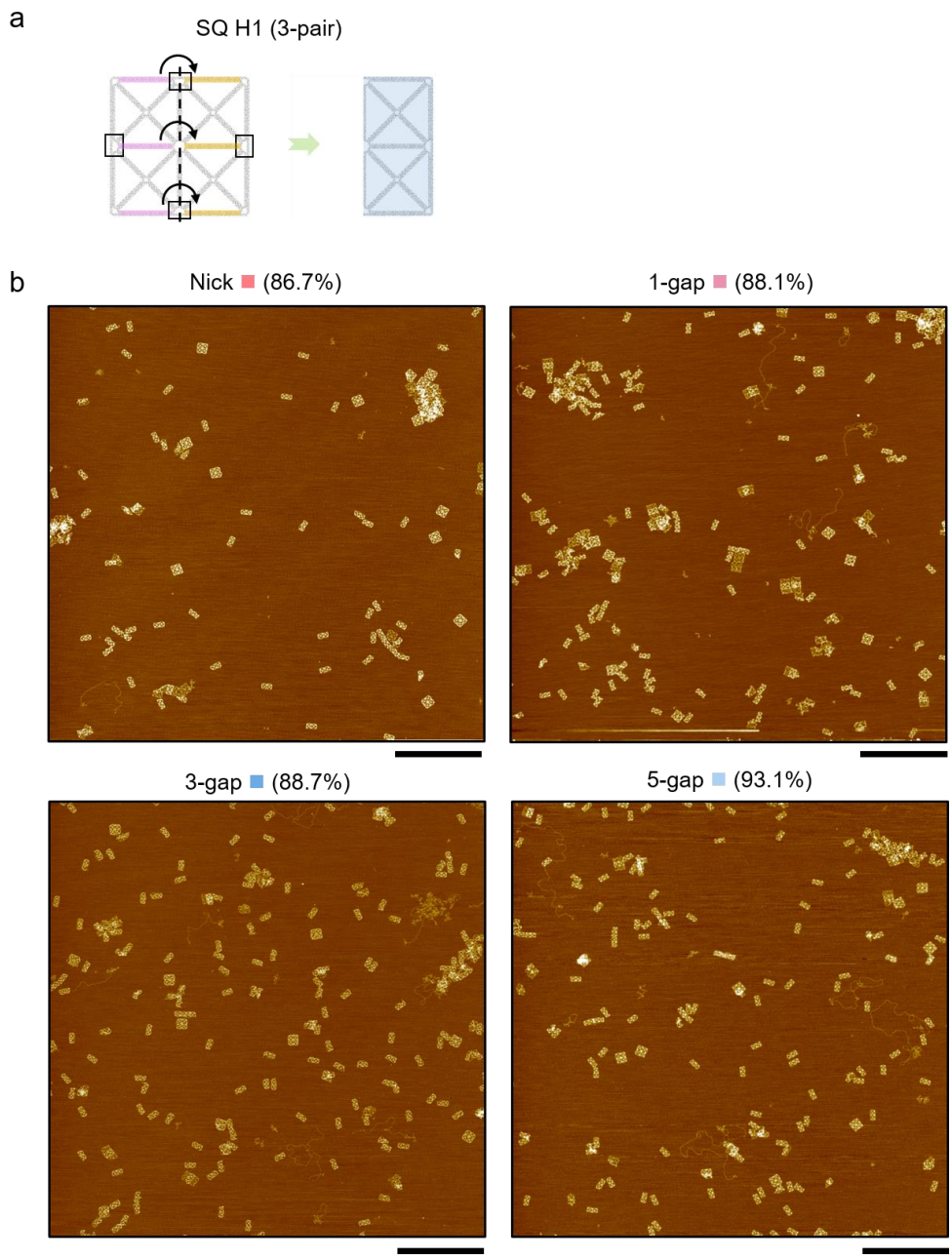

Figure 18. Representative AFM images of SQ H1 (3-pair, gap).

(a) Crease pattern of SQ H1 with three pairs of crease handles and different lengths of gaps on the four vertices (black box). (b) Representative AFM images of SQ H1 3-pair with nick, 1-, 3-, and 5-nt long gaps. At least three AFM measurements were conducted to estimate the folding yield and standard error. Scale bars, 1 μm.

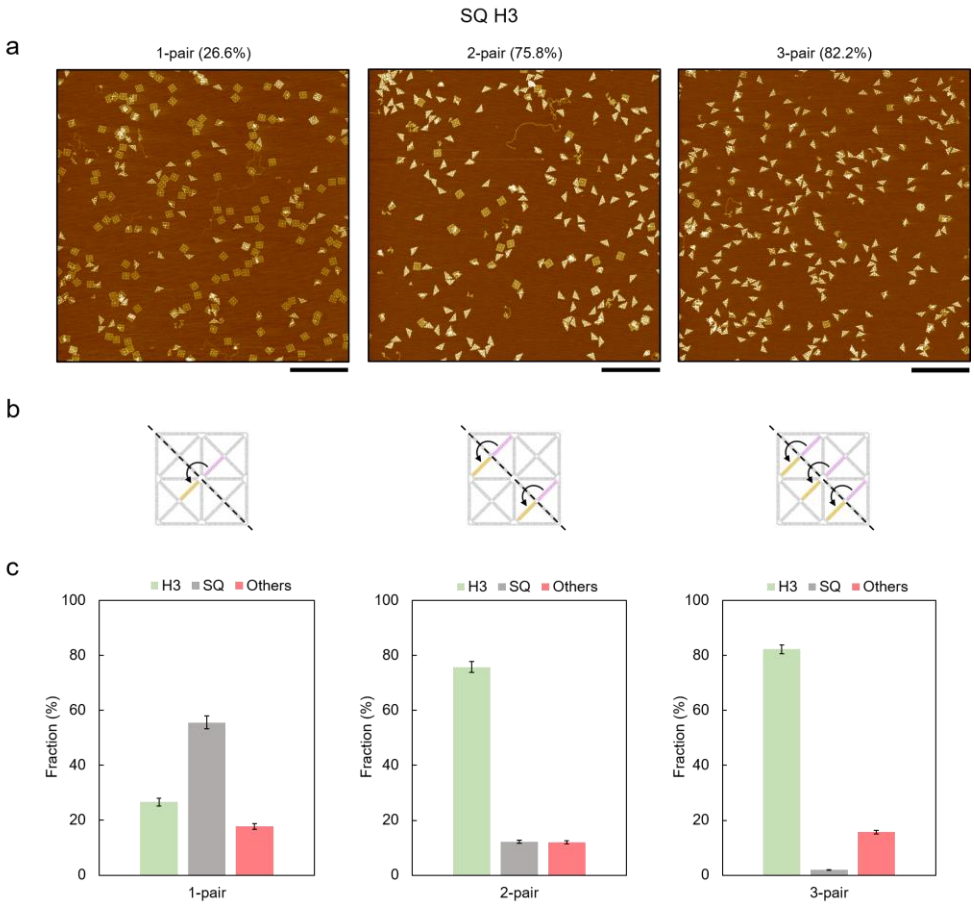

Figure 19. Representative AFM images of SQ H3 (pair).

(a) Representative AFM images of SQ H3 with three different numbers of crease handle pairs from one to three. Scale bars, 1 μm. (b) Crease patterns of corresponding SQ H3. Pink and orange edges represent DNA edges modified with 3` and 5` crease handles, respectively. (c) The fraction of H3, SQ (unfolded), and Others estimated by AFM measurements. At least three AFM measurements were conducted to estimate the folding yield and standard error. Detailed data were described in Table 1.

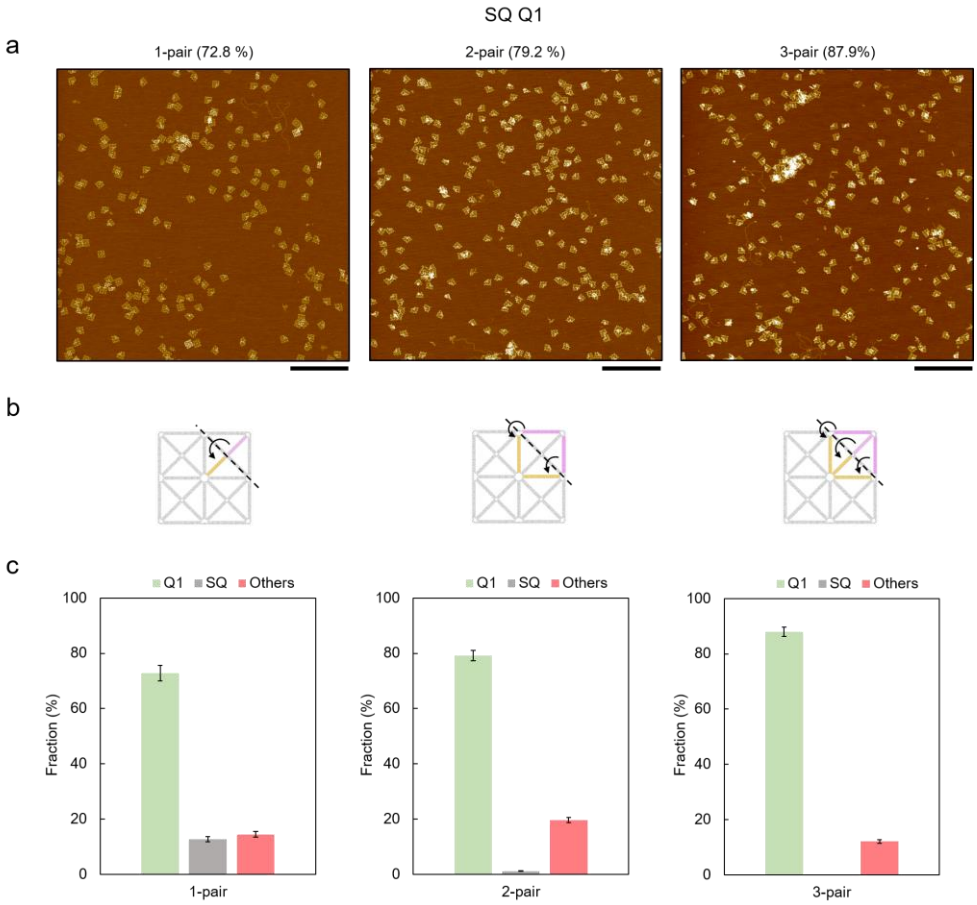

Figure 20. Representative AFM images of SQ Q1 (pair, nick).

(a) Representative AFM images of SQ Q1 with three different numbers of crease handle pairs from one to three. Scale bars, 1 μm. (b) Crease patterns of corresponding SQ Q1. Pink and orange edges represent DNA edges modified with 3` and 5` crease handles, respectively. (c) The fraction of Q1, SQ (unfolded), and Others estimated by AFM measurements. At least three AFM measurements were conducted to estimate the folding yield and standard error. Detailed data were described in Table 1.

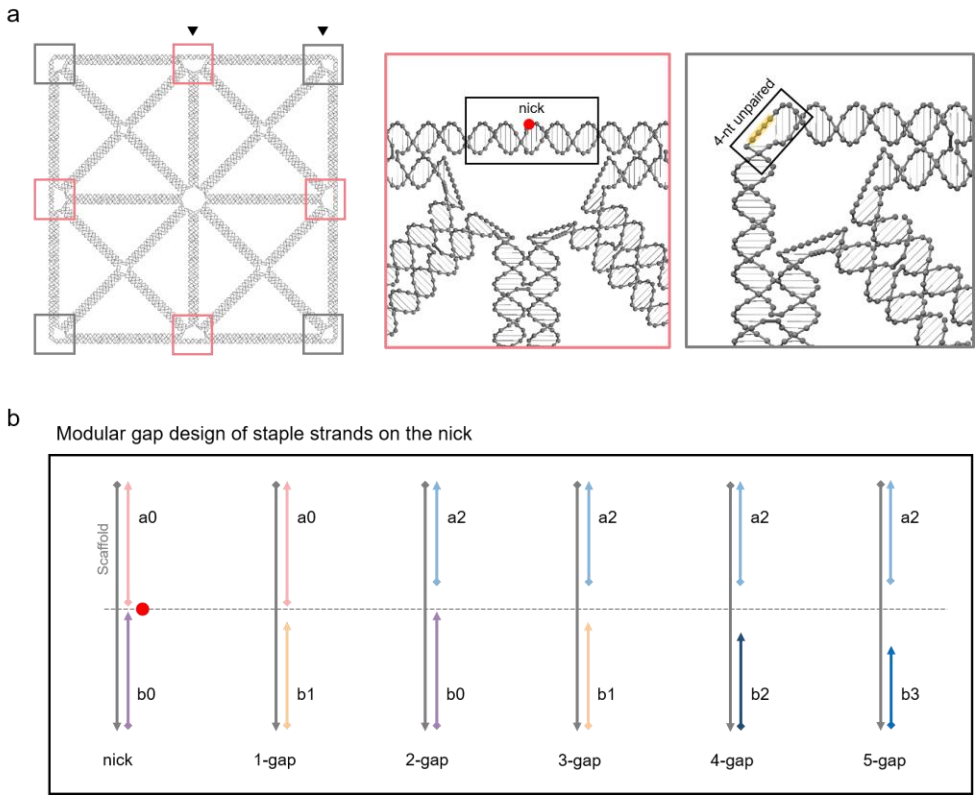

Figure 21. Modular gap design on vertices SQ.

(a) Composition of vertices of square DNA paper (left), stiff regions with nick (middle), and flexible regions with unpaired 4-nt long ssDNA (right). (b) The modular design of staple strands to replace nick (red dot) with gaps of various lengths. The suffixal number represents the gap length of the staple. Various length of the total gap was modularly obtained by adding two shorter lengths of staples than those of nick, expressed as $Gap(m+n)=a(m)+b(n)$.

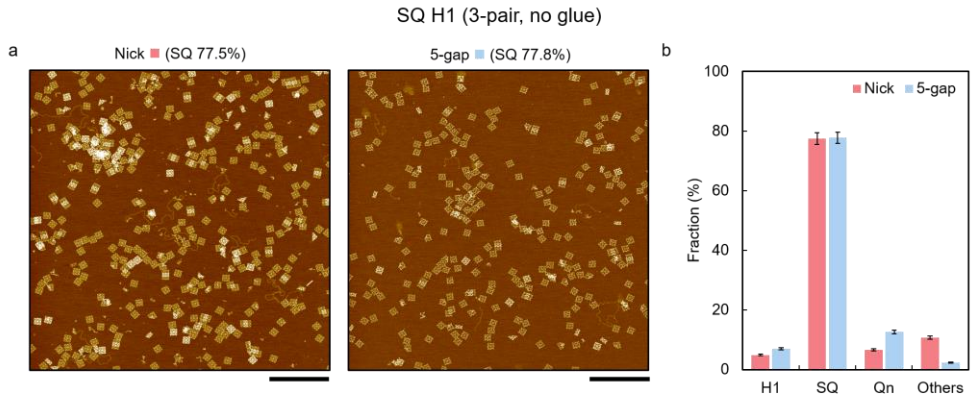

Figure 22. Gap effect on the structural integrity of SQ.

(a) Representative AFM images of SQ H1 3-pair with nick and 5-gap, respectively, before adding glue strands. Scale bars, 1 μm. (b) Fraction of H1, SQ (unpaired), Qn (single and multiple quarter-folding), and others. When 5-gap was applied on four vertices of SQ, the yield of SQ maintained near 80% similar to nick, which confirmed the structural integrity of SQ even with gaps.

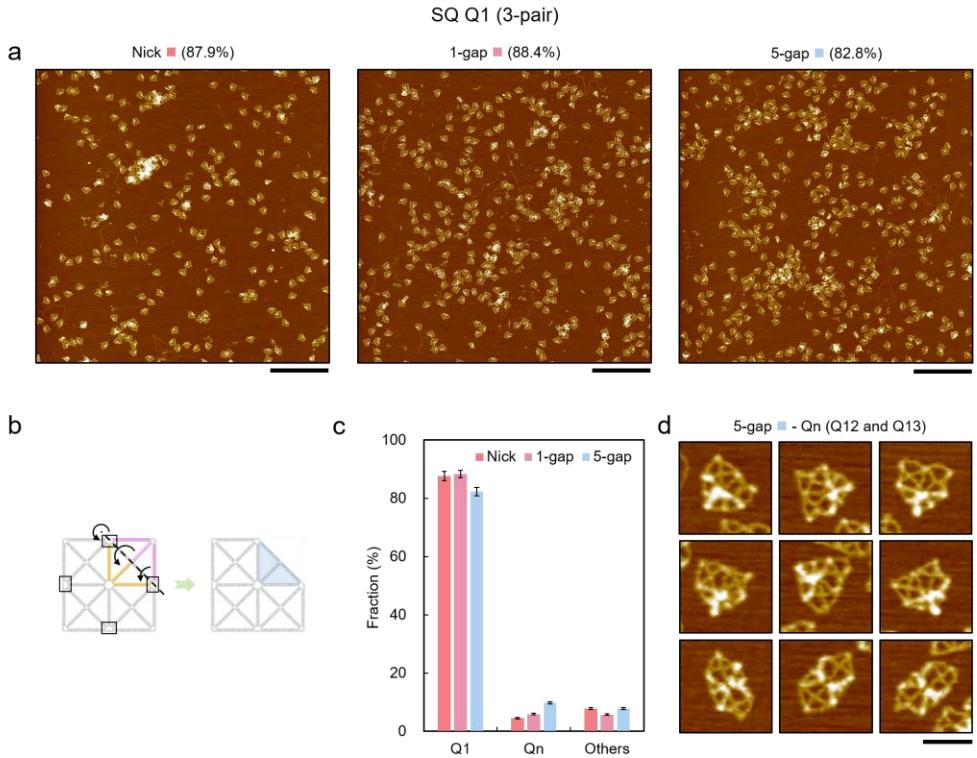

Figure 23. Additional quarter-folding of SQ by applying gap.

(a) Representative AFM image for SQ Q1 3-pair with 5-gap. Scale bars, 1 μm. (b) Crease pattern of SQ Q1 3-pair with four structural motifs for gap (black box). (c) Fraction of Q1, Qn (multiple quarter-folding), and Others of SQ Q1 3-pair for the cases of nick, 1-gap, and 5-gap. When gaps were applied, the Qn fraction increased from ~4.5% of nick to ~5.9% of 1-gap and finally doubled to ~9.8% while the folding yield (Q1) slightly decreased. Considering that the combined portions of Q1 and Qn were similar over 90% for 1-gap and 5-gap, and intended quarter-folding by designed crease handles (Q1) could not prevent other quarter-folding by gap unlike H1 gap cases, the slightly lower folding yield of SQ Q1 with 5-gap than 1-gap could be explained. (d) Exemplary AFM images of Qn shown in the image of 5-gap in (a). Scale bar, 100 nm.

Note 2. The flexural rigidity of DNA wireframe paper.

In the Kirchhoff-Love plate theory[37], the governing equation of isotropic and homogeneous plate of constant thickness was derived with zero external force as $D\nabla^2\nabla^2 w + 2\rho h\ddot{w} = 0$, where the w is the transverse displacement of place, h is the half of the plate thickness, ρ is the density, ∇^2 is the Laplacian operator, and D represents the flexural rigidity defined by $D = Eh^3/12(1-\nu^2)$ with the elastic modulus (E), and the Poisson's ratio (ν), respectively. The separation of the spatial and temporal variables of the governing equation yields the proportional relation between natural frequency and the plate bending stiffness in the free vibration as $D/\rho = \omega^2\alpha^4/\beta^2$ for the square plate where α is the square width, ω is natural frequency, and β is the numerically determined constant for the lowest mode as β~13 for the rectangular plate[37]. This suggests that the bending stiffness of a DNA wireframe paper can be estimated by its natural frequency by assuming the structure as square plates. Also, the bending stiffness of DNA wireframe paper consisting of different structural motifs (nicks or gaps) can be quantitatively compared using the eigenvalues corresponding to the lowest bending mode shape (λ), which were related to the natural frequency as $\lambda = \omega^2$. The bending mode shapes and eigenvalues of the DNA structures were calculated by performing the normal mode analysis in SNUPI[32]. The calculated rigidity of each structure with the corresponding gap was normalized to the value of the nick as shown in the figure below.

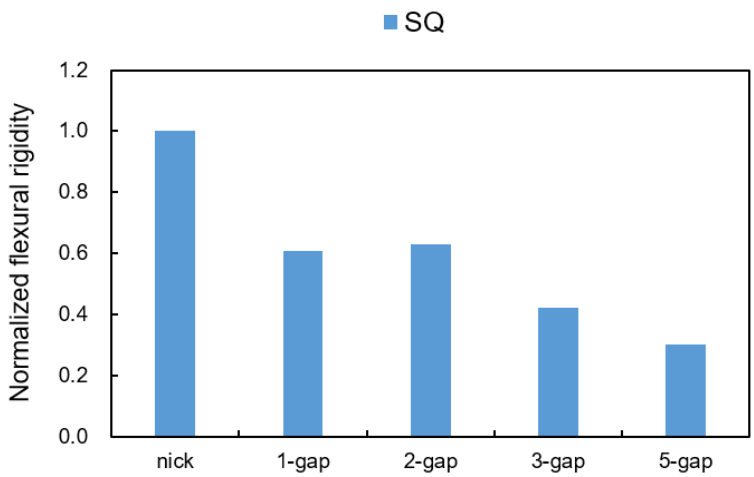

Note 3. Elastic energy cost of folding DNA wireframe paper.

In the DNA wireframe paper, the elastic energy cost (E) for each folding could be estimated from the general expression of the elastic polymer model. Assuming a single DNA helix as a rod cylinder, the derivative of the energy with the contour length (s) on the vertices along the target crease could be expressed as

$$dE = \frac{1}{2} k_B T (A\beta^2 + Bu^2 + C\omega^2 + 2Du\omega) ds$$

where s is the contour length, β is the bend vector as $\beta(s) = d\theta / ds$ for the bend angle (θ), u is stretch as $u(s) = \Delta(ds) / ds$, ω represents the twist density as $\omega(s) = d\phi / ds$ for the twist angle (ϕ), and Ak_BT, Bk_BT, Ck_BT, and Dk_BT are bend stiffness, stretch stiffness, twist stiffness, and twist-stretch coupling, respectively.

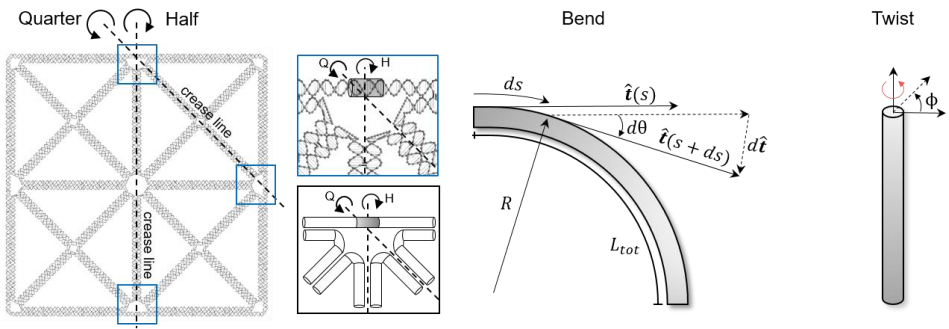

Considering the simplified rod model with bend and twist, the total elastic energy cost of the crease point (E_p) for the total contour length (L_{tot}) could be derived as below.

$$E_p = \frac{1}{2} k_B T \int_0^{L_{tot}} (A\beta^2 + C\omega^2) ds = \frac{1}{2} k_B T \int_0^{R\theta} ds \left(A\left(\frac{1}{R}\right)^2 + C\left(\frac{\phi}{L_{tot}}\right)^2 \right)$$

$$E_p(A, C, \theta, \phi) = \frac{k_B T}{2 L_{tot}} (A\theta^2 + C\phi^2)$$

where R is the radius by the bend deformation.

The energy cost of the folding line (E_l) could be simply modeled assuming that the energy would be proportional to the length (*l*) of the line, then finally, the total elastic energy cost is obtained by adding two energy costs E_p and E_l.

$$E_p(A,C,\theta,\phi,l) = E_p + E_l = \frac{k_B T}{2L_{tot}}(A\theta^2 + C\phi^2) + \alpha l$$

where α is an arbitrary proportional factor.

It is notable that the elastic energy would cost less for the same folding line by reducing the bend and twist rigidity, *A* and *C*, of the vertices using gap[33].

$$E(A_{nick}, C_{nick}) > E(A_{gap}, C_{gap})$$

Based on this result, we reduced the rigidity of vertices along the target crease by applying gaps instead of nick of the original design and successfully obtained the increment of the folding yield.

2.3. Folding properties

With optimized designs, we investigated various folding properties of DNA wireframe papers: orthogonal folding, repeatable folding and unfolding, and folding-based signal control. First, we explored the orthogonal folding by embedding both H1 and H2 folding patterns on the SQ DNA wireframe paper (Figure 24a). Glue strands for H1 and H2 foldings were designed to have complementary sequences to corresponding crease handles but be orthogonal to each other (Table 4). Without any glue strand, the unfolded state was dominant (82.6%) in AFM images (Figure 25 and Table 1). It could be successfully reconfigured into the folded state H1 (96%) and H2 (93%) by adding corresponding glue strands (glue1 and glue2, respectively). This high-yield orthogonal folding property would enable us to implement multiple and more complex reconfigurations on a single DNA wireframe paper.

Next, we checked the repeatable folding and unfolding of DNA wireframe papers using H1 folding design by adding alternately glue and releaser strands (Figure 24b). Agarose gel electrophoresis confirmed the repeatability of folding and unfolding through clear migration differences when glue or releaser strands were added. The initial band position of the unfolded state descended to a lower band position of the folded state as glue strands were added. It ascended back to the original position if we added releaser strands. AFM images obtained for each gel band (Figure 26) additionally verify properly folded and unfolded shapes. For the unfolded state, 81% unfolded SQ structures were observed, whereas, for the folded state, 97.6% H1 structures were found (Table 1). No significant degradation of the structural integrity was observed during folding and unfolding processes.

Orthogonality and repeatability of folding would offer a versatile way of programming the derived folding properties into DNA wireframe papers. To illustrate, we studied the folding-based control of fluorescent signals. We attached two quenchers (Q, EBQ) and fluorescence reporters (R, Cy3) on four inner vertices of the SQ with H1 and H2 folding patterns (Figure 24c and Figure 27). It was designed such that both quencher-reporter pairs became in close proximity with H1 folding while only one pair was quenched with H2 folding, leading to a folding-dependent change in fluorescent signals. Time-resolved fluorescence

measurements were conducted for 140 min in total consisting of three phases; Phase I (initial state), Phase II (folded state with glue strands), and Phase III (unfolded state with releaser strands) (Figure 4c). In Phase I, the normalized intensity level was maintained around 1.0 with minor fluctuations. After adding glue strands in Phase II, the normalized intensity decreased quickly and converged to around 0.25 and 0.65 with H1 and H2 foldings, respectively. As expected, H1 folding exhibited an approximately two-fold reduction in the fluorescent intensity compared to H2 folding. For both cases, the convergence was reached in about 10 min with the on-rate of $4.4\times10^{5}\,(\mathrm{M}\cdot\mathrm{s})^{-1}$ estimated from our kinetic model, which was similar to that of DNA nanostructure polymerization[34, 35] (Note 4). When releaser strands were added in Phase III, the normalized intensity increased slowly and finally converged to around 0.95 with the unfolding reaction time of about 40 min. AFM measurements in each phase also confirmed successful folding and unfolding consistent with the intensity profiles (Figure 28 and Table 1).

Finer tuning of the signal could be also possible by controlling the distance between quenchers and reporters by using mountain and valley folds for the same crease line. These folds were enabled by choosing the overhang direction of crease handles with respect to the surface to which quenchers and reporters attached (Figure 24d and Figure 29). With the mountain fold, relatively higher fluorescence intensities were expected due to slightly lower proximity between quenchers and reporters (ideally two layers of double-stranded DNA apart) than the valley fold. Measured time-resolved intensities for 15 minutes revealed the difference in the normalized intensity of approximately 0.1 between the mountain and valley folds. AFM measurements confirmed that these folds could be realized with a high yield (Figure 30 and Table 1).

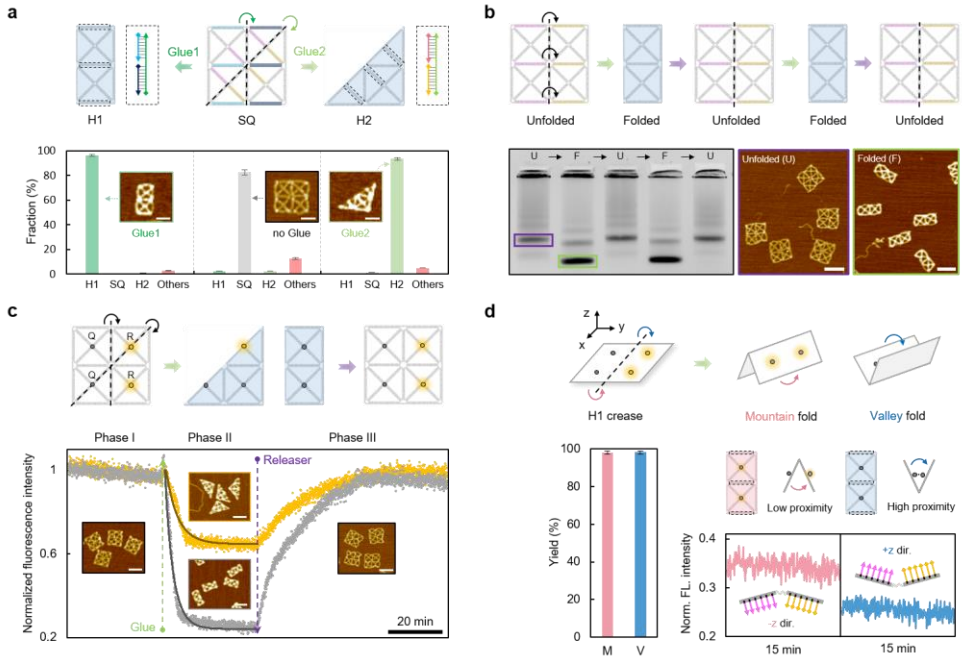

Figure 24. Validation of folding properties.

(a) Orthogonal folding. Top: schemes of orthogonal folding of the SQ having both H1 and H2 crease patterns. Two types of orthogonal crease handle pairs and corresponding glues, sky blue-blue (glue1, dark green) and pink-orange (glue2, green), were designed. The dominant state of SQ (unfolded) was reconfigured into H1 by adding glue1 and H2 by glue2. Representative AFM image for each dominant state. Scale bars, 50 nm. **(b)** Repeatable folding and unfolding. Top: schemes of repeatable folding and unfolding of SQ with a H1 pattern. Bottom: gel electrophoresis with EtBr stained 0.8wt% agarose to compare the migration during the repeatable folding and unfolding processes. AFM measurements were conducted after gel extraction to validate the shapes of the unfolded (U, purple box) and folded (F, green box) states in bands. Scale bars, 100 nm. **(c)** Folding-based signal control. Top: expected luminous states in initial, folded, and unfolded states. Two quenchers (Q, EBQ) and fluorescence reporters (R, Cy3) were placed at the end of the strand overhung from the inner vertices of the SQ (Figure 27). Bottom: Time-resolved normalized fluorescence intensity as measured in solution for a total of 140 min. Solid lines: forward reaction rates (k_{on}) were fit from our kinetic model (Note 4). SQ H1 (gray): $k_{on} = 4.35 \times 10^4 (\mathrm{M} \cdot \mathrm{s})^{-1}$ and SQ H2

(yellow): $k_{on} = 4.44 \times 10^4 (\mathrm{M} \cdot \mathrm{s})^{-1}$. Representative AFM images of corresponding phases. Scale bars, 100 nm. **(d)** Mountain and valley folds. Top: diagram of mountain and valley folds of SQ H1. Two quenchers and reporters (R, Cy3) were placed at the end of the overhang strand in the same direction as the valley fold. Bottom: estimated folding yield of mountain and valley folds. The time-resolved normalized fluorescence intensity as measured in solution for a total of 15 min after reaching the convergence of folded state. (c-d) The fluorescence intensity was normalized to compensate for the dilution effect.

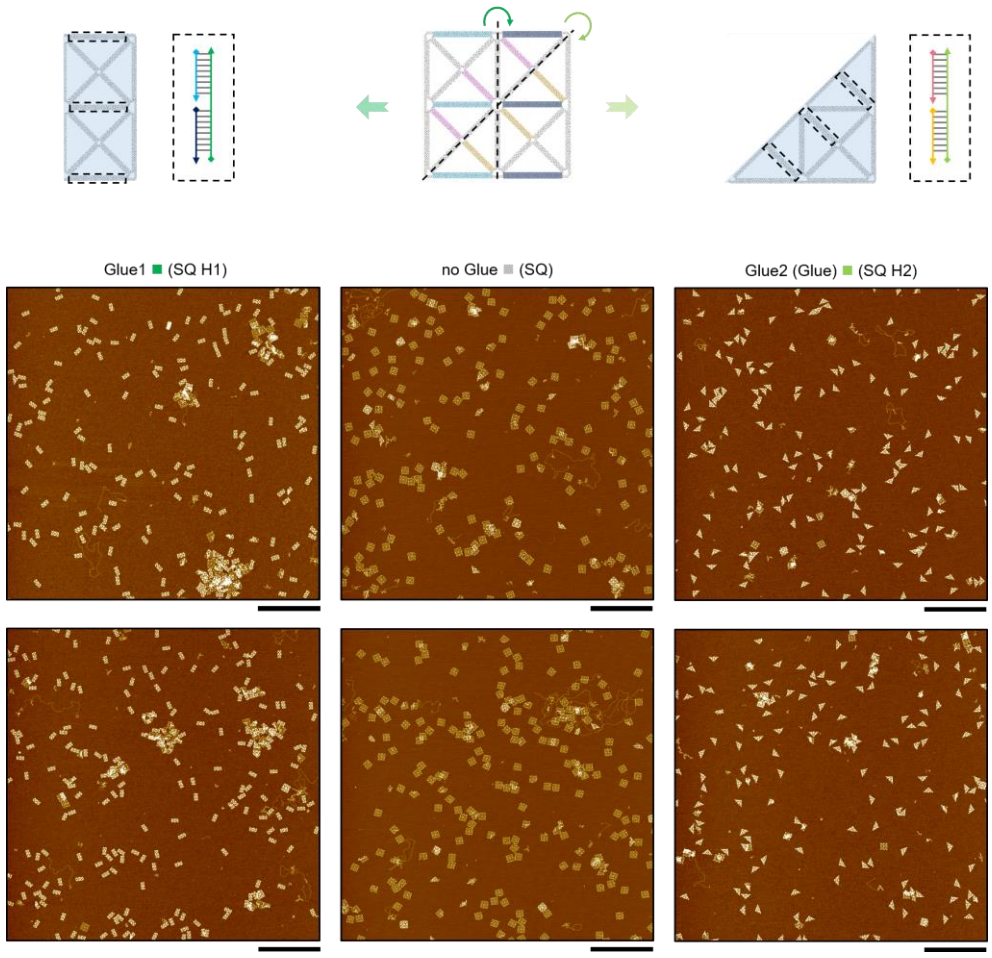

Figure 25. Representative AFM images of orthogonal folding.

Sky blue and blue edges indicate the modified DNA edges having 3` and 5` crease handles that bind with glue1 strands (dark green), respectively. Pink and yellow edges indicate the modified DNA edges having 3` and 5` crease handles that bind with glue2 strands (green), respectively. Scale bars, 1 μm.

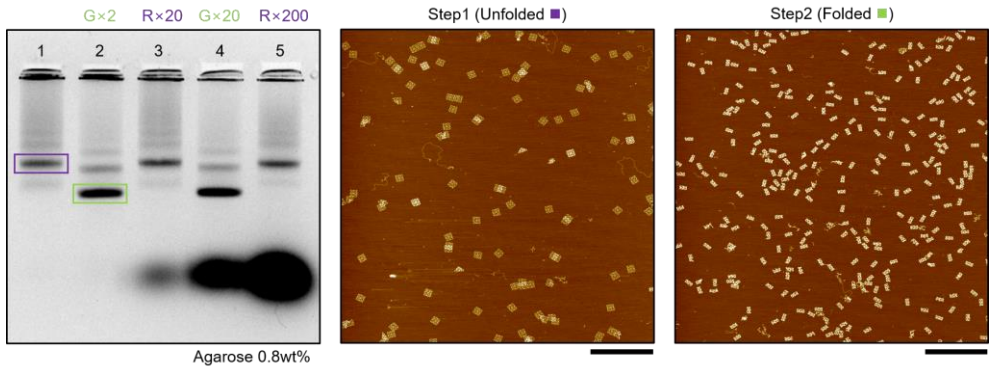

Figure 26. Representative AFM images and gel electrophoresis of repeatable folding and unfolding.

Gel electrophoresis with EtBr stained 0.8wt% agarose was conducted for 90 min at 75 V. Step 1: SQ H1 (3-pair). Step 2: two times of glue strands to the concentration of crease handle pairs of SQ H1 (3-pair) were added and incubated at room temperature overnight. Step 3: 20 times of releaser strands to the concentration of crease handle pairs were added and incubated at 37℃ for an hour. Step 4: 20 times of glue strands to the concentration of crease handle pair were added and incubated at room temperature overnight. (Since 18 times of unbound releaser strands remained in step 3, the final concentration of glue strands in step 4 would be two times the concentration of crease handle pairs). Step 5: 200 times of releaser strands to the concentration of crease handle pairs were added and incubated at 37℃ for an hour. AFM measurements were conducted after taking gel extraction and filtration for the bands (purple and green box). Scale bars, 1 μm.

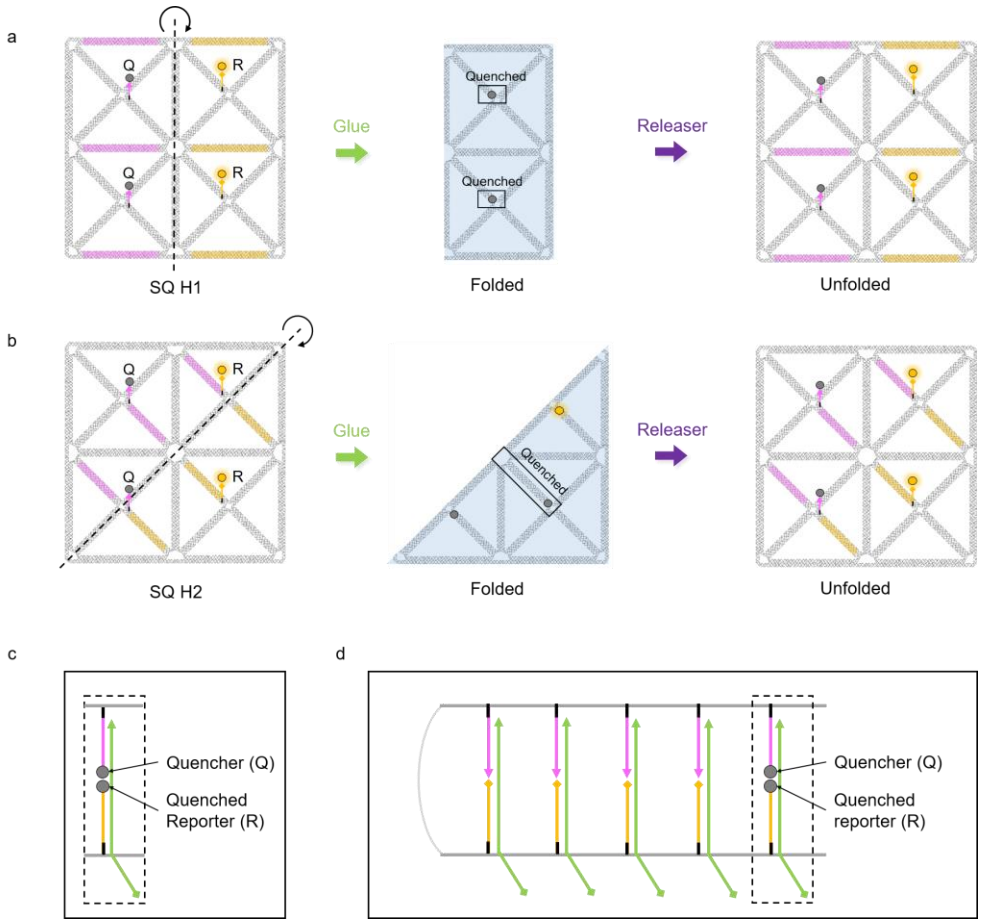

Figure 27. Design of folding-dependent fluorescence signal control.

(a) Crease pattern of SQ H1 3-pair with two quenchers (Q) and reporters (R). Both reporters would be quenched by induced proximity after adding glue strands (detail in **c**) and recovered after adding releaser strands. (b) Crease pattern of SQ H2 3-pair with two quenchers and reporters. Only a single reporter would be quenched after adding glue strands (detail in **d**) and recovered after releaser strands. (c) Schematic illustration of quenched reporter of SQ H1. (d) Schematic illustration of quenched reporter of SQ H2.

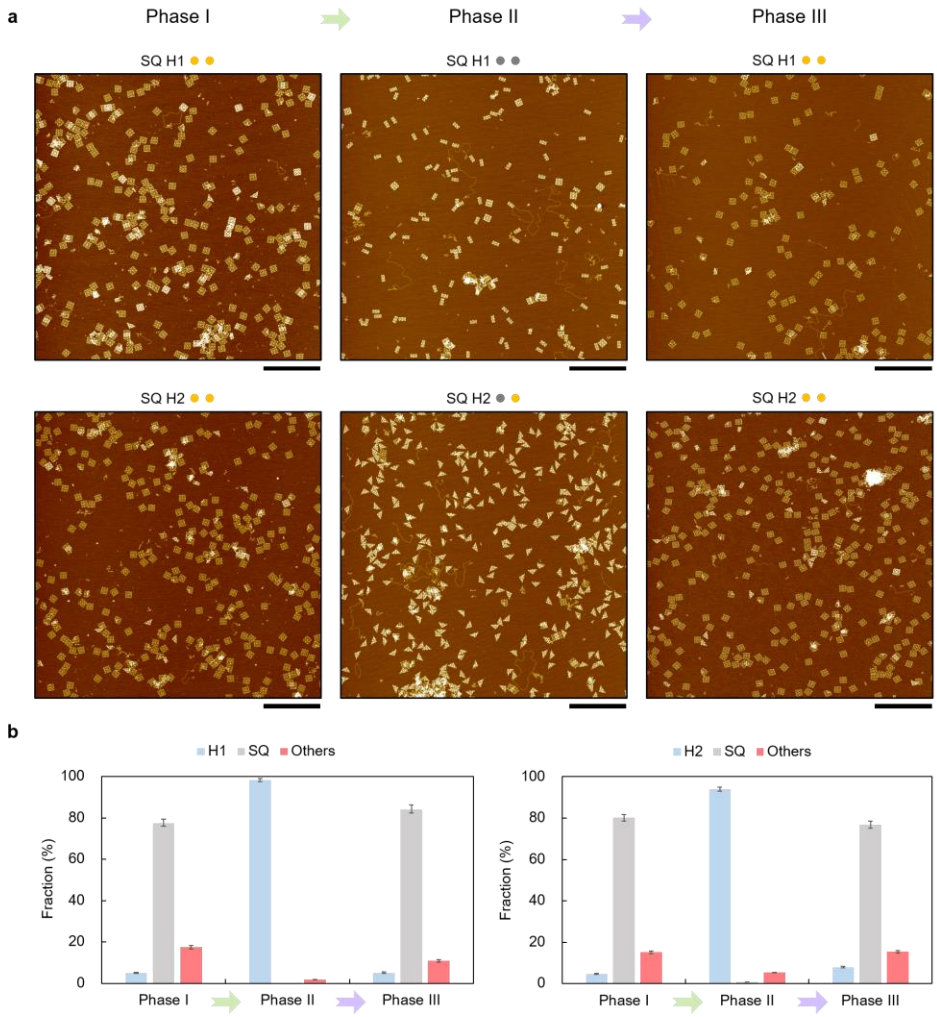

Figure 28. Representative AFM images of folding-dependent signal control.

(a) Phase I: initial state. Phase II: glue strands were added. Phase III: releaser strands were added. All AFM images were obtained after the fluorescence intensity of each phase was fully converged. Color dots represent the states of the two reporters (Cy3), orange = emit and gray = quenched. Scale bars, 1 μm. (b) Fraction change of SQ H1 and SQ H2 according to the phase (SQ: unfolded).

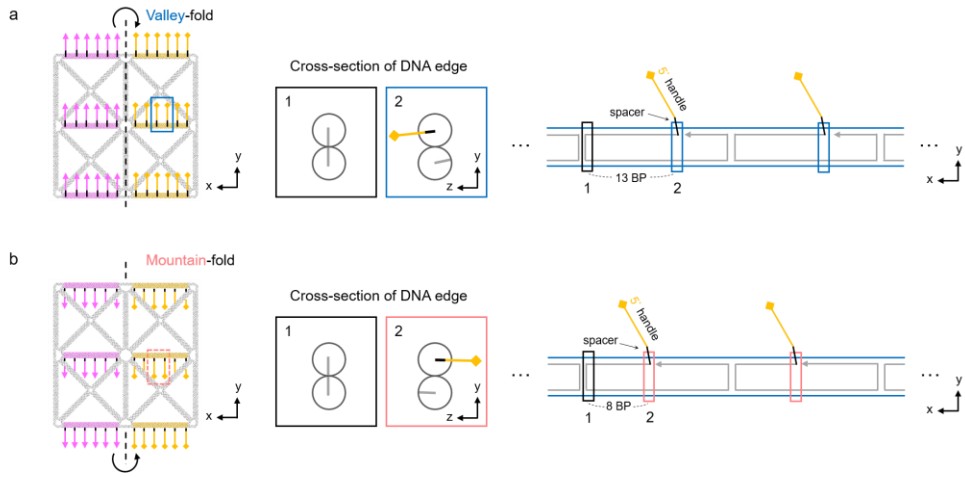

Figure 29. The crease handle design of mountain and valley fold.

(a) Conceptual design of valley fold with an example of SQ H1 (3-pair). (b) Conceptual design of mountain fold with an example of SQ H1 (3-pair). Based on the crossover direction (box 1), the overhang positions of crease handles on DNA edges were designed to protrude perpendicular to the plane of DNA paper (box 2) with a positive z-direction for valley fold and a negative z-direction for mountain fold.

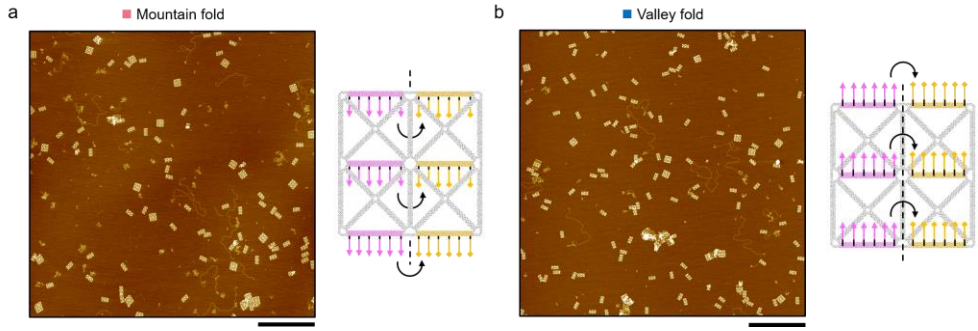

Figure 30. Representative AFM images of mountain and valley fold of SQ H1.

(a) Representative AFM image and crease pattern of mountain fold. (b) Representative AFM image and crease pattern of valley fold. Scale bars, 1 μm.

Table 4. Staple sequence for structural folding and unfolding.

• Glue and releaser strands (toehold)

Name	Sequence (5`→3`)
Glue2 (Glue) ■	CGATGCACACACCTCAGCAGC
PC-Glue■	CGATGCACACACC **[PC]** TCAGCAGC
Releaser2 (Releaser)■	GCTGCTGAGGTGTGTGCATCG
Glue1 ■	AACGATGCACCTTAGCGCCCT
Releaser1 ■	AGGGCGCTAAGGTGCATCGTT

• Crease handles of SQ: ■ & ■ (glue2) and ■ & ■ (glue1) (**overhang**, spacer)

Name	Sequence (5`→3`)
5` crease handle ■	**GGTGTGTG**TTT (edge sequences)
3` crease handle ■	(edge sequences) TTT**GCTGCTGA**
5` crease handle ■	**GCATCGTT**TTT (edge sequences)
5` crease handle ■	(edge sequences) TTT**GCTAAGGT**

• pH-responsive crease handles (ssDNA: ■, Hairpin: ■)(**triplex**, spacer)

Name	Sequence (5`→3`)
3` ssDNA ■	(edge sequences) TTT**CTTTCTTCTTCTTCTCTCTC**
3` hairpin ■	(edge sequences) TTT**CTCTCTCTTCTTCTTCTTTC**TTTT**GAAAGAAGAAGAAGAGAGAG**

• Reporter (Cy3 ●) and quencher (EBQ ●) staples (**overhang**, spacer)

Glue strands	
Name	**Sequence (5`→3`)**
V10-1 (3`) ●	(V10-1 sequences) TTT**GCTGCTGA [EBQ]**
V12-1 (3`) ●	(V12-1 sequences) TTT**GCTGCTGA [EBQ]**
V11-1 (5`) ●	**[Cy3] GGTGTGTG**TTT (V11-1 sequences)
V13-1 (5`) ●	**[Cy3] GGTGTGTGT**TTT (V13-1 sequences)

Table 4 (continued).

The pH-responsive triplex	
Name	**Sequence (5`→3`)**
V10-1 (3`) ●	(V10-1 sequences) TTT**CTTTCTTCTTCTTCTCTCTC**
V12-1 (3`) ●	(V12-1 sequences) TTT**CTTTCTTCTTCTTCTCTCTC**
V11-2 (vertex-hairpin) ●	(V11-2 sequences) TTT**CTCTCTCTTCTTCTTCTTTC**TTTT**GAAAGAAGAAGAAGAGAGAG**
V13-2 (vertex-hairpin) ●	(V13-2 sequences) TTT**CTCTCTCTTCTTCTTCTTTC**TTTT**GAAAGAAGAAGAAGAGAGAG**

• Modular composition of gap

Modular gap	**nick** ■	**1-gap** ■	**2-gap** ■	**3-gap**■	**5-gap** ■
a	a0 ■	a0 ■	a2 ■	a2 ■	a2 ■
b	b0 ■	b1 ■	b0 ■	b1 ■	b3 ■

• Gap staples of SQ vertices

Name	**Sequence (5`→3`)**
V02-1 a0 ■	ATGGTGGTTCCGAAATCGGCAAAATCATATCCAGAATTTTTTTTATATTA
V04-1 a0 ■	CTATTTTTGAGAGATCTACAAAGGCTAACGGGGTCATTTTTTTTGCCTTG
V06-1 a0 ■	AATTCGTAATCATGGTCATAGCTGTTTTGGATTATATTTTTTTTTCTGAA
V08-1 a0 ■	ATGGGATAGGTCACGTTGGTGTAGATAGCGAACCTCTTTTTTTACTTGCGGGAAAAAG
V02-3 b0 ■	AACATGCAACAGTGCTTTTTTTCACGCTGAGAGTGCCCCAGCAGGCGAAAATCCTGTTTG
V04-2 b0 ■	AGCACAACGCAAGGATTTTTTTTTAAAAATTTTTCTGATAAATTAATGCCGGAGAGGGTAG
V06-3 b0 ■	TTAGTATTTAACAACTTTTTTTGCCAACATGTACTAGAGGATCCCCGGGTACCGAGCTCG
V08-3 b0 ■	AGCAGCTTTTTTTACCGTAATCAGGTGGGAACAAACGGCGGATTGACCGTA
V02-3-b1 ■	AACATGCAACAGTGCTTTTTTTCACGCTGAGAGTGCCCCAGCAGGCGAAAATCCTGTTT
V04-2-b1 ■	AGCACAACGCAAGGATTTTTTTTTAAAAATTTTTCTGATAAATTAATGCCGGAGAGGGTA
V06-3-b1 ■	TTAGTATTTAACAACTTTTTTTGCCAACATGTACTAGAGGATCCCCGGGTACCGAGCTC
V08-3-b1 ■	AGCAGCTTTTTTTACCGTAATCAGGTGGGAACAAACGGCGGATTGACCGT
V02-1-a2 ■	GGTGGTTCCGAAATCGGCAAAATCATATCCAGAATTTTTTTTATATTA
V04-1-a2 ■	ATTTTTGAGAGATCTACAAAGGCTAACGGGGTCATTTTTTTTGCCTTG
V06-1-a2 ■	TTCGTAATCATGGTCATAGCTGTTTTGGATTATATTTTTTTTTCTGAA
V08-1-a2 ■	GGGATAGGTCACGTTGGTGTAGATAGCGAACCTCTTTTTTTACTTGCGGGAAAAAG
V02-3-b3 ■	AACATGCAACAGTGCTTTTTTTCACGCTGAGAGTGCCCCAGCAGGCGAAAATCCTGT
V04-2-b3 ■	AGCACAACGCAAGGATTTTTTTTTAAAAATTTTTCTGATAAATTAATGCCGGAGAGGG
V06-3-b3 ■	TTAGTATTTAACAACTTTTTTTGCCAACATGTACTAGAGGATCCCCGGGTACCGAGC
V08-3-b3 ■	AGCAGCTTTTTTTACCGTAATCAGGTGGGAACAAACGGCGGATTGACC

Note 4. Kinetic model of folding DNA wireframe paper.

The unfolded state (U) of DNA wireframe paper was transformed into the folded state (F) by adding glue strands (G). Corresponding kinetics of the folding reaction can be expressed with the forward reaction rate, k_{on}, and the reverse reaction rate, k_{off}, as the following equation.

$$[U]+[G] \underset{k_{off}}{\overset{k_{on}}{\rightleftharpoons}} [F]$$

$$\frac{dF}{dt} = k_{on}[U][G] - k_{off}[F]$$

The concentration of the unfolded structures and glue strands at time t could be substituted using the initial concentration of DNA nanostructures ($[U]_0$), the number of crease handle pairs per a DNA wireframe paper (n), and an input-factor of glue strands (ω) as below. Complete binding between glue strands and three pairs of crease handles was assumed at the folded state because single binding between crease handles and glue strands would enhance the rest binding of other pairs in that the pairs of crease handles would be located closer in a bent state. For instance, SQ H1 (3-pair) folding has parameters of $n = 3 \times 6 = 18$ and $\omega = 10$ (10-fold input).

$$\frac{dF}{dt} = k_{on}\left([U]_0 - [F]\right)\left(\omega n[U]_0 - n[F]\right) - k_{off}[F]$$

The folding yield (y) at time t can be expressed as $y = [F]/[U]_0$, therefore the differential equation was expanded as the equation below.

$$\frac{dy}{dt} = k_{on}\left(1-y\right)n\left(\omega - y\right) - k_{off}\,y = k_{on}\left\{n(1-y)(\omega - y) - K_D y\right\}$$

The dissociation constant, K_D, at quasi-steady state could be estimated using the equilibrated folding yield (y_{eq}) from AFM measurements.

$$K_D = \frac{[U]_{eq}[G]_{eq}}{[F]_{eq}} = \frac{[U]_0(1-y_{eq})(\omega n[U]_0 - n[F]_{eq})}{[F]_{eq}}$$

$$\therefore K_D = n[U]_0 \frac{(1-y_{eq})(\omega - y_{eq})}{y_{eq}}$$

Considering that the initial folding yield (y_0) from AFM measurements was typically less than 5%, it might occur by the projection problem in 2-D images while depositing on mica. Hence, for the simplicity of our model, we assumed the initial folding yield in the solution would be zero. Finally, the folding yield was derived as

$$nk_{on}dt = \frac{dy}{(1-y)(\omega - y) - \frac{K_D}{n}y} = \frac{dy}{y^2 - \left(1 + \omega + \frac{K_D}{n}\right)y + \omega}$$

$$= \frac{dy}{(y-\alpha)(y-\beta)} \qquad (\alpha > \beta)$$

$$n\int_0^t k_{on}dt = \int_{y_0}^{y} \frac{1}{\alpha - \beta}\left(\frac{1}{y-\alpha} - \frac{1}{y-\beta}\right)dy \quad \left(y_0 = \frac{[F]_0}{[U]_0} \cong 0\right)$$

$$y = \frac{1 - e^{nk_{on}(\alpha-\beta)t}}{\frac{1}{\alpha} - \frac{1}{\beta}e^{nk_{on}(\alpha-\beta)t}}$$

where α and β are solutions of a second-order equation of the denominator.

Considering that the folding yield would converge to y_{eq} when time goes to infinite ($t \to \infty$), then, we could calculate the coefficients α and β. With this result, we could eventually derive the kinetic model of fluorescence intensity from the relation $y = (I_0 - I_t)/(I_0 - I_\infty)$ where I_0, I_t, and I_∞ were the normalized fluorescence intensity at time 0, after time t, and at the end of the reaction, respectively.

$$\lim_{t\to\infty} y = \beta = y_{eq,}, \quad \alpha = \frac{\omega}{\beta} = \frac{\omega}{y_{eq}}$$

$$\therefore I_t = I_0 - (I_0 - I_\infty)\frac{1 - e^{nk_{on}(\alpha-\beta)t}}{\frac{1}{\alpha} - \frac{1}{\beta}e^{nk_{on}(\alpha-\beta)t}}$$

It is notable that only k_{on} remained for the variable in the final equation. We performed the least square curve fitting procedures with the experimental data using the *lsqcurvefit* function of MATLAB R2019b to systematically fit the forward reaction rate. The rate k_{off} was then obtained using the relation as $k_{off} = K_D \cdot k_{on}$.

$$K_D = \begin{cases} 41.7\,\text{nM} \ \text{(H1)} \\ 97.8\,\text{nM} \ \text{(H2)} \end{cases}$$

$$k_{on} = \begin{cases} 4.35\times10^5\,\text{M}^{-1}\text{s}^{-1} \ \text{(H1)} \\ 4.44\times10^5\,\text{M}^{-1}\text{s}^{-1} \ \text{(H2)} \end{cases}$$

$$k_{off} = \begin{cases} 1.81\times10^{-3}\,\text{s}^{-1} \ \text{(H1)} \\ 4.34\times10^{-3}\,\text{s}^{-1} \ \text{(H2)} \end{cases}$$

2.4. Environmental folding control

Since paper folding mechanisms are universal, one can easily make DNA wireframe papers responsive to various environmental stimuli. To illustrate, we first constructed a pH-responsive SQ DNA wireframe paper with H1 folding pattern (Figure 31a). Three pairs of edges were newly designed. Each pair consisted of a 20-nt-long ssDNA overhang (green) and a 20-bp-long hairpin overhang (orange) with a 4-nt-long poly-T loop. 60% TAT sequences were designed to control the Hoogsteen interaction by pH change (Figure 32). Samples were annealed and ultrafiltrated with FoB5 (5mM $MgCl_2$ and 1×TAE, pH 8.0), and then mixed with buffers of six different pH values between 5.8 and 8.4 (Note 5). Both AFM and time-resolved fluorescence measurements confirmed the pH-responsive structural switch between the folded and unfolded configurations (Figure 31b and Figure 31c). The Hill coefficient (*n*) and pK_a value were estimated as $n = 2.16$ and $pK_a = 7.47$ by fitting AFM data to the Hill equation (Figure 31b and Figure 33). The estimated pK_a value was similar to one of the pH-activated DNA switches found to be 7.50[36]. As pH changed repeatedly between 6.4 and 8.0, the normalized fluorescence intensity changed between 0.35 and 1.0, similar to the previous results of unfolding and folding by strands (Figure 31c). AFM measurements in each pH also confirmed the successful environmental folding control by pH change. A small decrease in the normalized fluorescence intensity was observed at pH 8.0 corresponding to the unfolded state. It was probably owing to structural damage with pH changes as a similar case was reported for pH-activated DNA capsules[27]. Our AFM measurements also supported it (Figure 34).

We also explored the deprivation of the folding ability of DNA wireframe papers by the illumination of ultraviolet (UV) rays. It was realized by introducing a photo-cleavable (PC) site in the middle of glue strands where two handles met (Figure 31d). Under visible light, DNA wireframe papers could be folded, unfolded, and refolded into the designated configurations with corresponding glue and releaser strands. When UV light was applied, folded structures were unfolded as the glue strands became cleaved (Figure 31e and Figure 35). Unfolding by UV

light took approximately 15~30 min. Three types of folded structures, H1, H2, and Q1, were successfully unfolded by 15 min illumination of UV light (Figure 31f and Figure 36). These photo-cleaved structures could not be refolded anymore except for random folding due to thermal fluctuations.

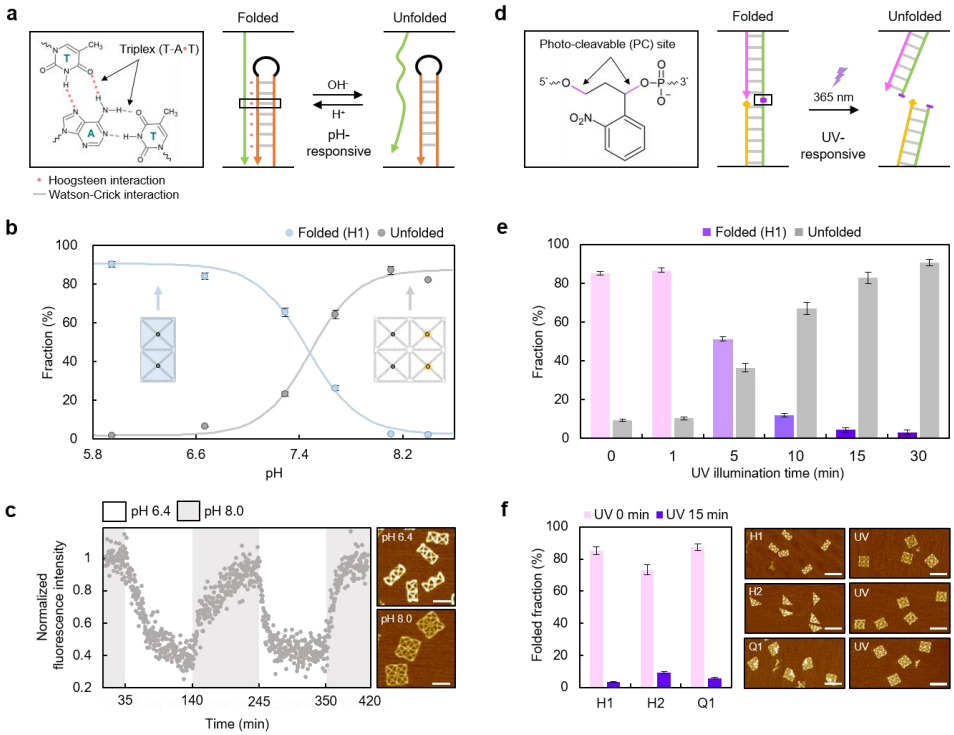

Figure 31. Environmental stimuli-responsive folding control by varying the pH value and UV illumination time.

(a) Schematic illustration for the pH-responsive folding control. The Hoogsteen interaction between ssDNA (green) and hairpin (orange) was designed to fold and unfold the assemblies between acidic and basic conditions. **(b)** Folded and unfolded fraction of SQ H1 according to pH value of buffers estimated by AFM measurement. The pH value was adjusted by adding 0.5 M acetic acid (CH_3COOH) and 0.5 M sodium hydroxide (NaOH). Hill equations are fitted to AFM data, and estimated Hill coefficient *n* and the value of pK_a are 2.16 and 7.47 for folded state and 2.33 and 7.49 for the unfolded state, respectively. **(c)** Time-resolved normalized fluorescence intensity as measured in solution for a total of 420 min. Representative AFM images at pH 6.4 and pH 8.0. Scale bars, 100 nm. **(d)** Schematic illustration for the deprivation of the folding ability by ultraviolet (UV) rays. Photo-cleavable site (violet) was designed in the middle of the glue strand to unable the folding of DNA assemblies through the illumination of UV. **(e)** Folded and unfolded fraction of SQ H1 according to UV illumination time estimated by AFM measurement. **(f)** Representative AFM images of the folded configuration by PC-glue and unfolded configuration by 15 min UV illumination Scale bars, 200 nm.

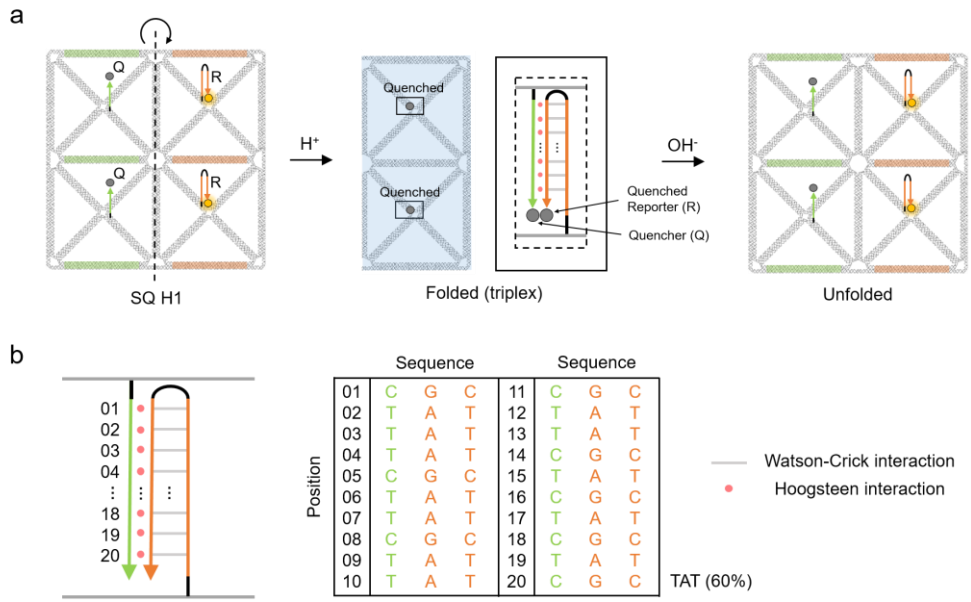

Figure 32. Design of pH-responsive folding and unfolding.

(a) Schematic illustration of pH-responsive folding and unfolding of DNA wireframe paper through the control of Hoogsteen interaction between ssDNA(green) and hairpin (orange). The attached two reporters would be quenched forming triplex by adding hydronium ion, and the intensity would be recovered by adding hydroxide. 0.5M acetic acid (CH_3COOH) and 0.5M sodium hydroxide (NaOH) was used for the pH adjustment. (b) Detailed sequences of a DNA triplex formed by 20-nt ssDNA and 20-bp hairpin motifs with 4-nt poly-T loop (black, half-arc). Black lines represent the 3-nt poly-T regions that serve as spacers. A 60% TAT content is designed for the pH-responsive structural reconfiguration between pH 6.4 and 8.0[36].

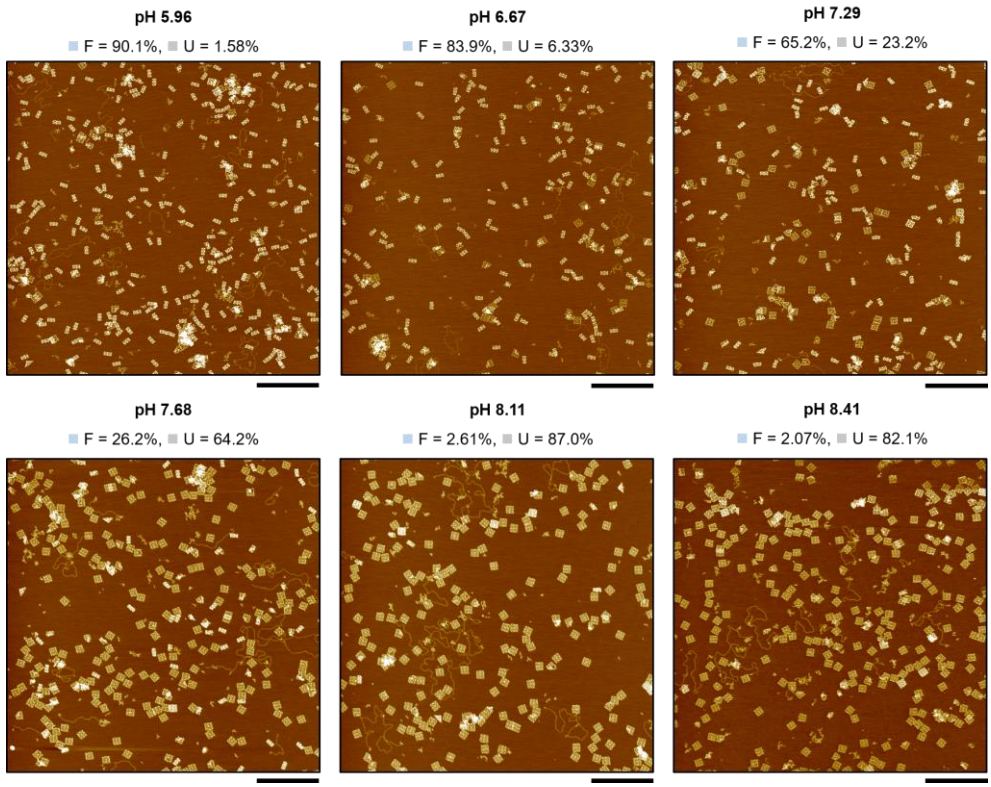

Figure 33. Representative AFM images of SQ H1 by varying the pH value.

The pH-responsive structural reconfiguration of SQ H1 by varying the pH value of the solution. Each sample was mixed with pH-adjusted buffer and incubated at room temperature for at least 2 hours. At least three AFM measurements were conducted to estimate the folded (F) and unfolded (U) fractions. Scale bars, 1 μm.

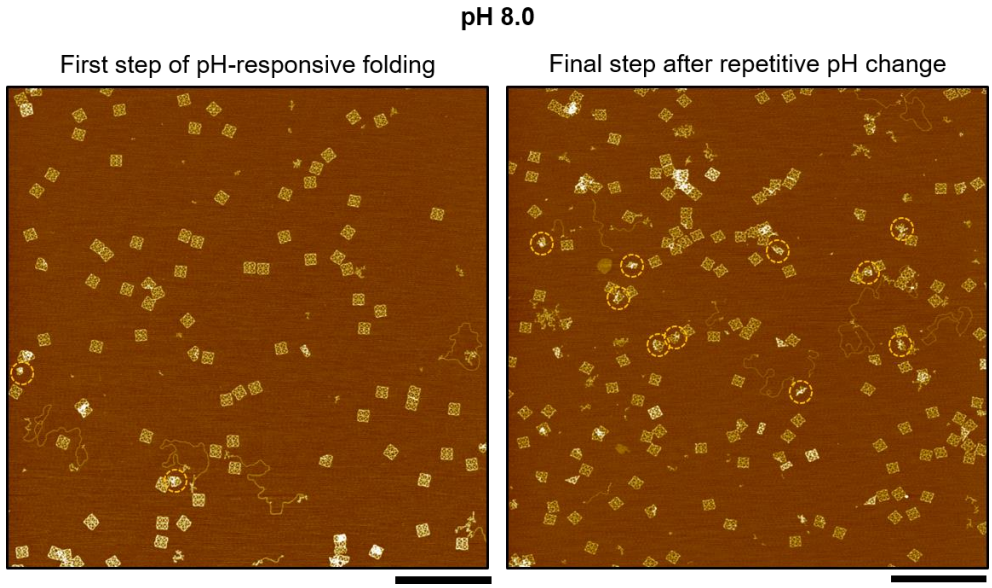

Figure 34. Structural damage of SQ H1 by repetitive pH changes.
Representative AFM images of the first and final step of pH-responsive folding and unfolding. More aggregated and irregular shapes (orange dotted circle) were observed in the final step image, guessed as one of the possible reasons for the slight decrease of normalized fluorescence intensity below 1.0 at pH 8.0 after repetitive pH changes. Scale bars, 1 μm.

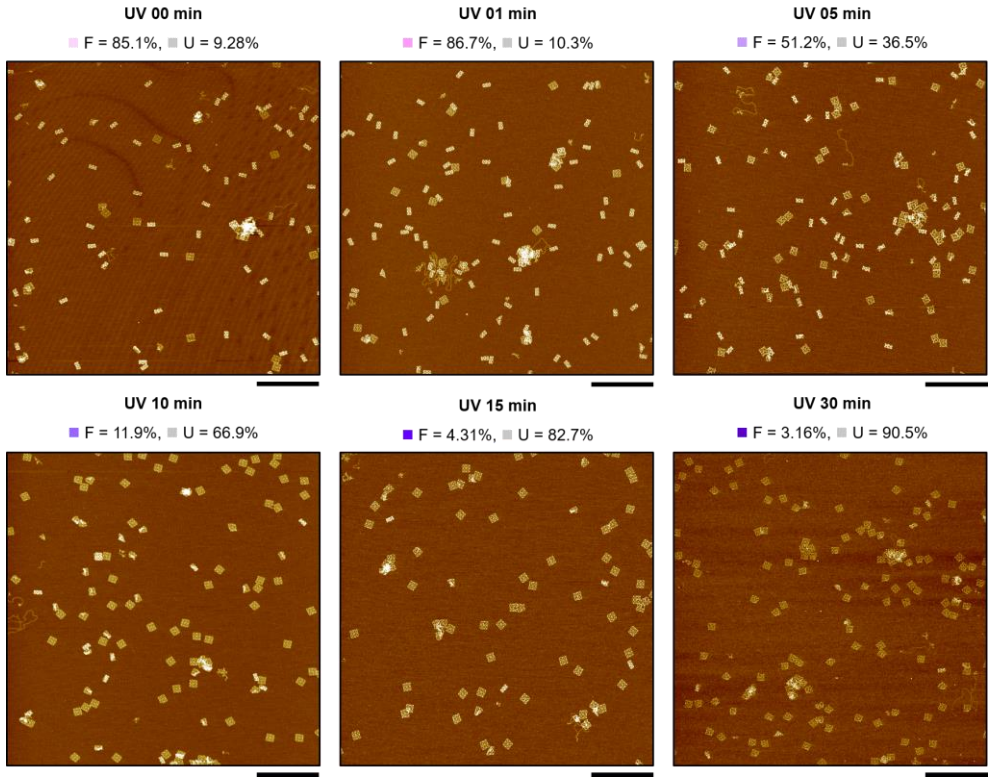

Figure 35. Representative AFM images of the unfolding of SQ H1 by varying the UV illumination time.

The UV-responsive unfolding of SQ H1 (3-pair) by varying the illumination time of UV light. Before UV illumination, DNA wireframe papers with an H1 3-pair crease pattern were mixed with the glue strand having a photo-cleavable (PC) site in the middle, PC-glue, and incubated at room temperature overnight. At least three AFM measurements were conducted to estimate the folded (F) and unfolded (U) fractions. Scale bars, 1 μm.

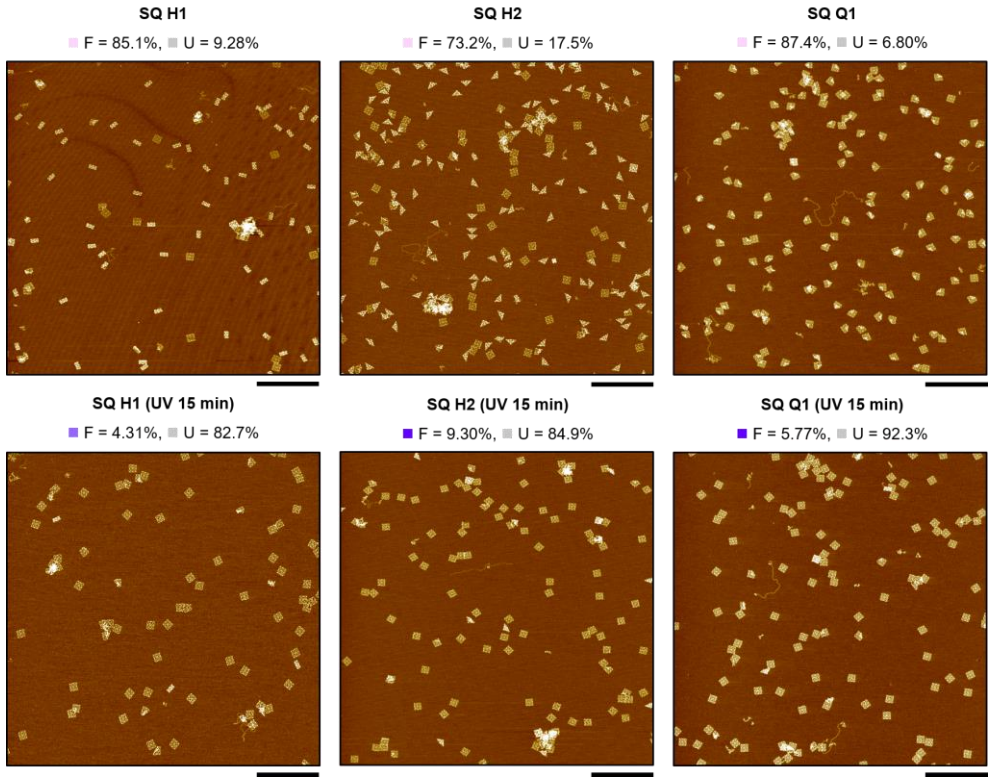

Figure 36. Representative AFM images of unfolding of SQ H1, H2, and Q1 by illuminating the UV.

The unfolding of three types of folded configurations (H1, H2, and Q1 3-pair) by PC-glue after the 15 min illumination of UV light. At least three AFM measurements were conducted to estimate the folded (F) and unfolded (U) fractions. Scale bars, 1 μm.

Note 5. The pH adjustment of Tris-acetate buffer.

Assuming that EDTA and $MgCl_2$ do not affect the hydrogen ion concentration of the solution, the pH of the buffer could be adjusted by considering the dissociation of acetic acid and $Tris^+$ ion. Then, two weak electrolyte buffer is considered[38] with the following equilibrium equations as

$$CH_3COOH \rightleftharpoons CH_3COO^- + H^+, \qquad K_A = \frac{[CH_3COO^-][H^+]}{[CH_3COOH]}$$

$$Tris - H^+ \rightleftharpoons Tris + H^+, \qquad K_B = \frac{[Tris][H^+]}{[Tris - H^+]}$$

where K_A and K_B are equilibrium constants of the acetic acid and $Tris^+$ ion, respectively.

The conservation equations for the two components can be expressed with two initial concentrations, c_A and c_B, and concentrations at equilibrium state.

$$c_A = [CH_3COOH]_{t=0} = [CH_3COO^-]_{eq} + [CH_3COOH]_{eq}$$

$$c_B = [Tris - H^+]_{t=0} = [Tris]_{eq} + [Tris - H^+]_{eq}$$

Also, given the electro-neutrality at moderate pH, the concentrations of acetate ion and $Tris^+$ ion would be equal to each other at equilibrium.

$$[CH_3COO^-]_{eq} = [Tris - H^+]_{eq}$$

The pH depending on c_A and c_B can finally be calculated by combining the above equations through substitution and infinite geometric series as follows.

$$pH = -\log \frac{K_A}{2}\left[\left(\frac{c_A}{c_B} - 1\right) + \sqrt{\left(1 - \frac{c_A}{c_B}\right)^2 + 4\frac{K_B}{K_A}\frac{c_A}{c_B}}\right]$$

Two equilibrium constants K_A and K_B are known values, and the initial $Tris^+$ ion concentration c_B is fixed as 40 mM according to the TAE buffer recipe. Therefore, the initial acetic acid concentration c_A is the only variable to lower the pH of the buffer, and hence, the reference volume of acetic acid to add to the solution can be estimated.

2.5. Larger-scale folding

In order to program more complex folding patterns, we need a larger DNA wireframe paper (Figure 37a). Toward this end, we constructed a four times larger DNA wireframe paper by hierarchically assembling four original-size papers (Figure 37b). We used six pairs of connectors and sticky edges at the interface of two monomeric papers to be connected, which showed the best polymerization yield at 12 mM $MgCl_2$ (Figure 38). Each monomeric DNA wireframe paper had two sets of six cohesive pairs in total to form a four times larger polymeric paper (Figures 39-40). Larger papers were built by mixing an equal amount of four monomeric papers in one place and incubating them at room temperature overnight (Figure 40).

These larger-scale DNA wireframe papers could be folded and unfolded successfully with glue and releaser strands as in the folding of monomeric papers. For example, AFM images clearly showed that the structure embedded with H2, Q1, Q2, and Q3 folding patterns could be folded into and unfolded from a diamond-like shape (Figure 37c and Figure 41). Furthermore, because of a large number of combinations in monomeric folding patterns, one can design various folded shapes. To demonstrate, here we constructed nine additional reconfigurable structures by programming different sets of monomeric folding patterns into the larger-scale DNA wireframe paper (Figure 37d and Figure 42). They could be folded into the intended shape as shown in AFM images (Figures 43-44).

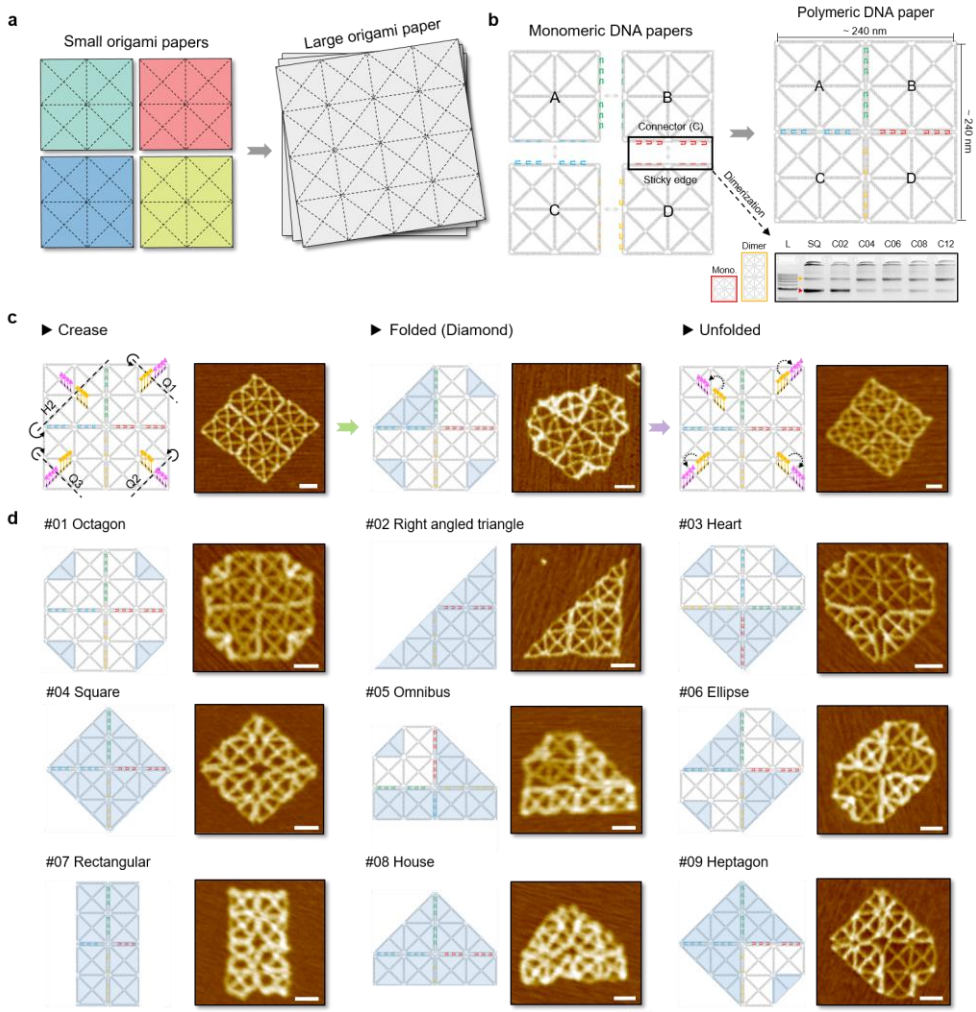

Figure 37. Larger-scale folding of a polymeric DNA paper.

(a) Conceptual illustration of forming a large origami paper by combining four small papers in macro-scale. **(b)** A polymeric DNA paper through the hierarchical assembly of four monomeric DNA papers in nano-scale. (Figure 39). The optimal number of connectors and sticky edges between two DNA papers was experimentally decided by comparing the intensity of the band in 1.5% agarose gel electrophoresis (Figure 38). **(c)** Larger-scale folding procedures of a polymeric DNA paper with an example of diamond folding. Four types of different crease patterns (H2, Q1, Q2, and Q3) were embedded on four types of original DNA wireframe papers (A, B, C, and D) and mixed at equal concentrations (Figure 41). A polymeric DNA paper was also folded and unfolded as intended by adding glue and releaser strands same with those of monomer. **(d)** Representative AFM images

of nine types of more complex and larger-scale folding (Detailed crease patterns and exemplary AFM images of larger-scale folding were described in Figure 42 and Figures 43-44, respectively). Scale bars, 50 nm.

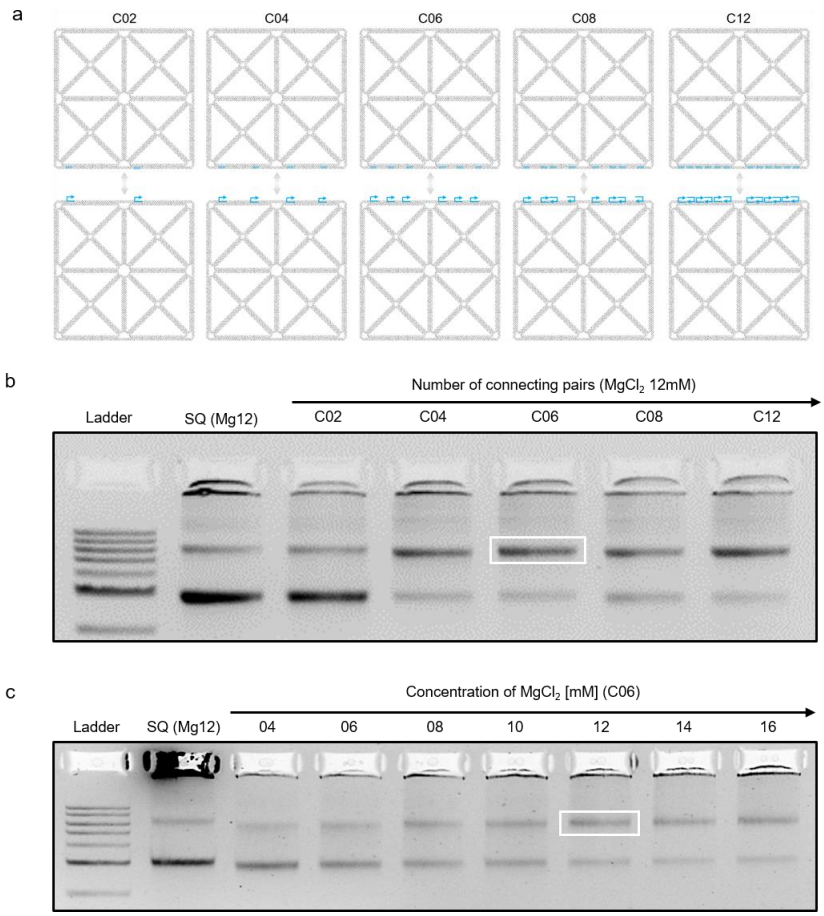

Figure 38. Connector number and cation concentration for polymerization of DNA wireframe papers.

(a) Schematic illustration of varying the number of connecting pairs (C) of sticky edges (top) and connectors (bottom). Five types of the number of pairs were designed to investigate the dimerization condition. (b) Agarose gel electrophoresis of the SQ dimers with the various number of pairs. The upper and lower band indicated the dimer and monomer, respectively. The brightness became stronger from the four pairs (C04) than those of the monomer. (c) Agarose gel electrophoresis of the SQ dimers with six connectors (C06, white box) and various cationic concentrations. From the 12 mM $MgCl_2$ concentration (white box), the brightness of the upper band became stronger than those of the monomer. The higher number of connectors and cationic concentration would cause irregular aggregation of structures, and therefore, six connecting pairs (C06) and 12 mM $MgCl_2$ were used.

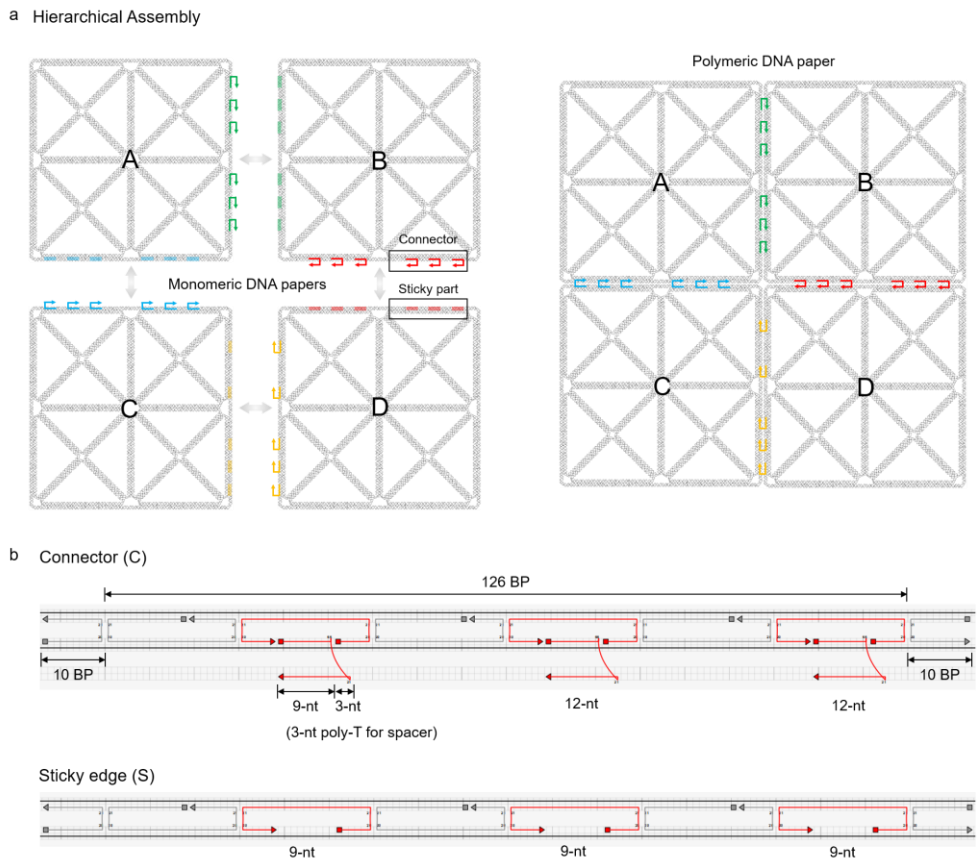

Figure 39. Design for hierarchical assembly of four types of DNA wireframe papers.

(a) Schematic illustration of hierarchical assembly of four DNA wireframe papers. Each monomer was designed to have six connectors and sticky parts that have complementary sequences to those of other monomers, which enable the polymerization. (b) Design diagram of the connector and sticky edge with an example of the connection between two DNA papers, B and D, in (a). 11-nt long overhang strands of connectors are desgined to have 9-nt long sequences that would combine with cohesive part of sticky edge and 3-nt long poly-T that serves as spacer.

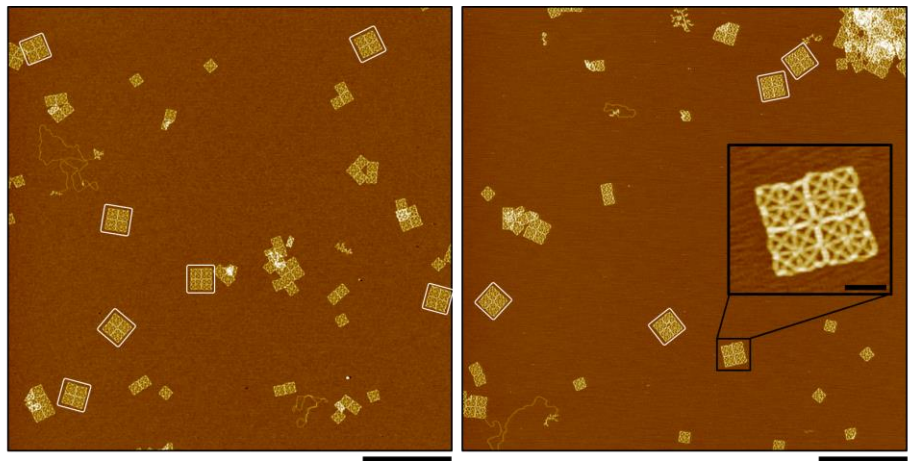

Figure 40. Representative AFM images of larger-scale DNA wireframe paper. Four types of square DNA wireframe papers with six connecting pairs were mixed at equal concentrations in 12 mM $MgCl_2$ and incubated at room temperature overnight. Scale bars, 1 μm (Inset, a magnified image. Scale bar, 100 nm.).

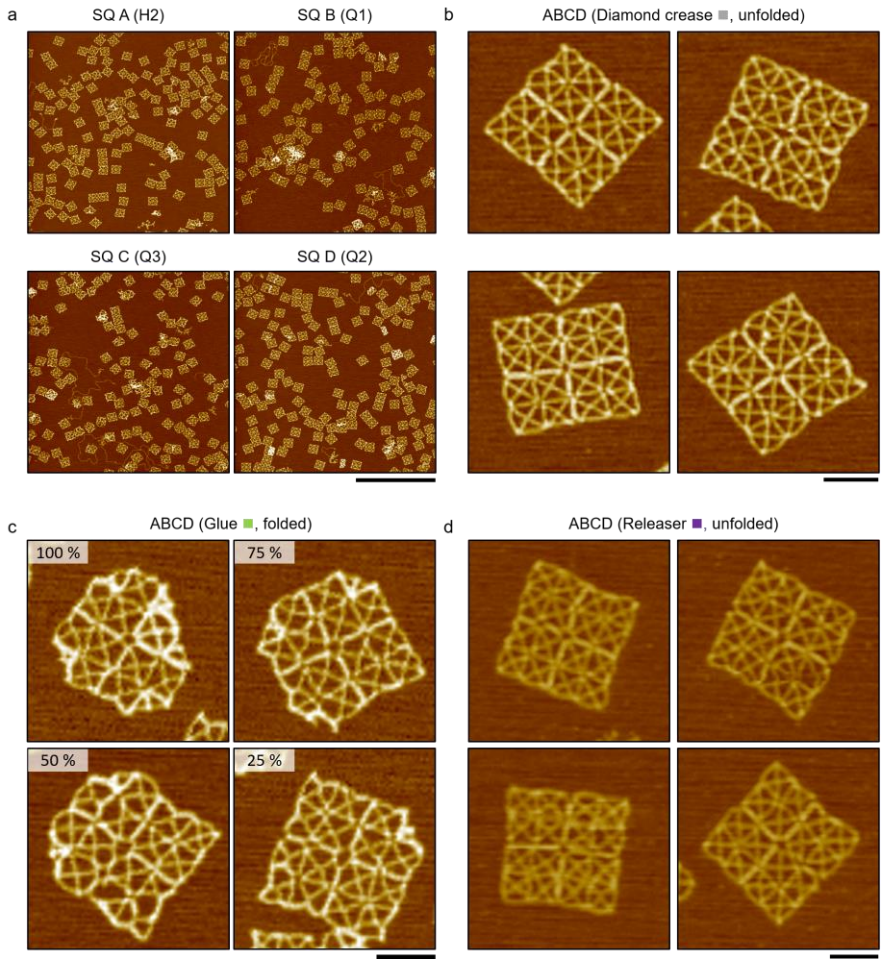

Figure 41. Representative AFM images of diamond-shaped folding.

(a) Representative AFM image for each monomer with its own crease pattern and connecting pairs. Without glue strands, most structures were unfolded. Scale bar, 1 μm. (b) Hierarchical assembly of four monomeric DNA papers into a polymeric DNA paper. (c) Diamond-shaped folding by adding glue strands. Partially folded configurations, 25%, 50%, and 75%, were also observed. (d) Unfolding by adding releaser strands. (b-d) Scale bars, 100 nm.

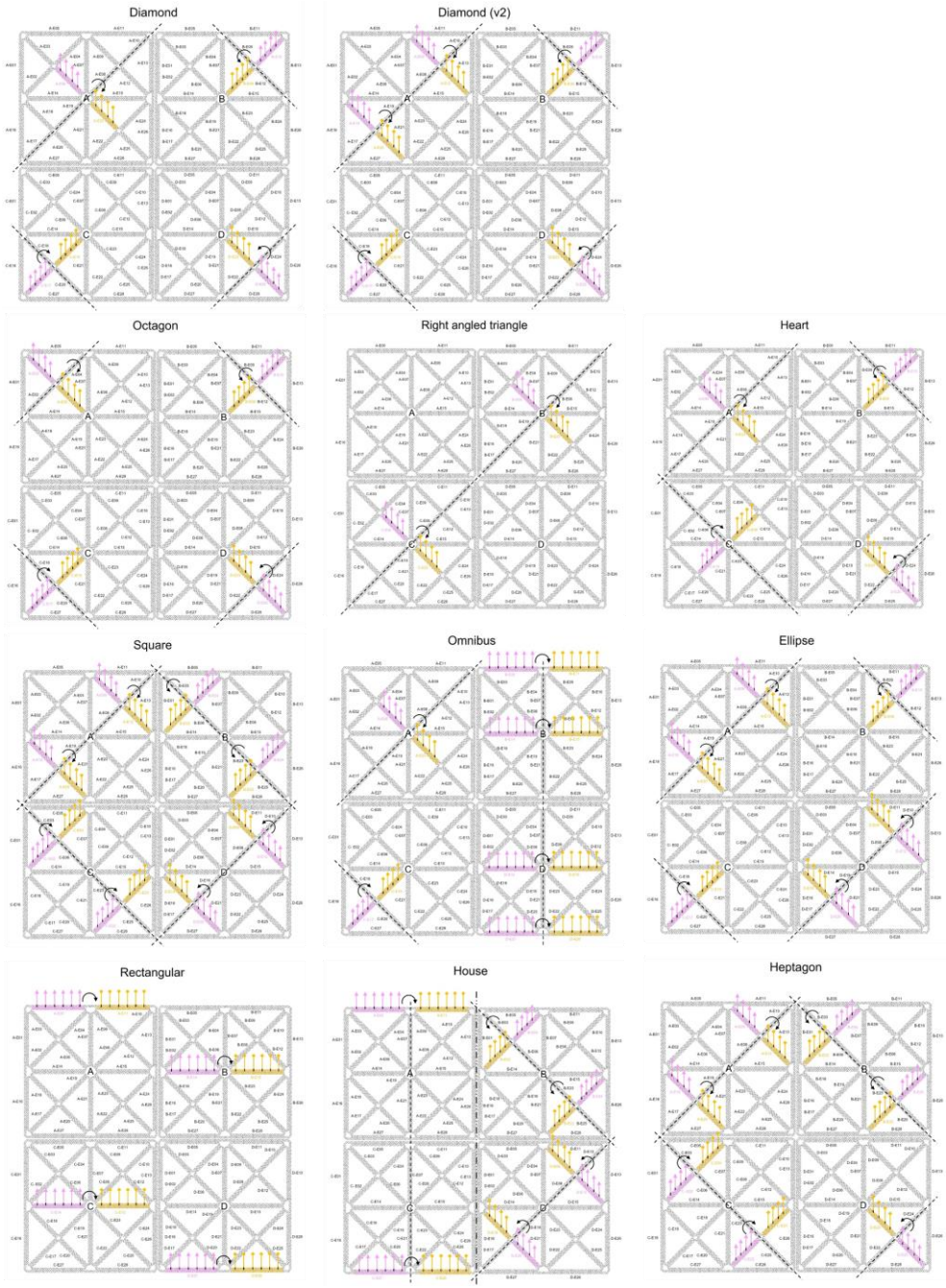

Figure 42. Detailed crease pattern of larger-scale folding.

Pink and yellow edges indicate the modified DNA edges having 3` and 5` crease handles that bind with the glue strand.

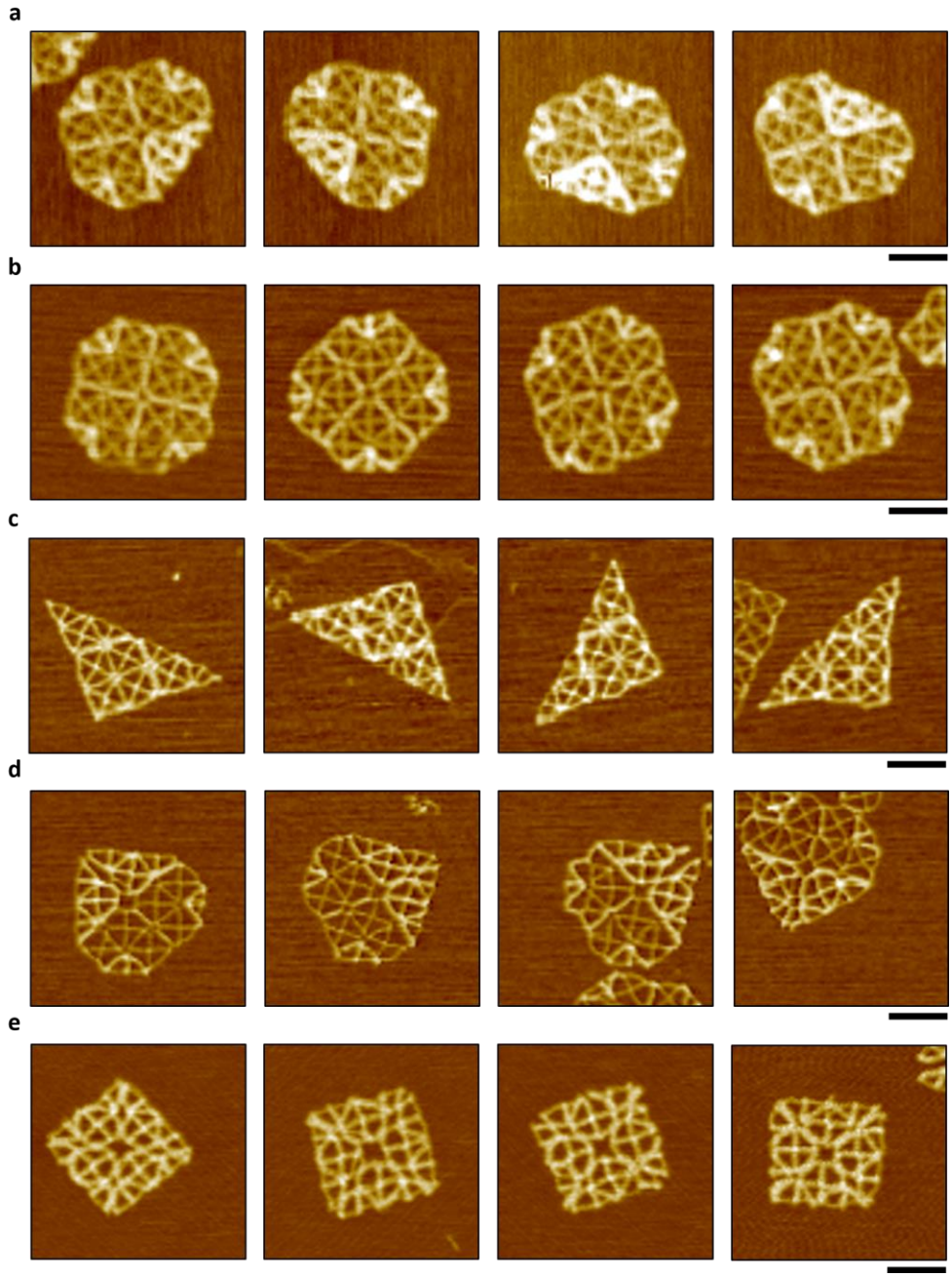

Figure 43. Representative AFM images of larger-scale folding (I).

(a) Diamond (v2). Compared to Diamond (v1), an H2 crease pattern with 2-pair was applied to SQ A to improve the folding yield. (b) Octagon. (c) Right-angled triangle. (d) Heart. (e) Square. Scale bars, 100 nm.

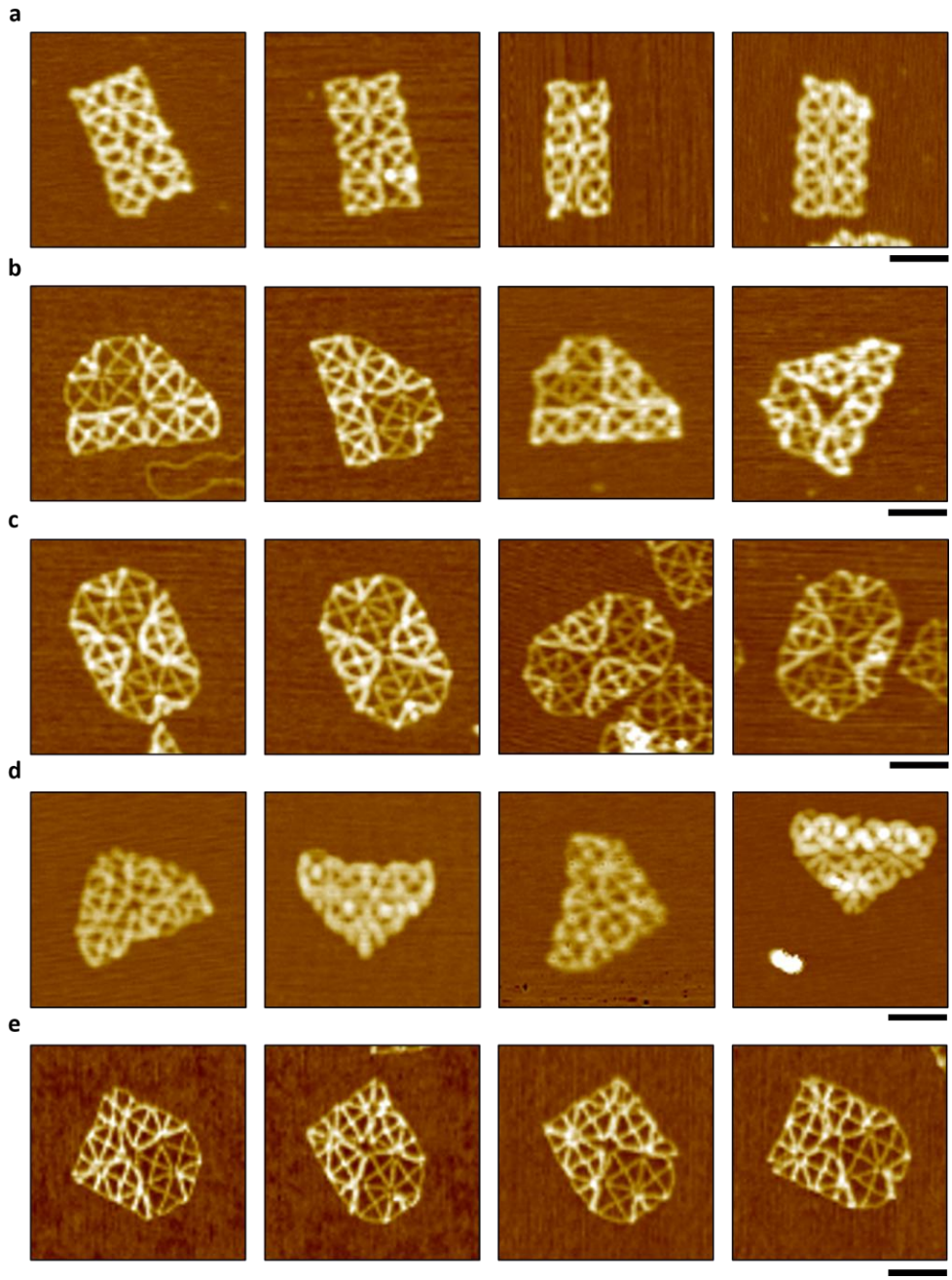

Figure 44. Representative AFM images of larger-scale folding (II).

(a) Rectangular. (b) Omnibus (H1, H2, and Q1). (c) Ellipse. (d) House. (e) Heptagon. Scale bars, 100 nm.

Table 5. Staple sequence for hierarchical assembly of DNA wireframe papers.

• Connecting pairs

Monomeric paper	A	B	C	D
Connector (C)	■	■	■	■
Sticky-edge (S)	■	■	■	■

• Connector (C) and sticky-edge (S)

Name	Sequence (5`→3`)
E01-2 (S) ■	GGGCGCGCGCTTAATGCGCCGCTACAGGAAAGC
E01-6 (S) ■	TTCTAGAGAACCCTCATATATTTTAAATATGAT
E13-1 (S) ■	TTATCCCATCAATATAATCCTGATTGTTCCTGT
E13-5 (S) ■	ATTAATTAACATTATCATTTTGCGGAAAGTGAG
E16-2 (S) ■	GAATCGCATGGCTTTTGATGATACAGGCTGGAG
E16-4 (S) ■	TGTACCGAAAGCGCAGTCTCTGAATTTAGCATG
E16-6 (S) ■	ATTGTATTGATATTCACAAACAAATAACCCAAA
E26-1 (S) ■	CGAAAGATGCAGAACGCGCCTGTTTATTATTAC
E26-3 (S) ■	CAGGGTTAATTCTGTCCAGACGACGACTAAGTT
E26-5 (S) ■	CCAAGCAGCCAGTAATAAGAGAATATAAAACGA
E01-2 (C) ■	GAAAGGAGCTTTCTAACTCAC
E01-6 (C) ■	ATTCAACCGTTTGTGAAATTG
E16-2 (C) ■	CAAACAAGATTTCGGCCAGTG
E16-4 (C) ■	TCAATCATATTTGGGTAACGC
E16-6 (C) ■	AACAGGAAGTTTGCCAGCTGG
E05-1 (S) ■	GAATAGAAACTATCGGCCTTGCTGGTACCTTAT
E05-3 (S) ■	AAGAGTCTTTGATTAGTAATAACATCAGTTCCA
E05-5 (S) ■	CGAAAAAGAGTCTGTCCATCACGCAAATCCAAC
E11-1 (S) ■	TGCGTAGGAAGGTTATCTAAAATATCTCGGGGA
E11-3 (S) ■	ACGGGCAATATCTGGTCAGTTGGCAAACTTTTC
E11-5 (S) ■	AGTTGCAAAGCATCACCTTGCTGAACCGCCTGG
E27-2 (S) ■	ACGCCATTGCCATCTTTTCATAATCAATTTTAA
E27-4 (S) ■	CTTTCACGTTTTCATCGGCATTTTCGGCCTTCC
E27-6 (S) ■	TTCTCCTAGCGACAGAATCAAGTTTGCTAACAA
E28-2 (S) ■	GACGACTATAGAAGGCTTATCCGGTATCTGCCA
E28-4 (S) ■	GCTTTCATCGTAGGAATCATTACCGCGATCGCA
E28-6 (S) ■	CCATTCAGTACCGCACTCATCGAGAACAAACCA

E27-2 (C) ■	CCAATAGGATTTGTCAAAGGG
E27-4 (C) ■	TGTAGCCAGTTTGTTTGGAAC
E27-6 (C) ■	CCCGTCGGATTTAAATCAAAA
E28-2 (C) ■	GTTTGAGGGTTTCCCTGAGAG
E28-4 (C) ■	CTCCAGCCATTTACCAGTGAG
E28-6 (C) ■	GGCAAAGCGTTTGAGGCGGTT
E01-1 (S) ■	AGGGAAGGCGCGTACTATGGTTGCTTTCGTGGC
E01-3 (S) ■	TGTAGCGGTCAGGGTGAGAAAGGCCGGAGGTAAAGAT
E01-4 (S) ■	TCAAAACGCTGCGCGTAACCACCACACCCGCCTAGGGC
E01-5 (S) ■	CATCAATGCAATGCCTGAGTAATGTGTAGACAG
E13-2 (S) ■	CAACATGATTATCAGATGATGGCAATTGCTCAC
E13-4 (S) ■	CTAATGCAAAGAAACCACCAGAAGGAGTAAAGC
E13-6 (S) ■	GCCCGCTATTAATTTTAAAAGTTTGAGTGCGTT
E16-1 (S) ■	GAGAGTAGTGTACTGGTAATAAGTTTTATCAGG
E16-3 (S) ■	AAAACTACCGTTCCAGTAAGCGTCATAATGAAC
E16-5 (S) ■	AAAAGCATCCTCATTAAAGCCAGAATGCCGGTT
E26-2 (S) ■	GGCGATAATAAACAACATGTTCAGCTAGGGGAT
E26-4 (S) ■	GTTGTAAAGTACCGACAAAAGGTAAAGTTTCCC
E26-6 (S) ■	TCGACTATTTAGGCAGAGGCATTTTCGTTGCAT
E13-2 (C) ■	AATTCCACATTTTCAAATCAC
E13-4 (C) ■	CTGGGGTGCTTTGCTGGCAAG
E13-6 (C) ■	GCGCTCACTTTTGAGAAAGGA
E26-2 (C) ■	GTGCTGCAATTTGATAATCAG
E26-4 (C) ■	AGTCACGACTTTGGTAATCGT
E26-6 (C) ■	GCCTGCAGGTTTTCATTGCCT
E05-2 (S) ■	AGTGTTCTTGCCTGAGTAGAAGAACTCCCCGAG
E05-4 (S) ■	GTGGACTTAACCGTTGTAGCAATACTTCCACTA
E05-6 (S) ■	CTAAATTCAGTGAGGCCACCGAGTAAAACCGTC
E11-2 (S) ■	GTTTTTTCAACAGTTGAAAGGAATTGATTGGGC
E11-4 (S) ■	TTCACCTCAAATATCAAACCCTCAATCAACAGC
E11-6 (S) ■	CTGGTTCCAGCAGCAAATGAAAAATCTAGCAAG
E27-1 (S) ■	CTCATTAATCACCGGAACCAGAGCCACTTTTTG
E27-3 (S) ■	GTCTGGTCATAGCCCCCTTATTAGCGTTCAAAA
E27-5 (S) ■	AGCGAGCTTTAGCGTCAGACTGTAGCGTCAACA
E28-1 (S) ■	GTGCATTCTAAGAACGCGAGGCGTTTTGGGCGC
E28-3 (S) ■	AGGAAGCCCAATAGCAAGCAAATCAGAGACAGT

E28-5 (S) ■	TGCCGGAAGCAAGCCGTTTTTATTTTCCGGCAC
E05-2 (C) ■	ATAGGGTTGTTTTTAAATGTG
E05-4 (C) ■	TTAAAGAACTTTATAATTCGC
E05-6 (C) ■	TATCAAGCATTTTTAAATCAG
E11-2 (C) ■	GCCAGGGTGTTTCGCTTCTGG
E11-4 (C) ■	TGATTGCCCTTTATCGGCCTC
E11-6 (C) ■	CGGTCCACGTTTATCGTAACC

Chapter 3. Conclusion

Here, we introduced the paper folding mechanism to program various crease patterns on square DNA wireframe assemblies and implemented eight types of reconfigurable folding of the nanostructures using toehold-mediated strand displacement. The folding yield was optimized above 90% by increasing the binding sites along the target crease and decreasing the structural rigidity using gap motifs. With the high yield obtained, various folding properties such as orthogonal folding, repeatable folding and unfolding, and folding-based fluorescence signal were successfully designed and implemented. Besides, embedding pH and UV-responsive crease handles enable the environmental folding control of DNA wireframe papers. Furthermore, through the hierarchical assembly of four original DNA papers with each crease pattern, we were able to show the possibility of our method to form much more complex and various folding patterns by representing 10 types of larger-scale folding of polymerized DNA papers.

Based on our effective reconfiguration mechanisms in nanoscale, we expect more complicated structural systems that interact with various inputs could be established by introducing more diverse types of orthogonal sequences of glue strands or applying both strand- and environment-responsive crease handles together. Building a larger paper beyond the current 2×2 assembly system, such as 4×4 and 8×8, would also enhance the complexity of the folding-based system. In addition, attaching various types and numbers of fluorophores to the folding-dependent system will lead to the development of sensitive DNA nanosensors with multi-wavelength and intensity. As in the versatile and effective use of a paper folding mechanism in macroscale engineering, our reconfigurable folding methods for DNA wireframe assemblies with high yield, programmability, and scalability, would contribute to the advancement of folding-based engineering applications in nanoscale.

Chapter 4. Materials and methods

Design and synthesis of DNA wireframe paper.

Structural draft of DNA wireframe paper was designed using PERDIX[31] (Note 1). Staple designs were edited to have crease handles perpendicular to the plane of the structure. Detailed design and sequences were described in Figure 2 and Table 3, respectively.

Scaffold M13mp18 (New England Biolabs) was used, and every staple was ordered at a 50 nmole scale and initially diluted to 100 pmole/μL (BioRP purification, Bioneer Corporation). The final concentration of the mixture was 20 nM scaffold, 100 nM each staple, 1×TAE buffer (40 mM Tris-acetate and 1 mM EDTA, Sigma-Aldrich), and 12 mM $MgCl_2$. A total of 42 hour PCR annealing process was performed using a thermocycler (T100, Bio-Rad) with the followed process: heated to 80℃ at 1℃/s, 80℃ to 65℃ in 1 h (1℃ per 4 min), 65℃ to 25℃ in 40 h (1℃ per 1 hour), and cooled and held at 4℃.

A larger-scale DNA wireframe paper was assembled by explicitly mixing equal concentrations of four types of ultrafiltrated DNA wireframe papers having their own connectors and sticky-edge and incubated at room temperature overnight. Detailed designs and sequences were included in Figure 39 and Table 5, respectively.

Ultrafiltration.

The synthesized sample was purified with 50 kDa molecular weight cut-off filters to remove excess staples. First, the filters were wet with a 500 μL amount of 12 mM $MgCl_2$ buffer and spun at 5,000 rcf (relative centrifugal force) for 8 min at 20℃. After discarding the filtrate, the sample and the buffer were sequentially poured into the filter and centrifuged at 5,000 rcf for 8 min at 20℃. Buffer exchange and centrifugation were repeated twice. Finally, the purified sample was collected by inverting the filter and spinning the tube at 10,000 rcf for 3 min at 20℃. The final concentration of the purified sample was measured by DNA absorbance measurements at 230 nm, 260 nm, and 280 nm using a NanoDrop spectrophotometer (Thermo Scientific), and detailed procedures were explained in Table 6.

Gel electrophoresis and extraction.

Samples were electrophoresed on from 0.8% to 1.5% agarose gels for 90 min at 75 V bias voltage (~3.7 V/cm) in an ice-filled water bath (i-Myrun, Cosmo Bio Co. Ltd.). Running buffer was composed of 0.5× TBE (45 mM Tris-borate and 1 mM EDTA, Sigma-Aldrich), 12 mM $MgCl_2$, and 0.5 μg/mL ethidium bromide (EtBr, Noble Bioscience Inc.). Gel images were laser scanned using GelDoc XR+ device and Image Lab v5.1 program (Bio-Rad). The electrophoresed samples were then carefully extracted by a razor blade and scrambled several times inside the freeze N squeeze tube (Bio-Rad) using a tweezer. They were frozen at -27℃ for 5 min and centrifuged at 7,000 rcf and 20℃ for 5 min to extract the samples.

AFM measurement.

Samples were diluted with the buffer composed of 20 mM $MgCl_2$, 40 mM Tris-acetate, and 1 mM EDTA, and deposited for 5 min onto freshly cleaved mica (highest grade V1 AFM Mica, Ted-Pella Inc.). They were completely dried by N_2 gun (<0.1 Kgf/cm2) after carefully washing the substrate three times with a 200 μL amount of deionized water. NX10 (Park Systems) and PPP-NCHR probe with 42 N/m spring constant (Nanosensors) were used for the measurement. All images were taken in non-contact mode using SmartScan software and flattened with linear and quadratic order using XEI 4.1.0 program (Park Systems). Structural height was then measured using line profile analysis of the program.

FE simulation.

The equilibrated configuration and rigidity of the DNA wireframe nanostructures were estimated using the finite element framework in SNUPI[32] where partition and relocation methods are applied. Structural design, sequence files, and the nonlinear properties of short single-stranded DNA[33] were introduced to conduct the normal mode analysis of the structures. All configurational results and the parameters used were represented in Figures 10-11 and Table 2, respectively.

Folding yield analysis.

The pixel-scale area and location of all particles in AFM images were obtained using the customized codes with the Image Processing Toolbox of MATLAB R2019b. Then, the aggregated nanostructures beyond the area criteria were systematically filtered out, and individual images containing a single particle were automatically cropped and collected. Based on the collected individual images, the folding yield was finally estimated by counting the number of monomers with intended shapes among the total number of monomers in AFM images. Detailed procedures and all yield results were described in Figure 13 and Table 1, respectively.

$$Yield\,(\%) = \frac{Number\ of\ monomers\ with\ intended\ shape}{Number\ of\ total\ monomers} \times 100$$

Folding and unfolding of DNA wireframe paper.

The folding process was typically actuated by adding glue strands 10 times higher than the concentration of crease handle pair and incubating the sample at room temperature overnight. The unfolding process was conducted by adding releaser strands 10 times higher than the concentration of the added glue strands and incubating the sample for an hour at 37℃. Folding and unfolding procedures of a polymeric DNA paper are the same as those of single DNA wireframe paper.

The pH-responsive crease handles were designed to have 60% T-A·T triplex content (Figure 32). They were ultra-filtrated with FoB5 (1×TAE buffer and 5 mM $MgCl_2$, pH 8.0) to relieve the aggregation of DNA assemblies. The 0.5 M acetic acid (Sigma-Aldrich) and 0.5 M sodium hydroxide (Officeahn) were used to adjust the pH values from 6.0 to 8.4 (Note 5), and the value was confirmed using the pH meter S2K922 (ISFETCOM) calibrated by pH 4.01 and 7.00 standard buffers (Thermo Scientific).

For the UV-responsive unfolding, the glue strand was internally modified to have the photo-cleavable (PC) sites in the middle (Bioneer). After adding the glue strands 10 times higher than the concentration of crease handle pairs and incubating the samples at room temperature overnight, they were carefully poured between two slide glasses (Duran) with a space of 1 mm and exposed to ultraviolet (UV) light illumination (Analytik Jena) of 365 nm wavelength.

Fluorescence measurements.

Inner vertex strands of square DNA paper were modified to have fluorescence reporters (Cyanine 3, Bioneer) and quencher (EBQ, Bioneer) at the end of the strands as shown in Figure 27 and Figure 32. Samples were ultrafiltrated and diluted to 20 nM before the measurement, and samples without fluorescence molecules were measured in advance for the use of the blank. Emission spectra analysis and kinetics at 563 nm wavelength, when excited at 546 nm wavelength, were performed using Dual-FL software 3.7 and HORIBA Scientific Jobin Yvon Spectrofluorometer with a 100-μL cuvette (Hellma) of 10×2 mm light path. All fluorescence intensity data were normalized to compensate for the dilution effect.

Hill coefficient and dissociation constant.

A Hill equation for the pH-responsive folding was fitted to AFM results using the *lsqcurvefit* function of MATLAB R2019b in order to obtain the effective Hill coefficient *n* and the values of pK_a as $pK_a = -\log K_a$ with the acid dissociation constant K_a, expressed as

$$F = F_{\min} + (F_{\max} - F_{\min}) \frac{(10^{-pH})^n}{(10^{-pK_a})^n + (10^{-pH})^n}$$

where $F_{\min}$ and $F_{\max}$ refer to the minimum and maximum folded fraction (F) estimated from AFM images, respectively. Before AFM measurements, samples were incubated at room temperature for at least two hours after being adjusted to each pH value (Note 5 and Figure 33).

Table 6. The effective concentration of DNA wireframe paper.

The concentration of DNA wireframe paper can be simply estimated by calculating the length of single-stranded DNA (ssDNA, nt) and double-stranded DNA (dsDNA, bp) of the structure. The total length of the unpaired scaffold, unpaired staples, and base pairs can be obtained from PERDIX[31]. The length of a scaffold loop was calculated by comparing the used length of the scaffold for the structure with the length of M13mp18. Based on these lengths obtained, we estimated the absorption coefficient by performing linear interpolation with the values of 33 for ssDNA and 50 for dsDNA and calculated the total molecular weight using the approximate average molecular weight of four types of nucleic acids. With the absorption coefficient and molecular weight obtained, the effective concentration of structures can be obtained using spectrophotometers.

Strand type	Pairing type	Square DNA paper (SQ)	Unit
ssDNA	Unpaired scaffold	42	[nt]
	Unpaired staple	324	[nt]
	Scaffold loop	63	[nt]
dsDNA	Base pair	7144	[bp]
Absorption coefficient		49.04	-
Molecular weight		4,469,632	[g/mol]

Appendix

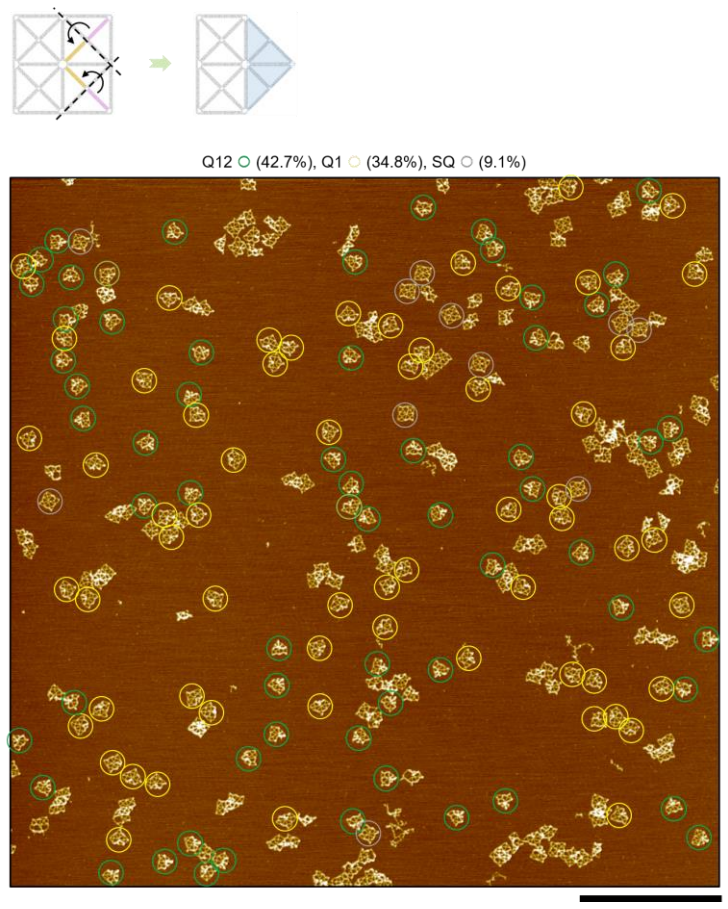

Figure A1. Representative AFM image of SQ Q12 (1-pair).

Pink and orange edges represent DNA edges modified with 3` and 5` crease handles, respectively. The green arrow indicates the process of adding glue strands. Well folded (intended), partially folded, and unfolded (SQ) structures were represented with corresponding colored circles. At least three AFM measurements were performed, and the total fraction for all shapes is described in Figure A5. Scale bar, 1 μm.

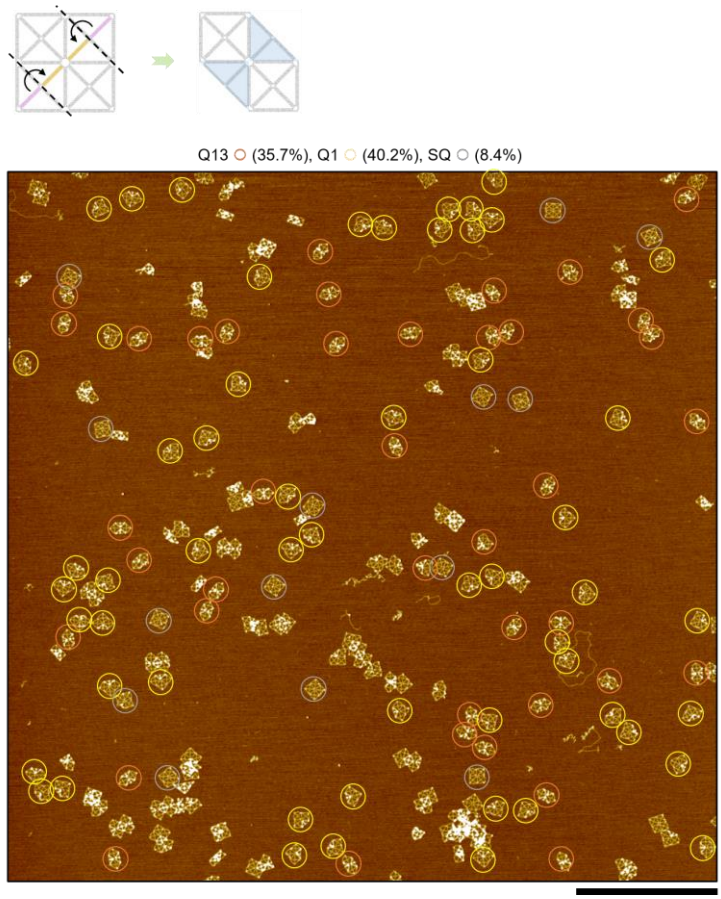

Figure A2. Representative AFM image of SQ Q13 (1-pair).

Pink and orange edges represent DNA edges modified with 3` and 5` crease handles, respectively. The green arrow indicates the process of adding glue strands. Well folded (intended), partially folded, and unfolded (SQ) structures were represented with corresponding colored circles. At least three AFM measurements were performed, and the total fraction for all shapes is described in Figure A5. Scale bar, 1 μm.

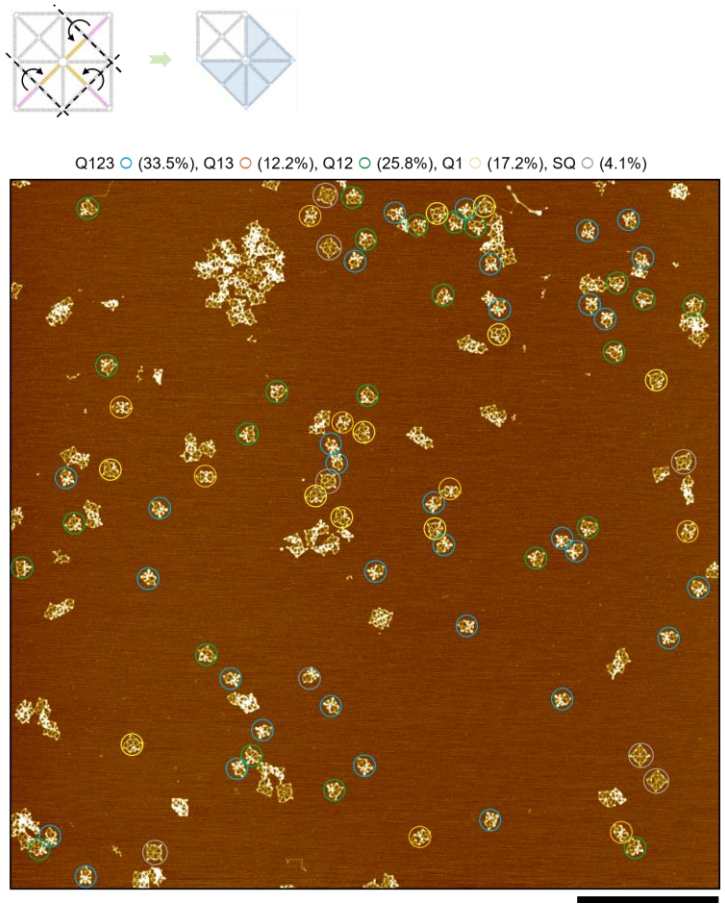

Figure A3. Representative AFM image of SQ Q123 (1-pair).

Pink and orange edges represent DNA edges modified with 3` and 5` crease handles, respectively. The green arrow indicates the process of adding glue strands. Well folded (intended), partially folded, and unfolded (SQ) structures were represented with corresponding colored circles. At least three AFM measurements were performed, and the total fraction for all shapes is described in Figure A5. Scale bar, 1 μm.

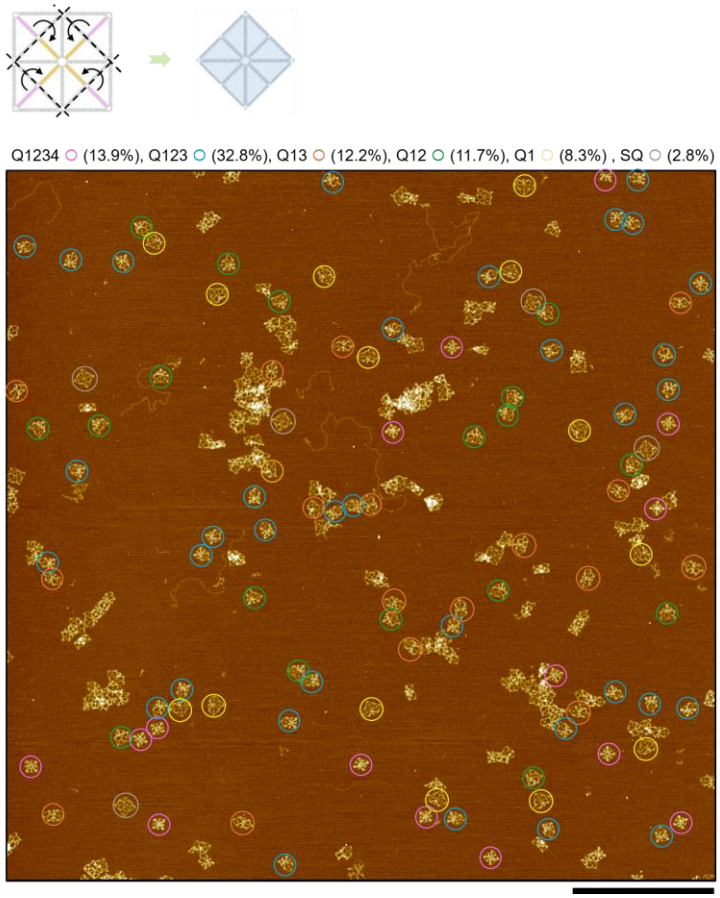

Figure A4. Representative AFM image of SQ Q1234 (1-pair).

Pink and orange edges represent DNA edges modified with 3` and 5` crease handles, respectively. The green arrow indicates the process of adding glue strands. Well folded (intended), partially folded, and unfolded (SQ) structures were represented with corresponding colored circles. At least three AFM measurements were performed, and the total fraction for all shapes is described in Figure A5. Scale bar, 1 μm.

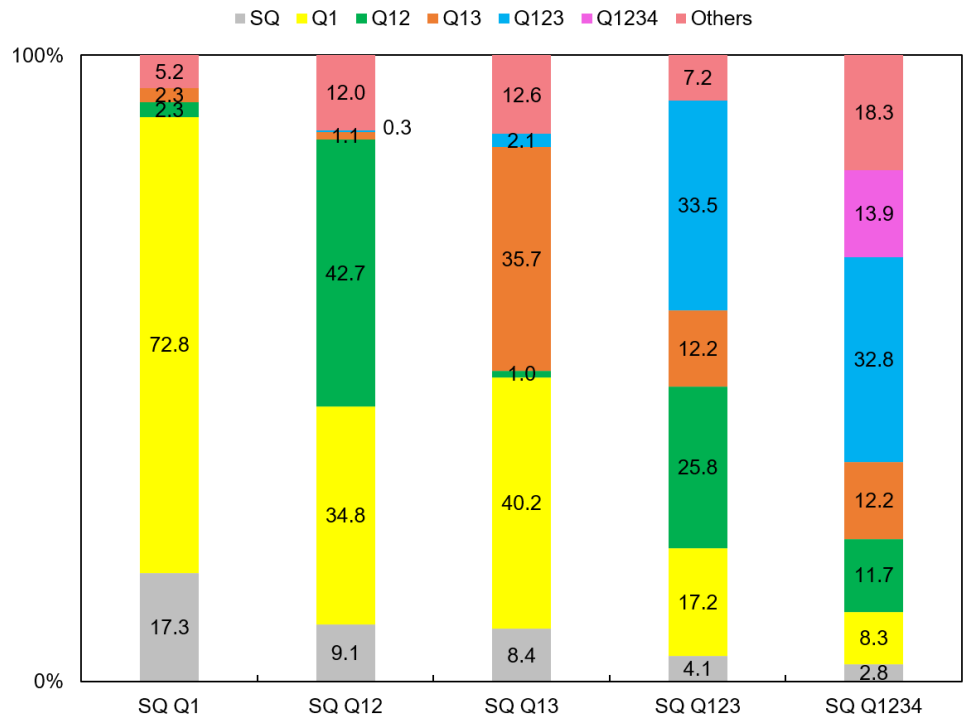

Figure A5. The total fraction of multiple quarter-folding of SQ (1-pair).

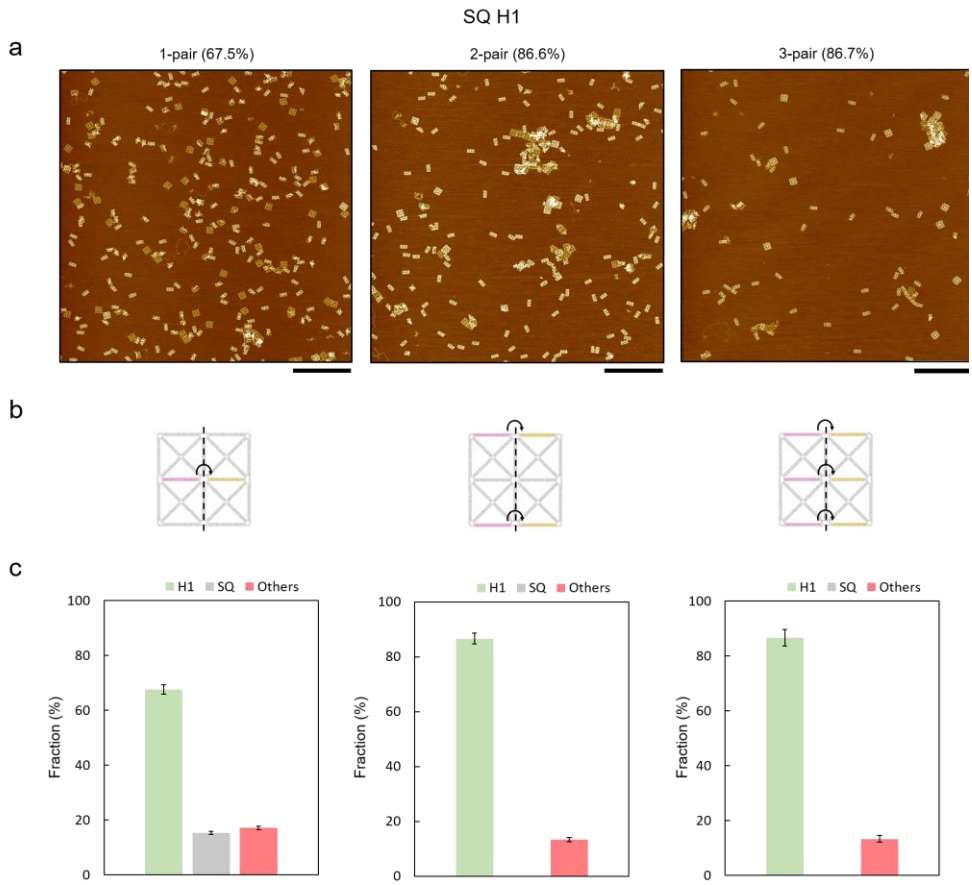

Figure A6. Representative AFM images of SQ H1 (pair, nick).

(a) Representative AFM images of SQ H1 with three different numbers of crease handle pairs from one to three. Scale bars, 1 μm. (b) Crease patterns of corresponding SQ H1. Pink and orange edges represent DNA edges modified with 3` and 5` crease handles, respectively. (c) The fraction of H3, SQ (unfolded), and Others estimated by AFM measurements. At least three AFM measurements were conducted to estimate the folding yield and standard error. Detailed data were described in Table 1.

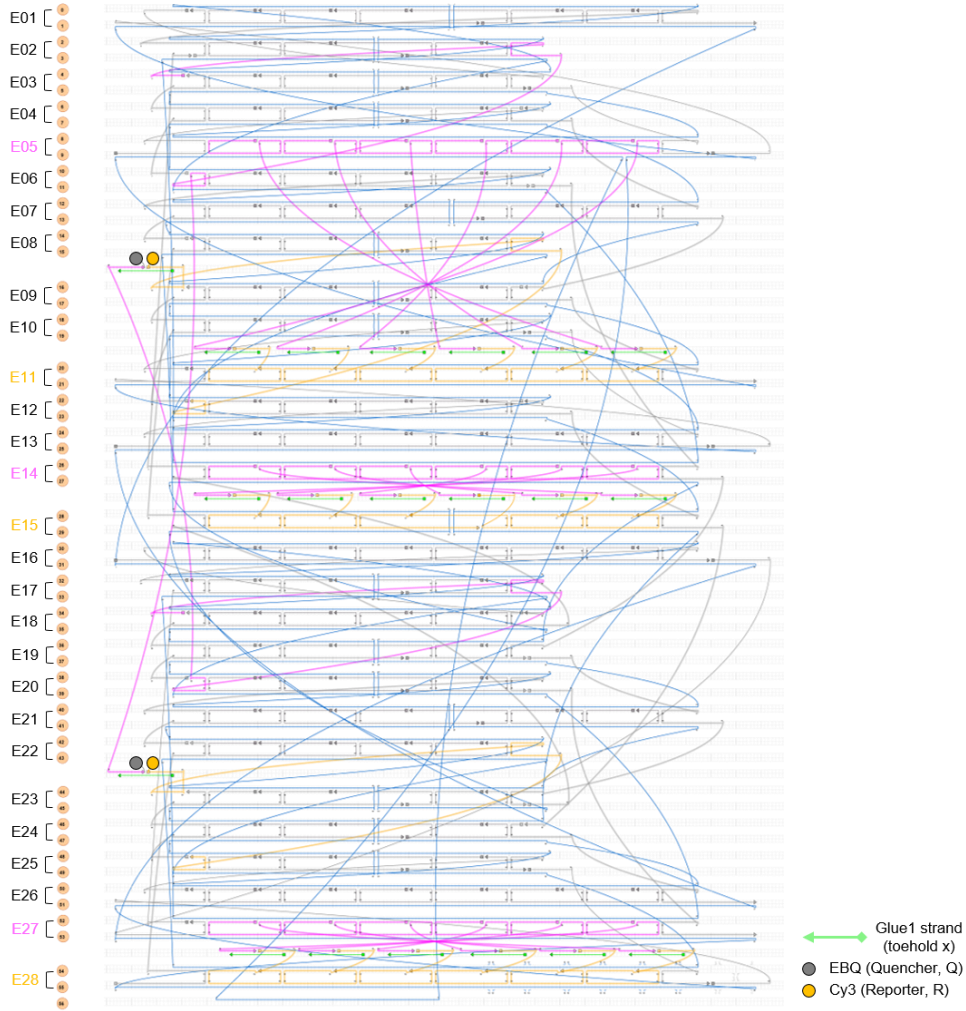

Figure A7. caDNAno blueprint of SQ H1 (3-pair) with two reporters and quenchers.

The blueprint represents the completely folded SQ H1 (3-pair) by glue strands (green). Two reporters and quenchers are attached at the 3` (pink) and 5` (orange) end of crease handles overhung from the inner vertex staples, respectively. In this blueprint, the toehold part of the glue strand is omitted.

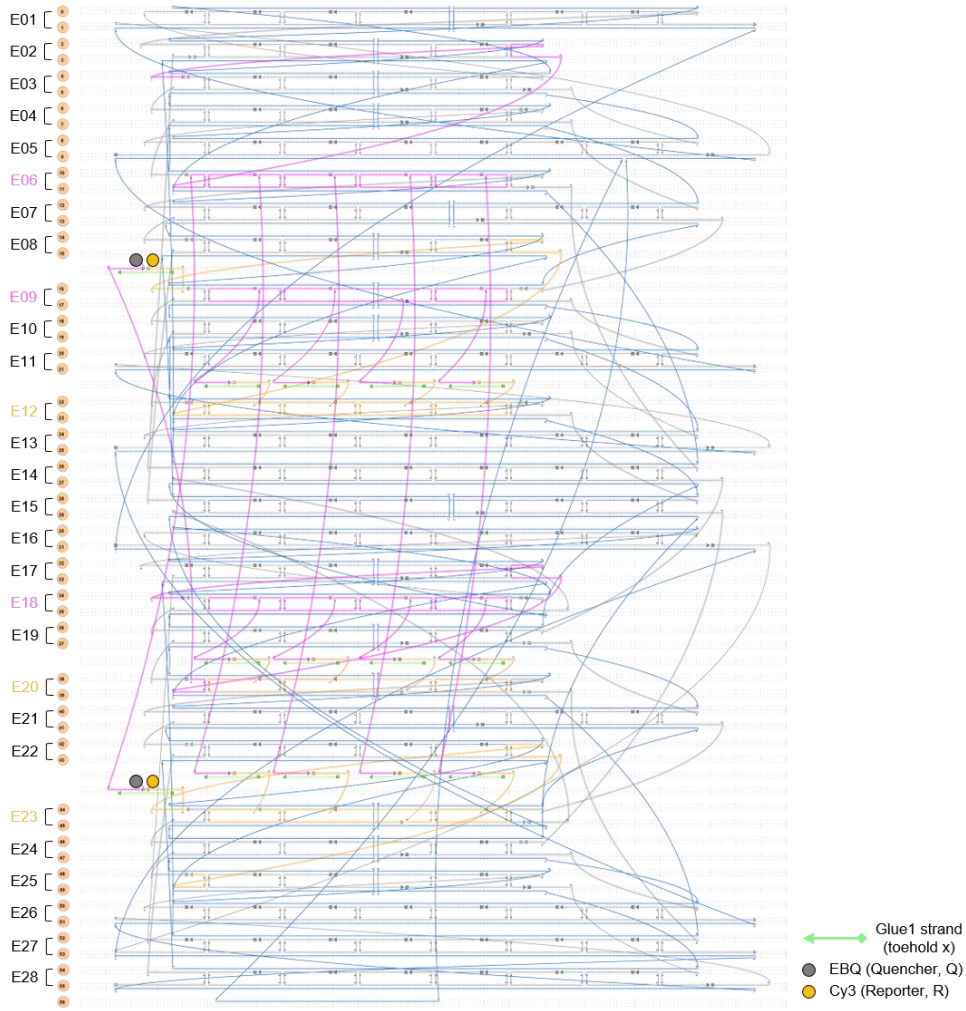

Figure A8. caDNAno blueprint of SQ H2 (3-pair) with two reporters and quenchers.

The blueprint represents the completely folded SQ H1 (3-pair) by glue strands (green). Two reporters and quenchers are attached at the 3` (pink) and 5` (orange) end of crease handles overhung from the inner vertex staples, respectively. In this blueprint, the toehold part of the glue strand is omitted.

Bibliography

1. Freeland R, Bilyeu G, Veal G, Steiner M, Carson D. Large inflatable deployable antenna flight experiment results. *Acta Astronautica* 1997, **41**(4-10)**:** 267-277.

2. Lee D-Y, Kim J-K, Sohn C-Y, Heo J-M, Cho K-J. High–load capacity origami transformable wheel. *Science Robotics* 2021, **6**(53).

3. Pesenti M, Masera G, Fiorito F. Exploration of adaptive origami shading concepts through integrated dynamic simulations. *Journal of Architectural Engineering* 2018, **24**(4)**:** 04018022.

4. Meloni M, Cai J, Zhang Q, Sang-Hoon Lee D, Li M, Ma R, *et al.* Engineering Origami: A comprehensive review of recent applications, design methods, and tools. *Advanced Science* 2021**:** 2000636.

5. Winfree E, Liu F, Wenzler LA, Seeman NC. Design and self-assembly of two-dimensional DNA crystals. *Nature* 1998, **394**(6693)**:** 539-544.

6. Rothemund PW. Folding DNA to create nanoscale shapes and patterns. *Nature* 2006, **440**(7082)**:** 297-302.

7. Douglas SM, Marblestone AH, Teerapittayanon S, Vazquez A, Church GM, Shih WM. Rapid prototyping of 3D DNA-origami shapes with caDNAno. *Nucleic acids research* 2009, **37**(15)**:** 5001-5006.

8. Dietz H, Douglas SM, Shih WM. Folding DNA into twisted and curved nanoscale shapes. *Science* 2009, **325**(5941)**:** 725-730.

9. Han D, Pal S, Nangreave J, Deng Z, Liu Y, Yan H. DNA origami with complex curvatures in three-dimensional space. *Science* 2011, **332**(6027)**:** 342-346.

10. Wei B, Dai M, Yin P. Complex shapes self-assembled from single-stranded DNA tiles. *Nature* 2012, **485**(7400)**:** 623-626.

11. Benson E, Mohammed A, Gardell J, Masich S, Czeizler E, Orponen P, *et al.* DNA rendering of polyhedral meshes at the nanoscale. *Nature* 2015, **523**(7561)**:** 441-444.

12. Kim Y-J, Lee C, Lee JG, Kim D-N. Configurational design of mechanical perturbation for fine control of twisted dna origami structures. *ACS nano* 2019, **13**(6)**:** 6348-6355.

13. Lee C, Kim KS, Kim Y-J, Lee JY, Kim D-N. Tailoring the mechanical stiffness of DNA nanostructures using engineered defects. *ACS nano* 2019, **13**(7)**:** 8329-8336.

14. Kim D-N, Kilchherr F, Dietz H, Bathe M. Quantitative prediction of 3D solution shape and flexibility of nucleic acid nanostructures. *Nucleic acids research* 2012, **40**(7)**:** 2862-2868.

15. Castro CE, Kilchherr F, Kim D-N, Shiao EL, Wauer T, Wortmann P, *et al.* A primer to scaffolded DNA origami. *Nature methods* 2011, **8**(3)**:** 221-229.

16. Tikhomirov G, Petersen P, Qian L. Fractal assembly of micrometre-scale DNA origami arrays with arbitrary patterns. *Nature* 2017, **552**(7683)**:** 67-71.

17. Wagenbauer KF, Sigl C, Dietz H. Gigadalton-scale shape-programmable DNA assemblies. *Nature* 2017, **552**(7683)**:** 78-83.

18. Chen H, Weng T-W, Riccitelli MM, Cui Y, Irudayaraj J, Choi JH. Understanding the mechanical properties of DNA origami tiles and controlling the kinetics of their folding and unfolding reconfiguration. *Journal of the American Chemical Society* 2014, **136**(19)**:** 6995-7005.

19. Li S, Jiang Q, Liu S, Zhang Y, Tian Y, Song C, *et al.* A DNA nanorobot functions as a cancer therapeutic in response to a molecular trigger in vivo. *Nature biotechnology* 2018, **36**(3)**:** 258-264.

20. Liu S, Jiang Q, Zhao X, Zhao R, Wang Y, Wang Y, *et al.* A DNA nanodevice-based vaccine for cancer immunotherapy. *Nature Materials* 2021, **20**(3)**:** 421-430.

21. Zhou L, Marras AE, Su H-J, Castro CE. DNA origami compliant nanostructures with tunable mechanical properties. *ACS nano* 2014, **8**(1)**:** 27-34.

22. Lee C, Lee JY, Kim D-N. Polymorphic design of DNA origami structures through mechanical control of modular components. *Nature communications* 2017, **8**(1)**:** 1-8.

23. Lavella GJ, Jadhav AD, Maharbiz MM. A synthetic chemomechanical machine driven by ligand–receptor bonding. *Nano letters* 2012, **12**(9)**:** 4983-4987.

24. Selnihhin D, Sparvath SM, Preus S, Birkedal V, Andersen ES. Multifluorophore DNA origami beacon as a biosensing platform. *ACS nano* 2018, **12**(6)**:** 5699-5708.

25. Marras AE, Shi Z, Lindell III MG, Patton RA, Huang C-M, Zhou L, *et al.* Cation-activated avidity for rapid reconfiguration of DNA nanodevices. *ACS nano* 2018, **12**(9)**:** 9484-9494.

26. Goetzfried MA, Vogele K, Mückl A, Kaiser M, Holland NB, Simmel FC, *et al.* Periodic Operation of a Dynamic DNA Origami Structure Utilizing

the Hydrophilic–Hydrophobic Phase-Transition of Stimulus-Sensitive Polypeptides. *Small* 2019, **15**(45)**:** 1903541.

27. Ijäs H, Hakaste I, Shen B, Kostiainen MA, Linko V. Reconfigurable DNA origami nanocapsule for pH-controlled encapsulation and display of cargo. *ACS nano* 2019, **13**(5)**:** 5959-5967.

28. Marras AE, Zhou L, Su H-J, Castro CE. Programmable motion of DNA origami mechanisms. *Proceedings of the National Academy of Sciences* 2015, **112**(3)**:** 713-718.

29. Zhou L, Marras AE, Huang CM, Castro CE, Su HJ. Paper Origami-Inspired Design and Actuation of DNA Nanomachines with Complex Motions. *Small* 2018, **14**(47)**:** 1802580.

30. Zhang F, Jiang S, Wu S, Li Y, Mao C, Liu Y, *et al.* Complex wireframe DNA origami nanostructures with multi-arm junction vertices. *Nature nanotechnology* 2015, **10**(9)**:** 779-784.

31. Jun H, Zhang F, Shepherd T, Ratanalert S, Qi X, Yan H, *et al.* Autonomously designed free-form 2D DNA origami. *Science advances* 2019, **5**(1)**:** eaav0655.

32. Lee JY, Lee JG, Yun G, Lee C, Kim Y-J, Kim KS, *et al.* Rapid computational analysis of DNA origami assemblies at near-atomic resolution. *ACS nano* 2021, **15**(1)**:** 1002-1015.

33. Lee JY, Kim M, Lee C, Kim D-N. Characterizing and Harnessing the Mechanical Properties of Short Single-Stranded DNA in Structured Assemblies. *ACS nano* 2021.

34. Hariadi RF, Yurke B, Winfree E. Thermodynamics and kinetics of DNA nanotube polymerization from single-filament measurements. *Chemical science* 2015, **6**(4)**:** 2252-2267.

35. Zenk J, Tuntivate C, Schulman R. Kinetics and thermodynamics of Watson–Crick base pairing driven DNA origami dimerization. *Journal of the American Chemical Society* 2016, **138**(10)**:** 3346-3354.

36. Idili A, Vallée-Bélisle A, Ricci F. Programmable pH-triggered DNA nanoswitches. *Journal of the American Chemical Society* 2014, **136**(16)**:** 5836-5839.

37. Rao SS. *Vibration of continuous systems*. John Wiley & Sons, 2019.

38. Persat A, Chambers RD, Santiago JG. Basic principles of electrolyte chemistry for microfluidic electrokinetics. Part I: acid–base equilibria and pH buffers. *Lab on a Chip* 2009, **9**(17)**:** 2437-2453.

국 문 초 록

종이접기 메커니즘은 변형 가능한 특성을 통해 구조 재구성과 관련된 많은 공학 문제들에 대한 효과적인 해결 방안들을 제공해왔습니다. 하지만, 종이접기 기반 구조 재구성 방식을 거시규모에서 나노규모 공학으로 이전하는 것은 정밀한 나노구조체 설계 및 다양한 접힘 (주름 패턴) 설계에 대한 어려움으로 인해 여전히 난제로 남아 있습니다. 본 논문에서는 평면 시트 형태의 DNA 와이어프레임 구조체(DNA 와이어프레임 종이) 위에 종이접기 방식을 접목하여 핵산 기반 주름 설계 방법을 개발하였고 발판 매개 가닥 변위 반응을 통해 DNA 와이어프레임 종이의 8가지의 재구성 가능한 접힘을 구현하였습니다. 접힘 수율은 결합 확률 증대 및 주름의 구조적 강성 완화를 통해 90% 이상으로 최적화 되었습니다. 확보한 높은 수율을 바탕으로 직교 접힘, 반복 접힘과 펼침, 접힘 기반 신호 제어 등 여러가지 접힘 특성들을 설계하였고 원자력 현미경 및 형광 측정을 통해 이를 입증하였습니다. 또한 pH 값 및 자외선 조사에 따른 환경 자극 반응 접힘을 설계해 이를 성공적으로 제어하였습니다. 나아가, 계층적 조립 전략을 채택하여 보다 복잡한 주름 패턴들을 설계하였고, 최종적으로 4배 면적으로 중합된 더 큰 규모의 DNA 종이의 10가지 의도한 접힘을 구현하였습니다. 높은 수율, 다양한 접힘 설계 가능성, 그리고 큰 규모 확장성을 가진 본 연구의 DNA 구조체에 대한 종이접기 기반 구조 재구성 방법이 나노규모에서의 접힘 방식 기반 공학적 응용 분야의 발전에 기여할 것을 기대합니다.

주요어 : DNA 나노기술, DNA 오리가미, 와이어프레임 구조체, 종이접기 공학, 구조 재구성, 유한 요소 해석

학 번 : 2020-28211

Acknowledgments

First of all, I would like to thank Prof. Do-Nyun Kim for his interest and guidance in developing my research on DNA nanotechnology. Through a lot of support and care during the two years of my master's degree, I could be able to focus on my research with great interest and passion. I also hope to express my gratitude to Prof. Yongdae Shin for giving an enthusiastic lecture on cellular mechanics, which helped me become more interested in exploring biology and its dynamic implications. Besides, I appreciate the comment and interest of Prof. Howon Lee in my thesis presentation.

I wish to acknowledge my debt to all of my research colleagues in Simulation-driven Structure Design Laboratory. I especially thank my senior Ph.D. Chanseok Lee, Young-Joo Kim, and Jae Young Lee for carefully teaching experimental and computational parts from the start of my master's degree and giving helpful advice for my research. Through a lot of discussion and guidance with them, I could learn basic capabilities and how to grow as an independent researcher. In addition, it was a meaningful moment for me to study various papers on DNA nanotechnology every week with researchers Kyounghwa Jeon and Dongsik Seo. I also would like to express great thanks for the support of the rest members of our DNA team.

In this thesis, Chanseok Lee contributed to analyzing the data and designing the experiments. Young-Joo Kim gave me help to set up and conduct the fluorescence measurement. Kyounghwa Jeon performed the UV and pH-responsive experiments together. Jae Gyung Lee ran the FE simulation, and Jae Young Lee estimated the normal mode analysis for DNA wireframe structures. I especially thank Junho Park for his advice to conduct AFM measurements.

Lastly, I hope to take this opportunity to express my gratitude to my father in heaven, mother, and older sister for their devoted support and consideration for my studies. Without their endless love and dedication, I would not be here today. I would like to sincerely appreciate their support and care once again.